Memo version 1.0.0

BESIII Analysis Memo

BAM–

June 22, 2022

Study of $\Xi^0 \to \gamma\Lambda$ at BESIII

He Li[a], Jiajun Tang[a], and Xiaorong Zhou[a], and Haiping Peng[a]

[a]*State Key Laboratory of Particle Detection and Electronics, University of Science and Technology of China, Hefei 230026, China*
[b]*Institute of High Energy Physics*

Internal Referee Committee

xxxx(Chair)[d], xxx[e], and xxxx[f]

[d]
[e]
[f]*IHEP*

HN : http://hnbes3.ihep.ac.cn/HyperNews/get/paper397.html

Abstract

Based on $1.0087 \times 10^{1}0$ J/ψ events collected with the BESIII detector operating at BEPCII in 2009, 2012, 2018 and 2019, the radiative decay $\Xi^0 \to \gamma\Lambda$ is studied at collider experiment for the first time. After background subtraction, XXX±XXX events are observed in total from the two charge conjugated processes, and the absolute branching fraction (BF) is determined to be $\mathscr{B}(\Xi^0 \to \gamma\Lambda) = (xxx \pm xxx_{stat.} \pm xxx_{syst.}) \times 10^{-3}$, the decay parameter is determined to be $\alpha(\Xi^0 \to \gamma\Lambda) = (xxx \pm xxx_{stat.} \pm xxx_{syst.})$.

Contents

1 Introduction

1.1 Motivation

Hyperons, quasi-stable subatomic particles classified as baryons that are composed of three quarks, are more heavier than the nucleons (protons and neutrons). Distinct from nucleons, they contain one or more strange quarks. In order of increasing mass, the hyperon family includes the Lambda-zero (Λ^0) particle, a triplet of Sigma (Σ) particles, a doublet of Xi (Ξ) particles, the Omega-minus (Ω^-) particle and so on. In this work we will concentrate on the lightest hyperon: Λ .

Hyperon decays fall into three categories: the nonleptonic decays, semi-leptonic decays and weak radiative decays[1]. The most dominant with the branching fraction of nearly 100%, are the nonleptonic (or pionic) decays, for example $\Lambda \to p\pi^-$, $\Lambda \to n\pi^0$. The semi-leptonic (or β) decays, like $\Lambda \to pe^-\bar{\nu}_e$, are quite infrequent with the branching fraction(BF) in the range from 10^{-3} to 10^{-4}. The weak radiactive decays refer to that contain only one hadron in initial state as well as final state with a γ emission, like: $\Lambda \to \gamma n$.

The weak radiactive decays of hyperon represent effective $s \to d$ quark transitions. These unique decays combine the strong, weak, and electromagnetic interactions in a hardronic system. Searching for the weak radiative hyperon decays provides an important tool for investigating the interplay of the electromagnetic, weak, and strong interactions[2]. The description of these processes in terms of well-undertood electroweak forces in complicated by the presence of strong interactions[3][4].

The transition matrix element T for a general radiative decay of a hyperon B_i of momentum p to a baryon B_f of momentum p' and a photon momentum q,

$$B_i(p) \to B_f(p') + \gamma(q) \tag{1}$$

is given by[5],

$$T = G_F \frac{e}{\sqrt{4\pi}} \epsilon_\nu \bar{u}(p')(\boldsymbol{A} + \boldsymbol{B}\gamma_5)\sigma_{\mu\nu} q_\mu u(p) \tag{2}$$

where $\bar{u}(p')$ and $u(p)$ are the spinor wave functions of the baryon and hyperon, respectively, ϵ_ν is the polarization vector of the photon, $\boldsymbol{A}$ and $\boldsymbol{B}$ are the parity-conserving ($\boldsymbol{M}1$) and parity-violating ($\boldsymbol{E}1$) amplitudes, $\sigma_{\mu\nu}$ and γ_5 are the combinations of the Dirac gamma matrices, G_F is the Fermi constant, and e is the electron charge. The decay asymmetry parameter is [6]

$$\alpha_\gamma = \frac{2Re(\boldsymbol{A} * \boldsymbol{B})}{|\boldsymbol{A}|^2 + |\boldsymbol{B}|^2} \tag{3}$$

The long-standing questions associated with the hyperon weak radiative decays is the “Hara theorem”[7], which indicates the parity-violating amplitudes $\boldsymbol{B}$ vanishing for weak radiative decays in the limit of uni-

tary symmetry within the pole approximation[8]. For broken SU(3), according to the size of hadron-level SU(3)-breaking effects elsewhere, the asymmetry parameter is expected to be of the order of ±0.2[5]. However, fix target experimental measurements[2] for the weak radiative decays did not support the predictions and the decay parameters were found large as the order of ±1.0, according to Table 1.

Table 1: Branching fraction and decay asymmetry parameter measurement results for weak radiactive decays. "–" indicates "not available".

$B_i \to \gamma B_f$	$BF(10^{-3})$	α_γ
$\Lambda \to \gamma n$	1.75±0.15	–
$\Sigma^+ \to \gamma p$	1.23 ± 0.05	−0.76 ± 0.08
$\Sigma^0 \to \gamma n$	–	–
$\Xi^0 \to \gamma\Lambda$	1.17 ± 0.07	−0.70 ± 0.07
$\Xi^0 \to \gamma\Sigma^0$	3.33 ± 0.10	−0.69 ± 0.06
$\Xi^- \to \gamma\Sigma^-$	1.27 ± 0.23	1.0 ± 1.3
$\Omega^- \to \gamma\Xi^-$	$< 0.46(90\%C.L.)$	–

Basically, there are four fix target experimental measurements for $\Xi^0 \to \gamma\Lambda$, as shown in Table 2. According to the measurement results, we can see that the average value of the branching fraction of $\Xi^0 \to \gamma\Lambda$ is determined by Ref. [9], while the average value of decay parameter is determined by Ref. [12] with quite large statistic, however, the branching fraction is not determined in the experiment.

Table 2: Summary of experimental measurements for $\Lambda \to \gamma n$. "–" indicates the value not available.

Experiment	BF($\times 10^{-3}$)	α_γ	Signal yields
CERN SPS NA48[9]	1.17 ± 0.05 ± 0.06	−0.78 ± 0.18 ± 0.06	672
CERN SPS NA48[10]	1.91 ± 0.34 ± 0.19	–	31
FerrmiLab[11]	1.06 ± 0.12 ± 0.11	-0.43 ±0.44	161/87
CERN SPS NA48[12]	–	-0.704 ±0.019 ± 0.064	52000
PDG	1.17 ± 0.07	-0.704 ±0.019 ± 0.064	–

Abundant theoretical calculations and predictions for BF and decay parameter of weak radiative decay behind the Hara theorem are implemented. Recently, detailed dynamics for the hyperon weak radiative decay are revisited by theorists[13], predictions for $\Xi^0 \to \gamma\Lambda$ by different models are summarized in Table 3.

The theoretical models help explaining the physical essences of the weak radiative decays, but obvi-

Table 3: Predictions for branching fraction and decay parameters.

Model	$BF(10^{-3})$	α_γ
Broken SU(3) [14]	1.02	-0.97
ChPT [15]	1.17	0.46
Pole model I [16]	0.72±0.42	0.07
Pole model II [17]	3.0	-0.78
NRCQM [13]	0.96±0.32	-0.72±0.11

ous difference of the experimental and theoretical results was observed. Therefore , precise experimental measurements are urgent to cross-check with the models and the previous experiments.

At BESIII, more than 10 billion J/ψ events have been accumulated in 2009, 2012, 2018 and 2019. It is a good oppurtunity to search the radiative decay of $\Xi^0 \to \gamma\Lambda$ by using $J/\psi \to \Xi^0\bar{\Xi}^0$ process, the charge conjugate processes of $\Xi^0 \to \gamma\Lambda$ can cross-check with each other. Also it will be the first time to study hyperon weak radiative decays on e^+e^- collider with lower backgroud level than fix target experiments. Baryon polarization in baryon-antibaryon events from $J/\psi \to \Xi^0\bar{\Xi}^0$ events was observed at BESIII [18], based on the measurement result and experimental method, the decay parameter for $\Xi^0 \to \gamma\Lambda$ will be measured for the first time with spin-correlation of $J/\psi \to \Xi^0\bar{\Xi}^0$ decay.

In order to experimentally reconstruct and measure the $\Xi^0 \to \gamma\Lambda$, we can speculate that the most challenge lies in the requirement of γ detection in the presence of a generally large π^0 background, considering $\Xi^0 \to \gamma\Lambda$ with a branching fraction $BF \approx 10^{-3}$, versus $\Xi^0 \to \pi^0\Lambda$ with $BF \approx 0.99$ [1]. The decay channels and corresponding branching fraction of Ξ^0 is list in Table 4.

Table 4: The decay channels and corresponding branching fraction of Ξ^0 quoted from PDG.

Decay channels	BF
$\Xi^0 \to \pi^0\Lambda$	$(99.524 \pm 0.012)\%$
$\Xi^0 \to \gamma\Lambda$	$(1.17 \pm 0.017) \times 10^{-3}$
$\Xi^0 \to \gamma\Sigma^0$	$(3.33 \pm 0.1) \times 10^{-3}$
$\Xi^0 \to \Lambda e^+e^-$	$(7.6 \pm 0.6) \times 10^{-6}$

1.2 Analysis strategy

In this analysis, the radiative decay of $\Xi^0 \to \gamma\Lambda$ are searching in the subsequent decay of process $J/\psi \to \Xi^0\bar{\Xi}^0$, thus a double tag (DT) method, which may cancel several uncertiainties and is described

below detailly, is implemented. Throughout the text, the charged conjugated modes is not implemented if there is not mentioned specially.

To search for the decay of $\Xi^0 \to \gamma\Lambda$, we first tag the $J/\psi \to \Xi^0\bar{\Xi}^0$ events (namely signal tagged (ST) thereafter) by reconstructing a $\bar{\Xi}^0$ signal with its charged decay mode $\bar{\Xi}^0 \to \pi^0\bar{\Lambda}$, where $\bar{\Lambda}$ is reconstructed by $\bar{\Lambda} \to \pi^+\bar{p}$. The observed ST yields (N_{ST}) can be written as :

$$N_{ST} = N_{J/\psi\to\Xi^0\bar{\Xi}^0} \times \mathscr{B}_{\bar{\Xi}^0\to\pi^0\bar{\Lambda}} \times \mathscr{B}_{\bar{\Lambda}\to\pi^+\bar{p}} \times \mathscr{B}_{\pi^0\to\gamma\gamma} \times \varepsilon_{ST}, \tag{4}$$

where $N_{J/\psi\to\Xi^0\bar{\Xi}^0}$ is the event number of event $J/\psi \to \Xi^0\bar{\Xi}^0$ in the using data sample, $\mathscr{B}_{\bar{\Xi}^0\to\pi^0\bar{\Lambda}}$ is the decaying branching fraction (BF) of $\bar{\Xi}^0 \to \pi^0\bar{\Lambda}$, and ε_{ST} is the corresponding ST detection efficiency.

We then search for the decay $\Xi^0 \to \gamma\Lambda$ recoiling against the ST $\bar{\Xi}^0$ (namely double tagged (DT) thereafter), and the corresponding DT yields (N_{DT}) is :

$$N_{DT} = N_{J/\psi\to\Xi^0\bar{\Xi}^0} \times \mathscr{B}_{\bar{\Xi}^0\to\pi^0\bar{\Lambda}} \times \mathscr{B}_{\bar{\Lambda}\to\pi^+\bar{p}} \times \mathscr{B}_{\pi^0\to\gamma\gamma} \times \mathscr{B}_{\Xi^0\to\gamma\Lambda} \times \mathscr{B}_{\Lambda\to\pi^-p} \times \varepsilon_{DT}, \tag{5}$$

where $\mathscr{B}_{\Xi^0\to\gamma\Lambda}$ is the BF of the signal interested, and the ε_{DT} is the corresponding DT efficiency.

Divide Eq. 5 by Eq. 4, the BF of the decay $\Xi^0 \to \gamma\Lambda$ is obtained :

$$\mathscr{B}_{\Xi^0\to\gamma\Lambda} = \frac{N_{DT}/\varepsilon_{DT}}{N_{ST}/\varepsilon_{ST}} \times \frac{1}{\mathscr{B}_{\Lambda\to\pi^-p}} \tag{6}$$

1.3 BESIII and BEPCII

The BESIII and BEPCII is major upgrade of the BESII and BEPC experiment for hardron spectroscopy and τ−charm physics. The BEPCII is a double-ring e^+e^- collider designed to provide a peak luminosity of 10 $^{33}\text{cm}^{-2}\text{s}^{-1}$ at the center of mass energy around 3770 MeV. The BESIII, a general purpose detector running at BEPCII, is cylindrically symmetric with a geometrical acceptance 93% of 4π. A superconductive solenoid magnet provides a 1.0 T magnetic field aligned with the beam axis for BESIII. The four main sub-detectors of BESIII is:

- **MDC** a drift chamber (MDC) with 43 layers, which is filled with helium-based gas. The average single wire resolution is 135 μm, and the momentum resolution in MDC is 0.5% for transverse momenta of 1 GeV/c;

- **TOF** a time-of-flight system (TOF) for particle identification composed of a barrel and two endcap. The barrel part is made of plastic scintillators in two layers, and the endcap part is made of multi-gap resistive plate chambers (MRPC) upgraded in 2015. The time resolution is 80 ps of the barrel, and 60 ps of the endcap, corresponding to a 2σ K/π separation for momenta up to about 1.0 GeV;

- **EMC** a electromagnetic calorimeter (EMC) for electron identification and photon detection. The EMC is totally consist of 6240 cells of CsI(Tl) crystal in the barrel section and endcap section. For 1.0 GeV photons, the energy resolution is 2.5% in the barrel and 5% in the endcap. and the position resolution is 6 mm in the barrel and 9 mm in the endcap;

- **MUC** a muon chamber system(MUC) made of 1000 m^2 of Resistive Plate Chamber (RPC) arranged in 9 layers in the barrel and 8 layers in the endcap. The position resolution of MUC is around 2 cm.

2 Data Set and Monte Carlo Samples

2.1 Data set

This analysis uses the sample of 10 billion J/ψ events collected with the BESIII detector in 2009, 2012, 2018 and 2019.

2.2 Software framework and monte carlo samples

These data samples are reconstructed using the BOSS (BESIII Offline Software System), which is developed based on Gaudi. This analysis is implemented in BOSS version 7.0.5.

Monte Carlo (MC) simulations of $e+e-$ annihilations are used to understand the backgrounds and also to estimate the detector efficiency of each channel. The response of the detector to the events is simulated with GEANT4 [19][20]. At BESIII, the simulation of the beam energy spread and the initial-state radiation (ISR) of the $e+e-$ collisions is considered with KKMC [21]. The subsequent decay of $\Lambda\bar{\Lambda}$ are produced with BesEvtGen [22][23]. We have used three types of MC events:

- **10 billion J/ψ inclusive MC sample**, which is provided by the BESIII offline group. The inclusive MC sample is used to investigate possible backgrounds, of which the branching fractions of the known physics processes are set to world average values according to PDG;
- **400,000 DIY signal MC**, which is used to evaluate the signal detection efficiency and extract the signal shape used for the fit. This is about 40 times the number of signal events in data.
- **4 million Phase Space (PHSP) signal MC**, which is used to to caluculate the normalization factor of the maximum likelihood fit of the decay parameter. This is about 400 times the number of signal events in data.
- **20 million DIY background MC**, which decay channel is $J/\psi \to \Xi^0\bar{\Xi}^0, \bar{\Xi}^0 \to \pi^0\bar{\Lambda}, \Xi^0 \to \pi^0\Lambda$. The sample is used to study the dominant background. This is about five times the number of background events in data.

3 ST analysis

In this section, the interested ST decay process $\bar{\Xi}^0 \to \pi^0\bar{\Lambda}$ is studied in the subsequent decay of process $J/\psi \to \Xi^0\bar{\Xi}^0$, where the $\bar{\Lambda}$ is reconstructed by $\bar{\Lambda} \to \pi^+\bar{p}$ and π^0 is reconstructed by $\pi^0 \to \gamma\gamma$. The ST analysis, including event selection, background study, ST signal extraction and efficiency study *etc* will be presented detailly.

To have a clear physical image, the basic distribution of kinematics of final state particles for the ST process $\bar{\Xi}^0 \to \pi^0\bar{\Lambda}$ are shown in Fig. 1, where $\bar{\Xi}^0$s are of momenta between 0.8 and 0.84 GeV/c, and $\bar{\Lambda}$s are of momenta between 0.5 and 0.9 GeV/c, π^0s are of momenta between 0.0 and 0.3 GeV/c. The openning angle between $\bar{\Lambda}$ and $\bar{\Xi}^0$ is relatively very small, which indicates the $\bar{\Lambda}$ inherits most of the momentum and emits almost in the same direction of its mother particle $\bar{\Xi}^0$. The momenta scales of anti-protons ($\bar{p}$) and pions (π^+) are of large difference, which can be used to distinguish $\bar{p}$ and π^+. The charge conjugate process, $\Xi^0 \to \pi^0\Lambda$ are of identical distributions.

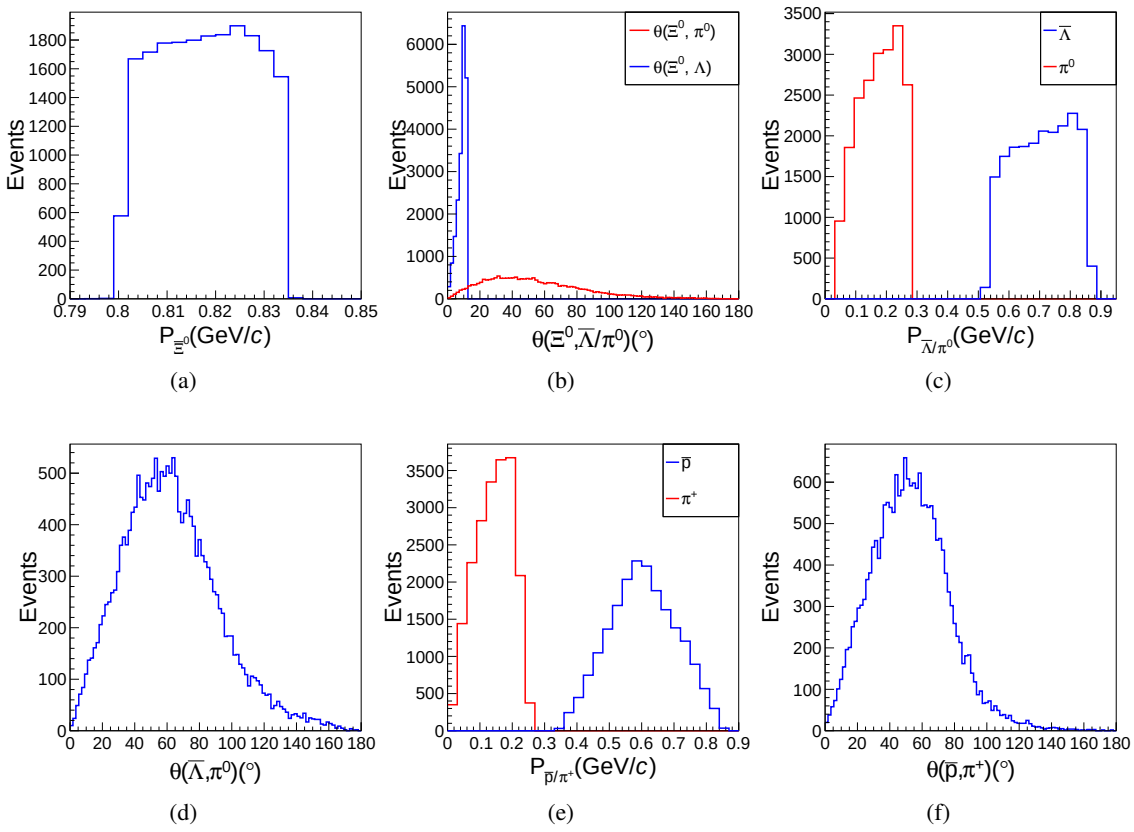

Figure 1: The kinematic distribution of ST final states from MC truth, (a) the momentum of $\bar{\Xi}^0$; (b) the openning angle between $\bar{\Lambda}$ and $\bar{\Xi}^0$; (c) the momentum of $\bar{\Lambda}$ and π^0, (d) the openning angle between $\bar{\Lambda}$ and π^0; (e)the momenta of anti-protons and pions; (f)the openning angle between anti-protons and pions;

3.1 Objects selection

- **Good charged tracks**

  Since Ξ^0 is long life particle ($c\tau$ = 8.71cm), there are no requiements on V_{xy} and V_z of the good charged particles, where V_{xy} and V_z are the closest distance of the charged tracks to interaction point (IP) in the plane perpendicular to and along the beam direction, respectively. The polar angle of the charged tracks is required within the acceptance of MDC, as:

  $\rightarrow |\cos\theta| < 0.93$

  where θ is the corresponding polar angle in the laboratory system.

- **Particle identification (PID)**

  According to Fig. 1, in the subsequent decay of $J/\psi \rightarrow \Xi^0\bar{\Xi}^0, \bar{\Xi}^0 \rightarrow \pi^0\bar{\Lambda}, \bar{\Lambda} \rightarrow \pi^+\bar{p}$, anti-protons and π^+ can be seperated through the momenta. Therefore, charged tracks with momenta larger than 0.3 GeV/c is assigned to be anti-protons, otherwise charged tracks with momenta smaller than 0.3 GeV/c is assigned to be pions. To further increasing the purity, dE/dx and TOF information are combined to form the PID confidence level for (anti-)protons, kaons, and pions. And we have requirement as:

  $\rightarrow prob(\bar{p}) > prob(\pi^+)\&\&prob(\bar{p}) > prob(K^+)$

  where, $prob(\bar{p}/\pi^+/K^+)$ are the probilities of charged tracks to be identified as anti-proton, π^+ and K^+, respectively.

- **Good EMC showers**

  The candidates of good EMC showers are required to have deposited energy beyond the threshold. A time window of TDC, t_{TDC}, is required to suppress the electronic noise and the cluster unrelated to events. The clusters are further required to be apart from the charged tracks to eliminate the showers originating from charged tracks.

  $\rightarrow E > 25$ MeV in barrel region ($|\cos\theta| < 0.8$) or $E > 50$ MeV in endcap region ($0.86 < |\cos\theta| < 0.92$), where θ is the polar angle of EMC showers.

  $\rightarrow 0 \leq t_{TDC} \leq 700$ ns.

  $\rightarrow \theta(\gamma, \text{track}) > 20^\circ$ for anti-proton, while $\theta(\gamma, \text{track}) > 10^\circ$ for other tracks, where $\theta(\gamma, \text{track})$ is the opening angle between an EMC shower and a charged track.

- **Reconstruction of π^0**

For a π^0candidate, at least two good EMC showers are needed. The π^0 candidates are reconstructed with two γs using one-constraint (1C) kinematic fit by enforcing the energy-momentum conservation under the hypothesis of $\pi^0 \to \gamma\gamma$, inwhich the invariant mass of the $\gamma\gamma$ is fixed to π^0 mass quoted from PDG. All possible combinations of $\gamma\gamma$ are looped in the 1C fit and reconstruct π^0 candidates. Candidates of π^0 are kept for further usage. In order to improve the purity of π^0s, invariant mass of the two γs, $M_{\gamma\gamma}$ is required as:

$\to$ 115 MeV $\leq M_{\gamma\gamma} \leq$ 150 MeV

the width of the mass window is corresponding to three times of $M_{\gamma\gamma}$ resolution.

3.2 ST candidate selection

The ST $\bar{\Xi}^0$ candidates are reconstructed through its dominant decay mode $\bar{\Xi}^0 \to \pi^0\bar{\Lambda}$ with $\bar{\Lambda} \to \pi^+\bar{p}$ and $\pi^0 \to \gamma\gamma$. Candidate events are required to have at least one $\bar{p}$ and π^+, and one π^0.

The ST $\bar{\Lambda}$ is reconstructed with one $\bar{p}$ and one π^+. A secondary vertex fit is carried out with the combinations of any $\bar{p}$s and π^+s. If there are more than one combinations of $\bar{p}$ and π^+ passing the fit, the one with the minimum $\chi^2_{\rm sec}$ is retained, where $\chi^2_{\rm sec}$ is the chi-square of the secondary vertex fit. According to the $\chi^2_{\rm sec}$ distributions of signal and backgrounds are shown in Fig 2, and the signal significance under different $\chi^2_{\rm sec}$ cut values are shown in Fig. 3, therefore we apply no requirement for the $\chi^2_{\rm sec}$. Due to the $\bar{\Xi}^0$ has relatively long lifetime in the laboratory frame ($c\tau$ = 8.71cm), the reconstructed $\bar{\Lambda}$ decay length (L) of signal process is expected longer than other combinatorial backgrounds, according to the decay length distributions in Fig. 4. To reject backgrounds, the decay length is required larger than 2.5, according to the signal significance distribution under different cut value, as shown in Fig 5. In order to improve the purity of $\bar{\Lambda}$ candidates, the distribution of the invariant mass of $\bar{p}$ and π^+ is required as $|M(\bar{p}\pi^+) - M^{PDG}_{\Lambda}| < 6$ MeV/c^2, as shown in Fig. 6. 6 MeV/c^2 corresponds to five times of resolution of the $M(\bar{p}\pi^+)$ distribution.

$\to N_{\bar{p}} \geq 1$, $N_{\pi^+} \geq 1$,

$\to L > 2.5$.

$\to |M(\bar{p}\pi^+) - M^{PDG}_{\Lambda}| < 6$ MeV/c^2

The ST $\bar{\Xi}^0$ is reconstructed by one $\bar{\Lambda}$ and one π^0. If there are more than one combinations of $\bar{\Lambda}$ and π^0, the one with minimum $|M(\pi^0\bar{\Lambda}) - M^{PDG}_{\Xi^0}|$ is retained. The $M(\pi^0\bar{\Lambda})$ is the invariant mass of π^0 and $\bar{\Lambda}$, and $M^{PDG}_{\Xi^0}$ is the nominal mass of Ξ^0 quoted from PDG. As shown in Fig. 7, a mass window requirement $|M(\pi^0\bar{\Lambda}) - M^{PDG}_{\Xi^0}| < 12$ MeV/c^2, which corresponds to the three times of resolution, is applied.

$\to |M(\pi^0\bar{\Lambda}) - M^{PDG}_{\Xi^0}| < 12$ MeV/c^2.

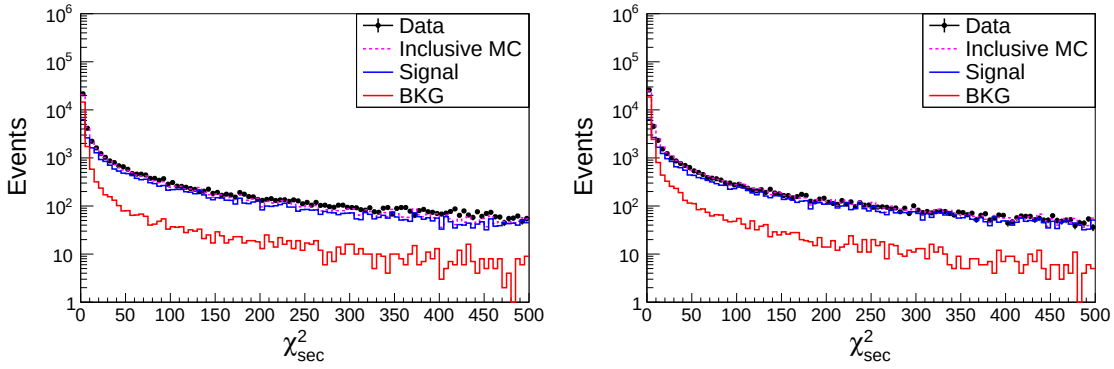

Figure 2: The distribution of chisqure of the vertex fit($\chi^2_{\rm sec}$) for (a) $\Lambda \to \pi^- p$ in ST $\Xi^0 \to \pi^0\Lambda$ process and (b) $\bar{\Lambda} \to \pi^+ \bar{p}$ in ST $\bar{\Xi}^0 \to \pi^0\bar{\Lambda}$ process. Dots with error bars indicate data and pink dashed lines show the inclusive MC. The blue solid and red solid lines represent the signal and backgrounds, respectively.

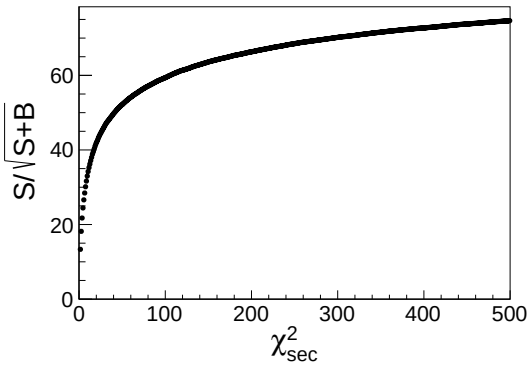

Figure 3: The optimization curve of $\chi^2_{\rm sec}$, where S and B stands for signal and background yields, respectively.

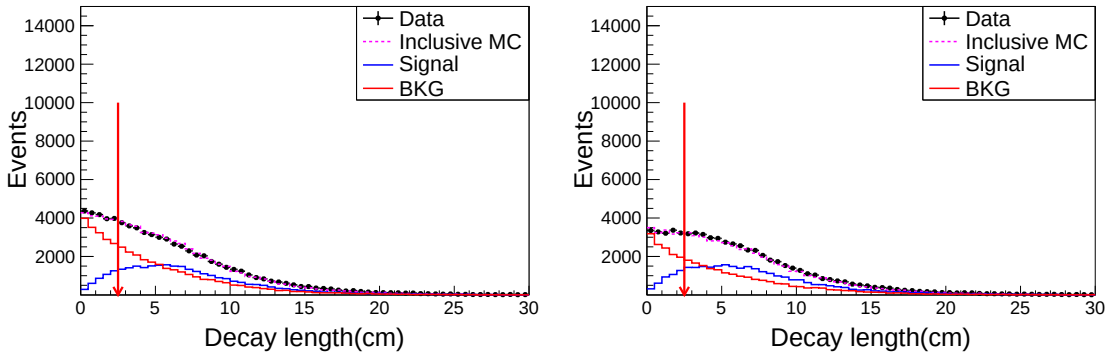

Figure 4: The distribution of decay length for (a) Λ in ST $\Xi^0 \to \pi^0\Lambda$ process and (b) $\bar{\Lambda}$ in ST $\bar{\Xi}^0 \to \pi^0\bar{\Lambda}$ process. Dots with error bars indicate data and pink dashed lines show the inclusive MC. The blue solid and red solid lines represent the signal and backgrounds, respectively.

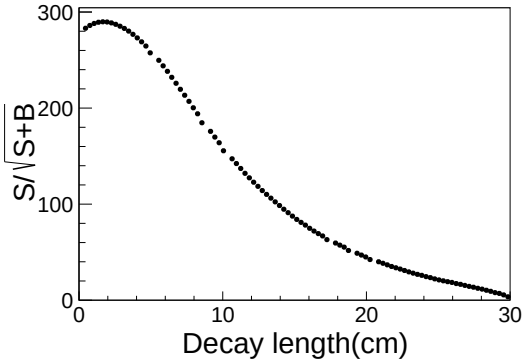

Figure 5: The optimization curve of decay length of Λ, where S and B stands for signal and background yields, respectively.

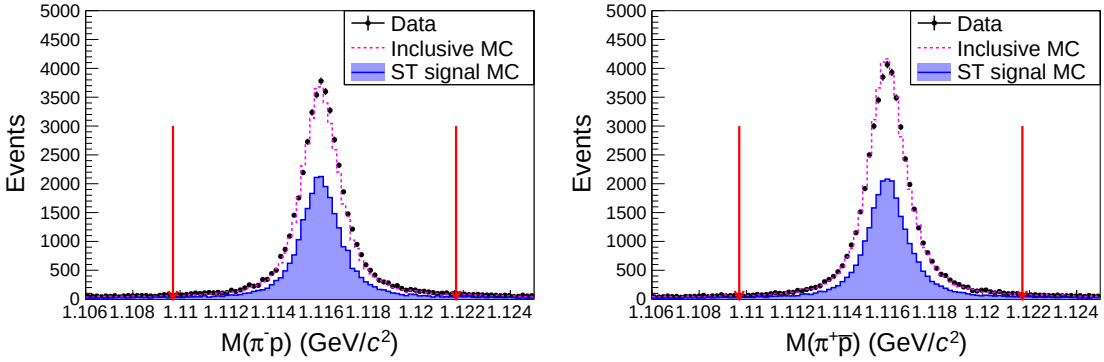

Figure 6: The distributions of (a) $M(\pi^- p)$ and (b) $M(\pi^+ \bar{p})$. The red arrows in the plot indicate the cut value.

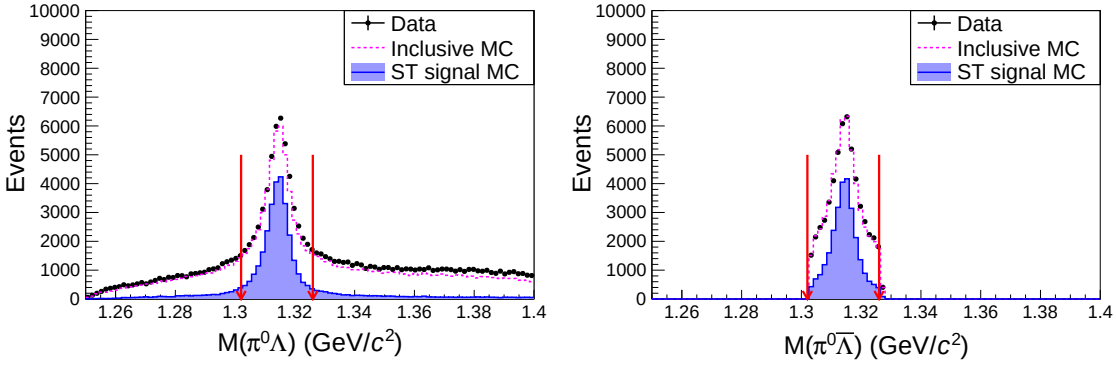

Figure 7: The distributions of (a) $M(\pi^0\Lambda)$ and (b) $M(\pi^0\bar{\Lambda})$. The red arrows in the plot indicate the cut value.

3.3 ST background studies

10 billion J/ψ inclusive MC sample provided by the offline software group is used to study the potential backgrounds. To identify the events $J/\psi \to \Xi^0\bar{\Xi}^0$ and reduce the background contributions from $J/\psi \to \bar{\Xi}^0 + anything$, which are not due to $J/\psi \to \Xi^0\bar{\Xi}^0$, a recoil mass, $M^{recoil}_{\bar{\Xi}^0} = \sqrt{(E_{\rm c.m.} - E_{\bar{\Xi}^0})^2 - P^2_{\bar{\Xi}^0}}$ is defined. This mass is required to be within $1.2 < M^{recoil}_{\bar{\Xi}^0} < 1.45$ GeV/c^2, where $E_{\rm c.m.}$ is the center-of-mass (c.m.) energy, $E_{\bar{\Xi}^0}$ and $P_{\bar{\Xi}^0}$ are the energy and momentum of ST $\bar{\Xi}^0$ cadidate.

After applying all the criteria, topology of survived events from inclusive MC shows the potential background processes, as summaried in Table 5. To reject these contributions from the non-$J/\psi \to \Xi^0\bar{\Xi}^0$ processes, the yield of ST events will be extracted from the recoil mass of tagged $\bar{\Xi}^0$ ($M^{recoil}_{\bar{\Xi}^0}$), which is shown in Fig. 8. The signal region is defined as $1.2 < M^{recoil}_{\bar{\Xi}^0} < 1.45$ GeV/c^2. Within this signal region, the total estimated backgrond after normalizing to the total J/ψ event number is 1146508 and 14494726 for tagging Ξ^0 and $\bar{\Xi^0}$, respectively, corresponding to 53.64% and 61.47% for the suvived events, individually.

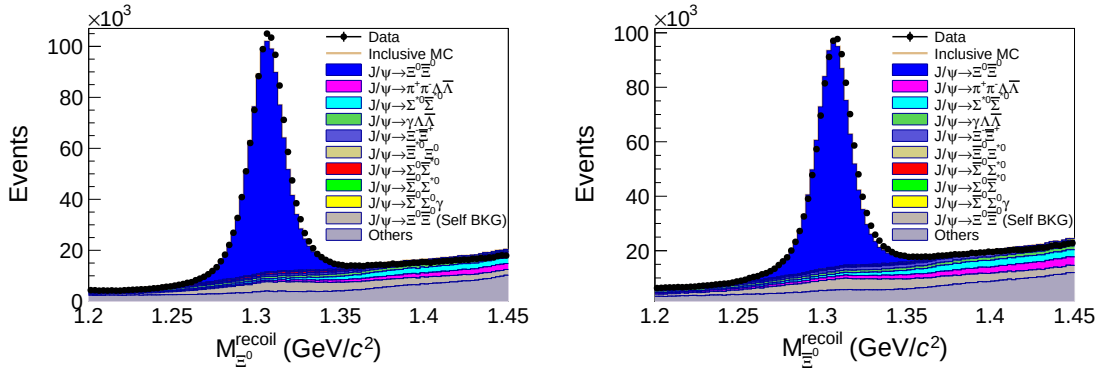

Figure 8: The recoil mass distribution of tagging $\bar{\Xi}^0$ within the signal region, defined as $1.2 < M^{recoil}_{\bar{\Xi}^0} < 1.45$ GeV/c^2. (a)ST $\Xi^0 \to \pi^0\Lambda$ process and (b) ST $\bar{\Xi}^0 \to \pi^0\bar{\Lambda}$ process.

Besides the already known background processes, unknow processes are also a concern for the background estimation. In order to study these potential processes, we studied the $M^{recoil}_{\bar{\Xi}^0}$ distribution of events in the sideband region of tagging $M(\pi^0\Lambda)$ spectrum, defined as $0.03\ {\rm GeV}/c^2 < |M(\pi^0\Lambda) - M^{PDG}_{\Xi^0}| < 0.042\ {\rm GeV}/c^2$. The corresponding distributions of these events are shown in Fig. 9, where no peaking background is observed.

3.4 ST efficiency

Signal MC samples, including a sample of 3.9×10^6 $J/\psi \to \Xi^0\bar{\Xi}^0, \Xi^0 \to \pi^0\Lambda, \bar{\Xi}^0 \to \pi^0\bar{\Lambda}$ are generated to estimate the ST signal efficiencies, as shown in Table 6.

Table 5: Main background processes after single tag event selection.

	Percentage(%)	
Process	ST $\Xi^0 \to \pi^0\Lambda$	ST $\bar{\Xi}^0 \to \pi^0\bar{\Lambda}$
$J/\psi \to \pi^+\pi^-\Lambda\bar{\Lambda}$	4.39	6.09
$J/\psi \to \Sigma^{*0}\bar{\Sigma}^{*0}$	5.32	5.81
$J/\psi \to \gamma\Lambda\bar{\Lambda}$	4.35	4.04
$J/\psi \to \Xi^-\bar{\Xi}^+$	2.45	3.81
$J/\psi \to \Xi^{*0}\bar{\Xi}^0$	0.20	0.66
$J/\psi \to \bar{\Sigma}^0\Sigma^{*0}$	2.00	0.73
$J/\psi \to \Sigma^0\bar{\Sigma}^{*0}$	1.15	0.65
$J/\psi \to \bar{\Sigma}^0\Sigma^0\gamma$	1.20	1.30
Self BKG	11.25	11.84
Others	21.35	26.53
Total	53.64	61.47

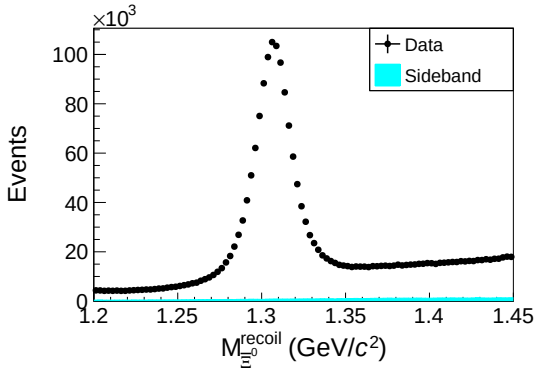

Figure 9: The recoil mass distribution of tagging $\bar{\Xi}^0$ of the sideband events which is in cyan-filled histogrms.

Table 6: The ST signal MC efficiencies of each step of event selection.

Efficiencies	ST $\Xi^0 \to \pi^0\Lambda$	ST $\bar{\Xi}^0 \to \pi^0\bar{\Lambda}$
Truth	100.0%	100.0%
Charge Tracks ($N_{trk} \geq 2$)	95.24%	95.24%
PID	59.62%	58.78%
Vertex fit	46.19%	45.50%
$L > 2.0$	37.17%	36.74%
$\lvert M(\bar{p}\pi^+) - M_{\Lambda}^{PDG}\rvert < 6$ MeV/c^2	31.91%	31.60%
Shower ($N_{\gamma} \geq 2$)	31.55%	31.26%
$N_{\pi^0} \geq 1$	27.59%	27.37%
$\lvert M(\pi^0\bar{\Lambda}) - M_{\Xi^0}^{PDG}\rvert < 12$ MeV/c^2(truth match)	13.17%	11.91%
$1.2 < M_{\bar{\Xi}^0}^{recoil} < 1.45$ GeV/c^2	13.15%	11.89%

3.5 ST yields extraction

The yield of ST (N_{ST}) is extracted by performing a binning extended maximum likelihood fit on the $M_{\bar{\Xi}^0}^{recoil}$ distributions between 1.2 and 1.45 GeV/c^2, as shown in Fig. 10. In the fit, the signal is modeled by the MC-simulated shape extracted from the signal MC, which is convoluted with a Guassian function to represent the resolution difference between data and MC simulation. The background is described by a 1^{st} order polynomial function. The signal yield from the fit as well as the detector efficiency estimated from the signal MC sample $J/\psi \to \Xi^0\bar{\Xi}^0, \Xi^0 \to \pi^0\Lambda, \bar{\Xi}^0 \to \pi^0\bar{\Lambda}$ are summarized in Table 7. It is worth noting that the signal yields exist 2.0% difference between two charge conjugated modes after the detection efficiency correction. Detail studies indicate that this difference is due to the MC efficiency which is corrected.(Details in Appendix D). Since the DT method is used in BF measurement, thus this effect do not affect the results, but improved the purity of ST sample.

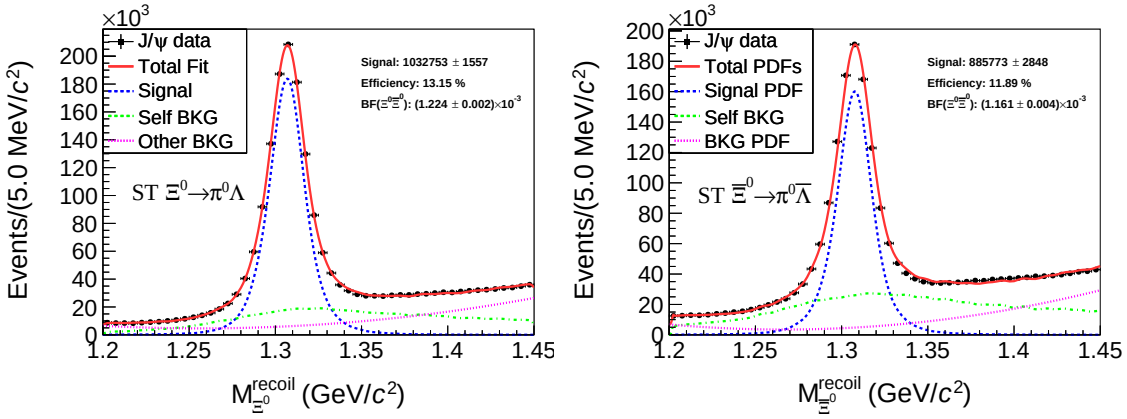

Figure 10: The fit on the distributions of (a) $M_{\bar{\Xi}^0}^{recoil}$ and (b) $M_{\Xi^0}^{recoil}$.

Table 7: The ST yields of charged conjugated processes.

Modes	$J/\psi \to \Sigma^+\bar{\Sigma}^-$,$\Sigma^+ \to \pi^0 p$, $\bar{\Sigma}^- \to$ *anything*	$J/\psi \to \Sigma^+\bar{\Sigma}^-$, $\bar{\Sigma}^- \to \pi^0\bar{p}$, $\Sigma^+ \to$ *anything*
Yield	319859 ± 703	276468 ± 642
Default efficiency	39.72%	35.02%

4 DT analysis

The interested decay process $\Xi^0 \to \gamma\Lambda$ is studied in the subsequent decay of process $J/\psi \to \Xi^0\bar{\Xi}^0$ by a DT approach. In this section, the DT analysis, including event selection, background study, DT signal extraction and efficiency study *etc* will be introduced detailly.

Before we start the analysis of the DT process, the distributions of kinematics of the final state particles in the DT $\Xi^0 \to \gamma\Lambda$ process are checked in Fig. 11. We can get information: the DT Ξ^0s are of momenta between 0.8 and 0.84 GeV/c, and Λs are of momenta between 0.5 and 0.9 GeV/c, γs are of momenta between 0.1 and 0.35 GeV/c. The openning angle between Λ and Ξ^0 is relatively very small, which indicates the Λ inherits most of the momentum and emits almost in the same direction of its mother particle Ξ^0. The momenta scales of protons (p) and pions (π^-) are of large difference, which can be used to distinguish the them. The charge conjugate process, $\bar{\Xi}^0 \to \gamma\bar{\Lambda}$ are of identical distributions.

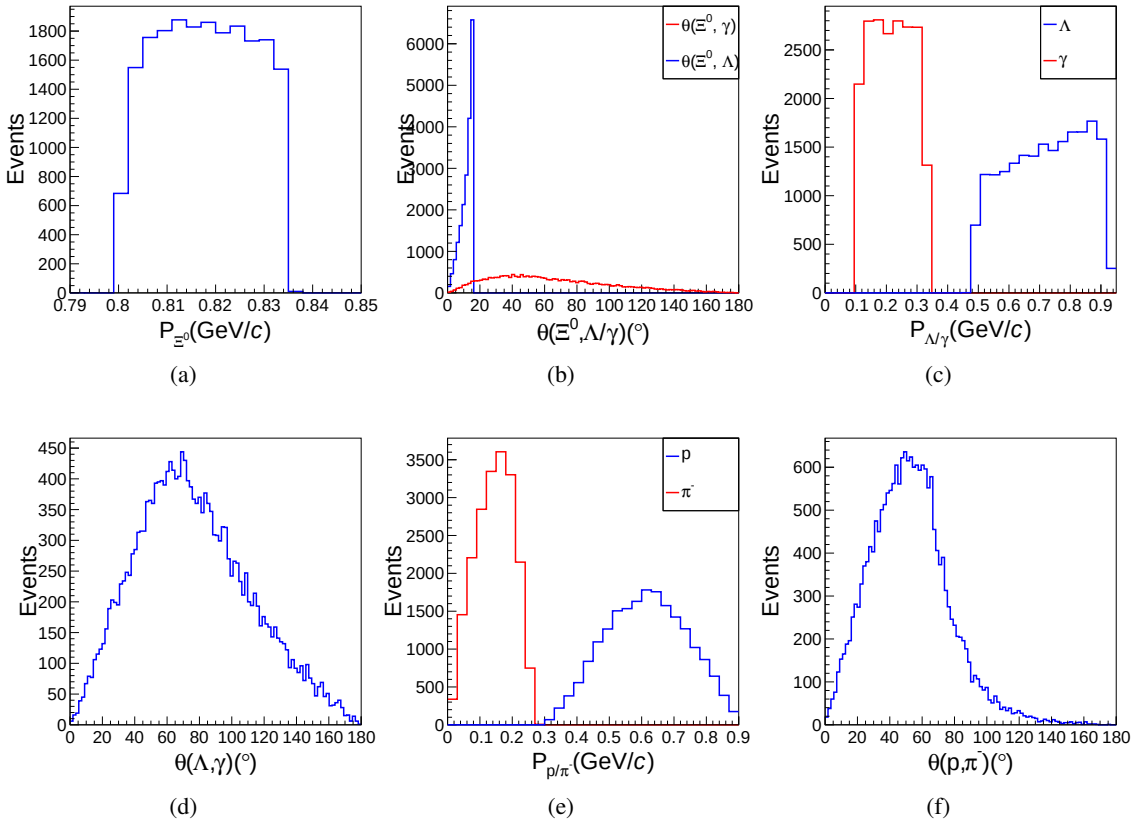

Figure 11: The kinematic distribution of DT final states from MC truth, (a) the momentum of $\Xi^0(\gamma)$; (b) the openning angle between Λ and Ξ^0; (c) the momentum of Λ and γ, (d) the openning angle between Λ and γ; (e)the momenta of protons and pions; (f)the openning angle between protons and pions;

4.1 Objects selection

Since the charged tracks and neutral showers are already selected in the ST event selection, here we have no more introductions on the objects selection.

4.2 DT candidate selection

- **Good charged tracks**

  Since the final state of interested signal $\Xi^0 \to \gamma\Lambda$ includes one photon, one proton, and one π^- in the final states, so we require:

  $\to N_p \geq 1$, $N_{\pi^-} \geq 1$,

  where the N_p and N_{π^-} are the track numbers for proton and π^-. Good charged tracks are of same defination as those in sec. 3.1

- **Good shower number**

  As mentioned above, in the process $\Xi^0 \to \gamma\Lambda$, the candidate events are required at least one good shower for DT, and there already exist two good showers from π^0 decay in ST process, thus at least three good showers are required:

  $\to N_{shower} \geq 3$.

- Λ **reconstruction**

  With the same method as ST $\bar{\Lambda}$ reconstruction, the DT Λ is reconstructed with one proton (p) and one π^-. A secondary vertex fit is carried out with the combinations of any ps and π^-s. If there are more than one combinations of p and π^- passing the fit, the one with the minimum $\chi^2_{\rm sec}$ is retained, where $\chi^2_{\rm sec}$ is the chi-square of the secondary vertex fit. In order to improve the purity of Λ candidates, the distribution of the invariant mass of p and π^- is required as $|M(p\pi^-) - M^{PDG}_{\Lambda}| < 6$ MeV/c^2, as shown in Fig. 12. 6 MeV/c^2 corresponds to five times of resolution of the $M(p\pi^-)$ distribution.

  $\to |M(\bar{p}\pi^+) - M^{PDG}_{\Lambda}| < 6$ MeV/c^2

  It is worth noting that there are no requirement for the $\chi^2_{\rm sec}$ and decay length of the DT Λ, because we will use another more strict criteria to suppress the backgrounds with short-life hyperons, such as $J/\psi \to \Sigma^{*0}\bar{\Sigma}^{*0}$.

- **Kinematic fit**

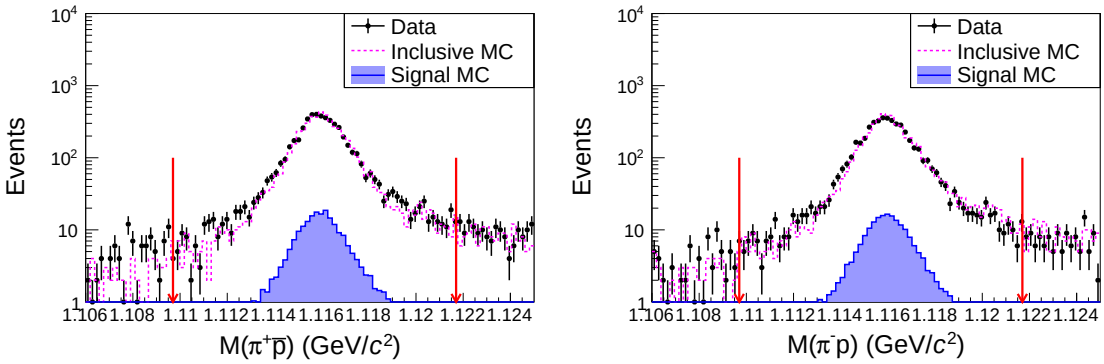

Figure 12: The distributions of (a)$M(\pi^+\bar{p})$ and (b)$M(\pi^-p)$ in process DT $\Xi^0 \to \gamma\Lambda$ and $\bar{\Xi}^0 \to \gamma\bar{\Lambda}$, respectively. The red arrows in the plot indicate the cut value.

A five-constraint (5C) kinematic fit by enforcing the energy-momentum conservation with the hypothesis of $J/\psi \to \bar{\Lambda}\gamma_1\gamma_2\Lambda\gamma$ is performed. Here the kinamatic variables of $\bar{\Lambda}$ as well as their uncertainties are from the second vertex fitof ST side. The invariant mass of γ_1 and γ_2 which are from the π^0 in the ST side, are constrained to the nominal mass of π^0. For the events with more than three good showers, all the photons (except γ_1 and γ_2) are looped in the 5C-fit and the one with the smallest $\chi^2_{3\gamma}(\Xi^0 \to \gamma\Lambda)$ is kept. The distributions of $\chi^2_{3\gamma}(\Xi^0 \to \gamma\Lambda)$ is shown in Fig. 13 (a-b) for the signal and background samples from inclusive MC. A requirement $\chi^2_{3\gamma} < 15$, which is considering both the signal efficiency and significance, is further implemented.

Detail background studies (as shown following) indicate that the dominate background is from $\Xi^0 \to \pi^0\Lambda$. To suppress this background, we performed the similar 5C kinematic fit for the hypothesis of $J/\psi \to \bar{\Lambda}\gamma_1\gamma_2\Lambda\gamma\gamma$. For the events with more than four good showers, all the photons (except γ_1 and γ_2) are looped in the 5C-fit and the one with the smallest chisqure ($\chi^2_{4\gamma}$) is kept. Finally we require

$\to \chi^2_{4\gamma} > \chi^2_{3\gamma}$

Figure 14 shows the the energy distribution of photon in the Ξ^0 rest frame E^{cms}_{γ}, which is the variable to extract the yields of signal, after each step of event selection.

- **Further suppresion of Σ-related background**

After above selection criteria, the energy distributions of photon candidates in the Ξ^0 rest frame (E^{cms}_{γ}) are shown in Fig. 14(e)(f), in which the backgrounds are dominanted from the processes like $J/\psi \to \bar{\Sigma}^0(\to \bar{\Lambda}\gamma)\Sigma^{*0}(\to \Lambda\pi^0)$, which are involving $\Lambda(\bar{\Lambda})$ from the $\bar{\Sigma}^0(\Sigma^{*0})$ decays. Due to the extremely short life time of Σ^0 or Σ^{*0}, the crossing point of the $\bar{\Lambda}$ and Λ tracks is expected very close to the initial point (IP). We performed a vertex fit with the Λ and $\bar{\Lambda}$ and reconstruct the decay

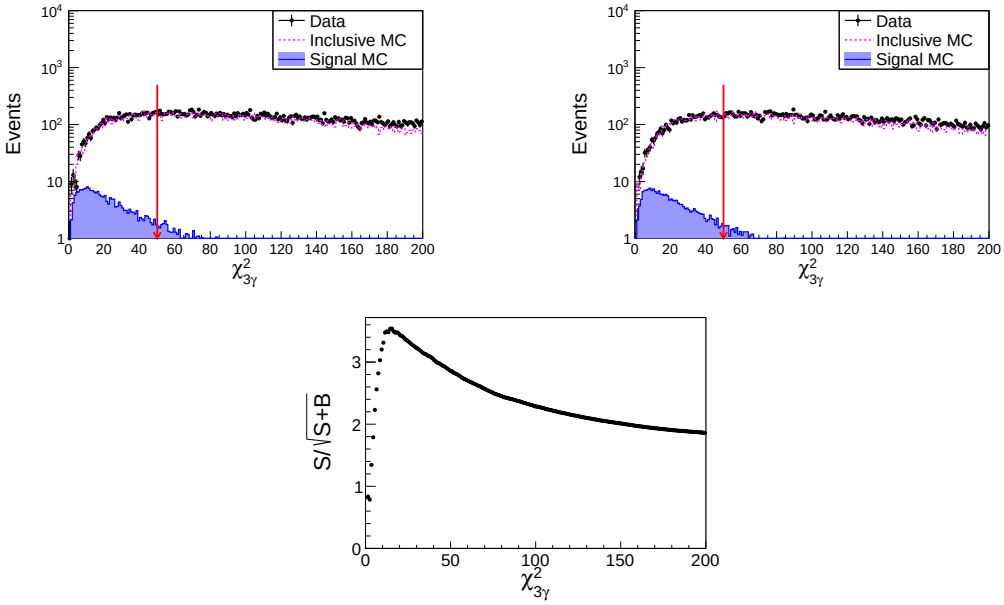

Figure 13: (a) The distribution of the 5C-fit $\chi^2_{3\gamma}(\Xi^0 \to \gamma\Lambda)$ and (b) $\chi^2_{3\gamma}(\bar{\Xi}^0 \to \gamma\bar{\Lambda})$ and (c)optimazation curve, where the S stands for Signal events number and B stands for Background events number

length ($L^{\Lambda\bar{\Lambda}}$), which refers to the closest distance between the crossing point of the $\bar{\Lambda}$ and Λ tracks to the IP. The $L^{\Lambda\bar{\Lambda}}/\sigma_{L^{\Lambda\bar{\Lambda}}}$ is used as a selection criteria to improve the signal efficiency, as shown in Fig. 15 (a). According to the optimized curve in Fig. 15 (b), events passing the vertex fit and $L^{\Lambda\bar{\Lambda}}/\sigma_{L^{\Lambda\bar{\Lambda}}} < 2.5$ is rejected.

$\to$ reject events passing the vertex fit and $L^{\Lambda\bar{\Lambda}}/\sigma_{L^{\Lambda\bar{\Lambda}}} < 2.5$

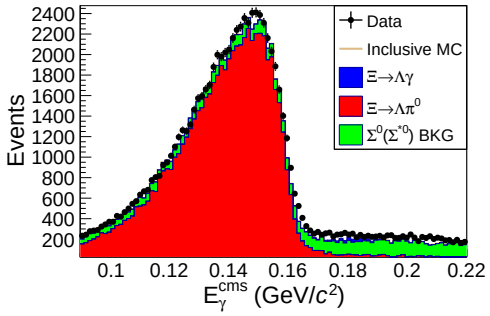

(a) After kinematic fit

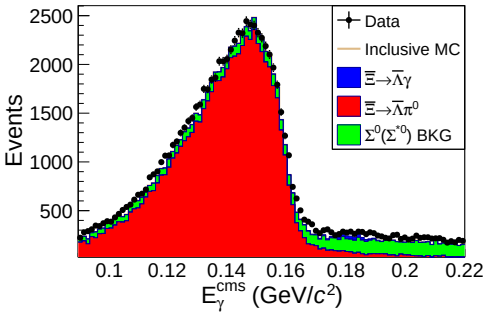

(b) After kinematic fit

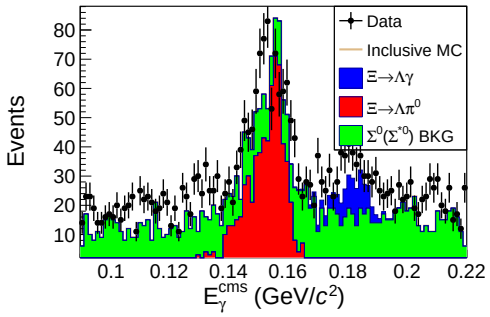

(c) After applying $\chi^2_{3\gamma} < 15$

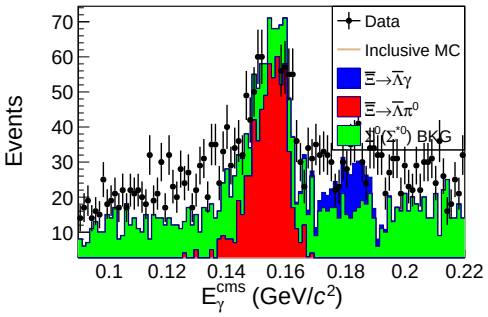

(d) After applying $\chi^2_{3\gamma} < 15$

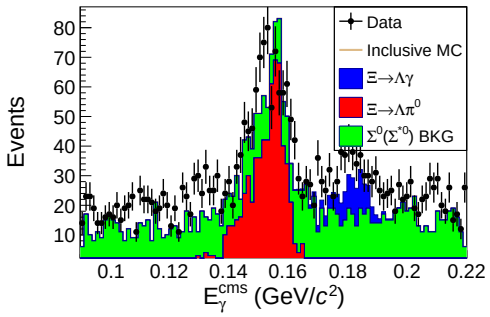

(e) After applying $\chi^2_{4\gamma} > \chi^2_{3\gamma}$

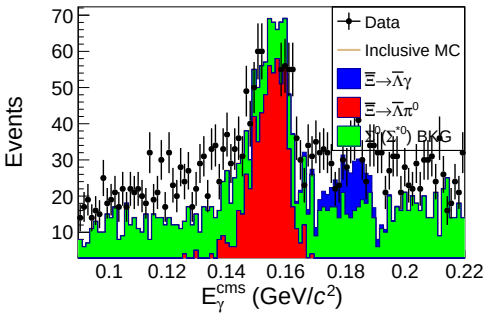

(f) After applying $\chi^2_{4\gamma} > \chi^2_{3\gamma}$

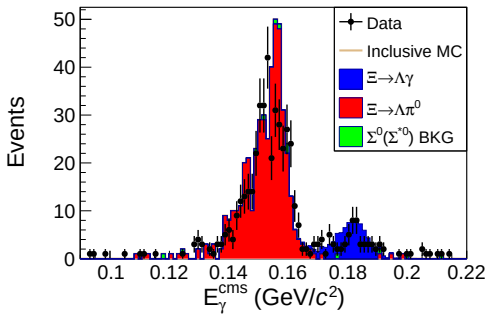

(g) After applying $\chi^2_{4\gamma} > \chi^2_{3\gamma}$

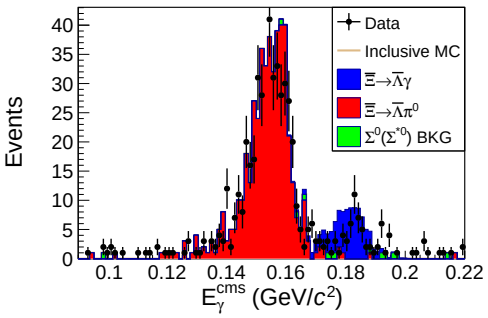

(h) After applying $|M(\gamma\gamma) - M_{\pi^0}| > 20$ MeV/c^2

Figure 14: The energy distributions of photon candidates in the $\Lambda(\bar{\Lambda})$ rest frame (E_γ) after every step of event selection about the kinematic fit.

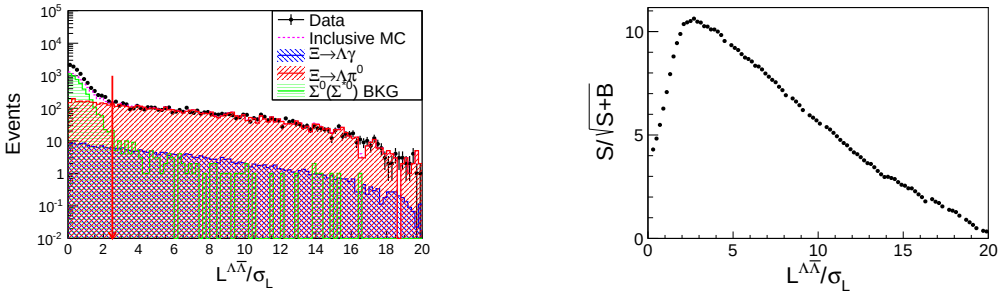

Figure 15: (a) The distribution of the $L^{\Lambda\bar{\Lambda}}$ and (b)optimazation curve, where the S stands for Signal events number and B stands for Background events number

- **Event selection efficiency**

After above selection criteria, the signal efficnecies are summaried in Table 8. The final efficiency is 0.84% for $\Xi^0 \to \gamma\Lambda$ and 0.92% for $\bar{\Xi}^0 \to \gamma\bar{\Lambda}$.

Table 8: The DT signal MC efficiencies of each step of event selection.

Efficiencies	$\Xi^0 \to \gamma\Lambda$	$\bar{\Xi}^0 \to \gamma\bar{\Lambda}$
Truth	100.0%	100.0%
Single tag	39.6%	45.2%
Kinematic fit($\chi^2_{3\gamma}$ <100)	31.6%	34.6%
$\chi^2_{4\gamma} > \chi^2_{3\gamma}$	31.0%	33.9%
L/σ_L	21.8%	23.8%
$\chi^2_{3\gamma}$ <30	19.1%	20.9%
Truth match	19.0%	20.9%

4.3 DT background studies

We use 10 billion inclusive J/ψ MC sample to study the potential backgrounds after applying all above selection criteria, and the distributions of E_{γ}^{cms} for the $\Xi^0 \to \gamma\Lambda$ and $\bar{\Xi}^0 \to \gamma\bar{\Lambda}$ are shown in Fig. 16, respectively, where the signals of $\Xi^0 \to \gamma\Lambda$ and $\bar{\Xi}^0 \to \gamma\bar{\Lambda}$ are observed clearly, but with large background from $\Xi^0 \to \pi^0\Lambda$ and $\bar{\Xi}^0 \to \pi^0\bar{\Lambda}$. The 10 billion inclusive J/ψ MC sample is performed with the same approaches, and the survived events are summaried in Table 9.

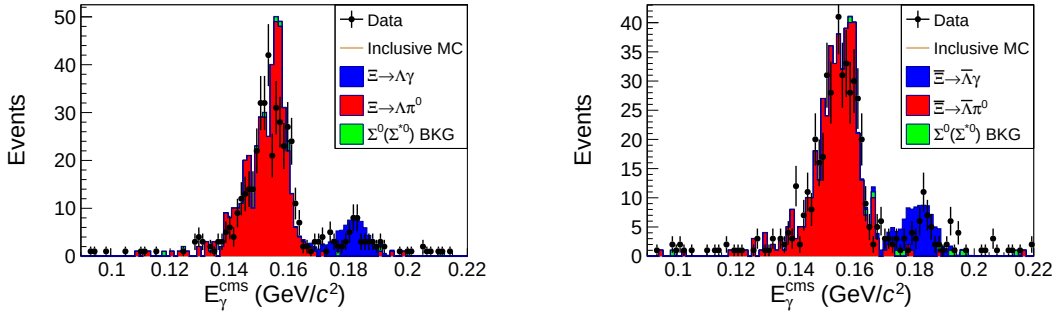

Figure 16: The distributions of γ energy in the $\Xi^0(\bar{\Xi}^0)$ rest frame after applying all the above selection. The dot with error bars are data, with histogrms with colors for different processes in inclusive mc.

Table 9: The yields of signal and backgrounds after the kinematic fit from inclusive MC sample.

Source	$\Xi^0 \to \gamma\Lambda$ channel	$\bar{\Xi}^0 \to \gamma\bar{\Lambda}$ channel
$\Xi^0 \to \gamma\Lambda$	91	79
$\Xi^0 \to \pi^0\Lambda$	478	447
Others	13	12

4.4 DT yields extraction

The double tag yield $N_{double-tag}$ is extracted by fitting the distribution of photon candidate energy in the $\Lambda(\bar{\Lambda})$ rest frame. As shown in Fig. 17, a 1-D unbinned extended maximum likelihood fit is performed on the distribution of the accepted events. The fitting range is from 0.08 GeV to 0.24 GeV. The PDFs are modeled by the shapes extracted from signal MC and background MC. Considering the resolution difference between data and MC, MC-simulated shapes of signal and BKG A are convoluted with a Gaussian function with same parameters.

Shape of BKG A is extracted from exclusive MC which photon candidates are matched with with the truth direction ($< 10°$). The BKG B is related to noise showers generated by reaction of $n(\bar{n})$ with matter, the MC cannot simulate these complex processes. The PDF for BKG B is described with a gaussian function which parameters are extracted from a data control sample of the BKG B (The details are introduced in Appendix B). The yields of the signal and background are set floated in the fit.

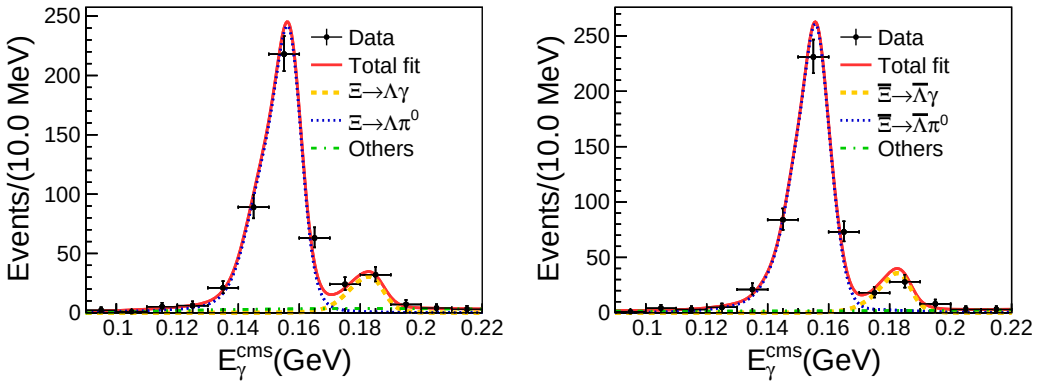

Figure 17: Fit of the energy distribution of photon candidates in the $\Xi^0(\bar{\Xi}^0)$ rest frame. The left plot is the fit for $\Xi^0 \to \gamma\Lambda$ process, right plot is the fit for $\bar{\Xi}^0 \to \gamma\bar{\Lambda}$ process.

Individual fits with accepted events for two charge conjugte processes are performed firstly. In fact, we assume the charge conjugate processes share a same branching fraction, a simultaneous fit with all accepted events is performed. The yields of individual and simultaneous fit are shown in Table 10.

Table 10: The DT yields obtained by individual and simultaneous fit.

Process	$\Xi^0 \to \gamma\Lambda$		$\bar{\Xi}^0 \to \gamma\bar{\Lambda}$	
Yields	Individual fit	Simultaneous fit	Individual fit	Simultaneous fit
Signal	52±9	45±6	42±9	51±7
$\Xi^0 \to \pi^0\Lambda$	393±22	392±22	409±23	412±23
Others	30±14	34±14	31± 17	23±15

4.5 Result of branching fraction

The BF of $\Xi^0 \to \gamma\Lambda$ is calculated with the yields determined by the individual fit and simultaneous fit, as shown in Table 11. The statistical uncertainties are indicated after the BF results by absolute values.

Table 11: Branching fraction results of $\Xi^0 \to \gamma\Lambda$ based on individual and simultaneous fit.

Modes	BF
$\Xi^0 \to \gamma\Lambda$	$(1.23 \pm 0.21_{stat.}) \times 10^{-3}$
$\bar{\Xi}^0 \to \gamma\bar{\Lambda}$	$(0.88 \pm 0.19_{stat.}) \times 10^{-3}$
Simultaneous fit	$(1.06 \pm 0.14_{stat.}) \times 10^{-3}$

5 Determination of Decay Parameter

5.1 Joint angular distribution

The total cjoint angular distribution amplitude for $e^+e^- \to J/\psi \to \Xi^0\bar{\Xi}^0$ is shown in Appendix A. And experimentally β and γ are reconstructed by an observable $\phi(\beta = (1-\alpha)^{1/2} sin\phi)$. So the final expression is a formula with 8 decay parameters space η $(\alpha_{J/\psi}, \Delta\Phi, \alpha_{\Xi^0}, \alpha_{\bar{\Xi}^0}, \phi_{\Xi^0}, \phi_{\bar{\Xi}^0}, \alpha_\Lambda, \alpha_{\bar{\Lambda}})$ and 9 kinematic variables space ξ $(\theta_{\Xi^0}, \theta_\Lambda, \phi_\Lambda, \theta_{\bar{\Lambda}}, \phi_{\bar{\Lambda}}, \theta_P, \phi_P, \theta_{\bar{P}}, \phi_{\bar{P}})$.

Where the kinematic variables are defined in the reference frame shown in Fig. 18. The θ_{Ξ^0} is the angle between momenta of positron and Ξ^0 in the e^+e^- C.M. frame and the polar angle $\theta_\Lambda(\theta_{\bar{\Lambda}}))$ and azimuth angle $\phi_\Lambda(\phi_{\bar{\Lambda}})$ of $\Lambda(\bar{\Lambda})$ are defined in it's mother particle $\Xi^0(\bar{\Xi}^0)$ rest frame and the corresponding coordinate system is rotated from e^+e^- C.M. frame to make the momentum direction of $\Xi^0(\bar{\Xi}^0)$ pointing along Z axis and Y axis is perpendicular to the decay plane which is defined by the e^+ momentum direction and Ξ^0 momentum direction. The polar angle $\theta_P(\theta_{\bar{P}}))$ and azimuth angle $\phi_P(\phi_{\bar{P}})$ of proton and anti-proton are defined in it's mother particle $\Lambda(\bar{\Lambda})$ rest frame.

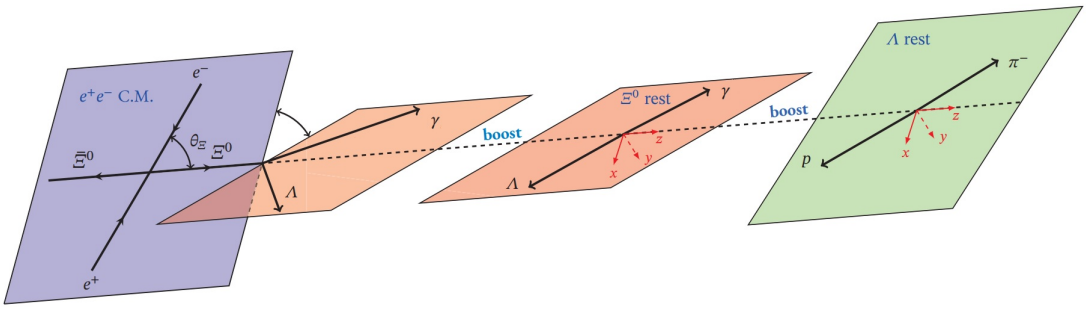

Figure 18: Definition of the helicity frame and coordinate system for $e^+e^- \to J/\psi \to \Xi^0\bar{\Xi}^0$.

5.2 Maximum likelihood fit

The maximum likelihood fit is a common procedure used for parameter estimation in analysis of experimental data, which is adopted to estimate the decay asymmetry parameter. The probability density function (PDF) for a single event is defined by:

$$p.d.f(\xi,\eta) = \frac{\omega(\xi,\eta)\epsilon(\xi)}{\int d\xi \omega(\xi)\epsilon(\xi)} \tag{7}$$

In this formula, $\omega(\xi,\eta)$ is the joint angular distribution amplitude, and the $\epsilon(\xi)$ is the detection efficiency. ξ is the kinematic variables $(\theta_{\Xi^0}, \theta_\Lambda, \phi_\Lambda, \theta_{\bar{\Lambda}}, \phi_{\bar{\Lambda}}, \theta_P, \phi_P, \theta_{\bar{P}}, \phi_{\bar{P}})$, and η is the decay parameters space η $(\alpha_{J/\psi}, \Delta\Phi, \alpha_{\Xi^0}, \alpha_{\bar{\Xi}^0}, \phi_{\Xi^0}, \phi_{\bar{\Xi}^0}, \alpha_\Lambda, \alpha_{\bar{\Lambda}})$. The integral term $\int d\xi \omega(\xi)\epsilon(\xi)$ is the normalization factor.

Considering the naive case, there are N independent signal events without backgrounds, the likelihood function is defined as:

$$\begin{aligned}\mathcal{L} &= p.d.f(\xi_1, \xi_2 ... \xi_N; \eta) \\ &= \prod_{i=1}^{i=N} p.d.f(\xi_i, \eta) \\ &= \prod_{i=1}^{i=N} \frac{\omega(\xi, \eta)\epsilon(\xi)}{\int d\xi \omega(\xi)\epsilon(\xi)}\end{aligned} \tag{8}$$

Take the -log value:

$$-\ln\mathcal{L} = -\sum_{i=1}^{i=N} \ln(\frac{\omega(\xi, \eta)}{\int d\xi \omega(\xi)\epsilon(\xi)}) - \sum_{i=1}^{i=N} \ln(\epsilon(\xi)) \tag{9}$$

The second term $-\sum_{i=1}^{i=N} \ln(\epsilon(\xi))$ is a constant number only depending on the acceptance. Supposing the normalization factor $\int d\xi \omega(\xi)\epsilon(\xi)$ is $\mathcal{S}$, the result is simplified as:

$$\begin{aligned}-\ln\mathcal{L} &= -\sum_{i=1}^{i=N} \ln\frac{\omega(\xi, \eta)}{\mathcal{S}} \\ &= -\sum_{i=1}^{i=N} \ln\omega(\xi, \eta) + N\ln\mathcal{S}\end{aligned} \tag{10}$$

The $\mathcal{S}$ can be obtained using PHSP MC integration. Suppose we have generated the signal MC sample in PHSP and reconstruct it, truth event number of this PHSP sample is N_{truth} and reconstructed event number is N_{rec}.The nomalization factor $\mathcal{S}$ can be obtained using PHSP MC which is at least 10 times of accepted data to improve the measurement accuracy:

$$\begin{aligned}\mathcal{S} &= \int d\xi \omega(\xi)\epsilon(\xi) \\ &= \frac{1}{N_{truth}} \int dN_{truth} \cdot \omega(\xi) \cdot \epsilon(\xi) \\ &= \frac{1}{N_{truth}} \int dN_{rec} \cdot \omega(\xi,) \\ &= \frac{1}{N_{truth}} \sum_{k=1}^{N_{rec}} \omega(\xi)\end{aligned} \tag{11}$$

In fact, the survived events are not pure and containing backgrounds, including: $\Xi^0 \to \pi^0\Lambda$ (BKG A) and other combinatorial backgrounds (BKG X). The contributions of BKG A and BKG X ($\ln\mathcal{L}_{BKGA}$, $\ln\mathcal{L}_{BKGX}$) are substracted, only the signal process is left: $-\ln\mathcal{L}_{SIG}$, as the equation below:

$$
\begin{aligned}
-\ln\mathcal{L}_{SIG} &= -\ln\mathcal{L}_{DATA} + \ln\mathcal{L}_{BKGA} + \ln\mathcal{L}_{BKGX} \\
&= -\sum_{i=1}^{N_{DATA}} \ln\omega(\xi_i,\eta) + \sum_{j=1}^{N_{BKGA}} \ln\omega(\xi_j,\eta) + \sum_{l=1}^{N_{BKGX}} \ln\omega(\xi_l,\eta) \\
&\quad + (N_{DATA} - N_{BKGA} - N_{BKGX})\ln\mathcal{S}
\end{aligned}
\tag{12}
$$

5.3 Fit and result

The likelihood function of signal events for $\Xi^0 \to \gamma\Lambda$ and $\bar{\Xi}^0 \to \gamma\bar{\Lambda}$ is defined as $-ln\mathcal{L}^I_{SIG}$ and $-ln\mathcal{L}^{II}_{SIG}$, respectively, as shown in equation 13 and 14. The N_{DATA}, N_{BKGA}, N_{BKGX} are the yields of data, BKG A and BKG X, respectively. In the fit, we only float two parameters α_{Ξ^0} (denoted as α_γ) and ϕ_{Ξ^0} (denoted as ϕ_γ) of signal process $\Xi^0 \to \gamma\Lambda$, with other parameters fixed. The normalization factors $\mathcal{S}^I$ and $\mathcal{S}^{II}$ are constructed with PHSP signal MC.

$$\begin{aligned}-\ln\mathcal{L}^I_{SIG} =& -\ln\mathcal{L}^I_{DATA}+\ln\mathcal{L}^I_{BKGA}+\ln\mathcal{L}^I_{BKGX}\\ =& -\sum_{i=1}^{N^I_{DATA}} \ln\omega^I(\xi_i,\alpha_\gamma,\phi_\gamma) + \sum_{j=1}^{N^I_{BKGA}} \ln\omega^I(\xi_j,\alpha_\gamma,\phi_\gamma) + \sum_{l=1}^{N^I_{BKGX}} \ln\omega^I(\xi_l,\alpha_\gamma,\phi_\gamma)\\ &+ (N^I_{DATA} - N^I_{BKGA} - N^I_{BKGX})\ln\mathcal{S}^I\end{aligned} \tag{13}$$

$$\begin{aligned}-\ln\mathcal{L}^{II}_{SIG} =& -\ln\mathcal{L}^{II}_{DATA}+\ln\mathcal{L}^{II}_{BKGA}+\ln\mathcal{L}^{II}_{BKGX}\\ =& -\sum_{i=1}^{N^{II}_{DATA}} \ln\omega^{II}(\xi_i,\bar{\alpha}_\gamma,\bar{\phi}_\gamma) + \sum_{j=1}^{N^{II}_{BKGA}} \ln\omega^{II}(\xi_j,\bar{\alpha}_\gamma,\bar{\phi}_\gamma) + \sum_{l=1}^{N^{II}_{BKGX}} \ln\omega^{II}(\xi_l,\bar{\alpha}_\gamma,\bar{\phi}_\gamma)\\ &+ (N^{II}_{DATA} - N^{II}_{BKGA} - N^{II}_{BKGX})\ln\mathcal{S}^{II}\end{aligned} \tag{14}$$

Only the accepted events in the region from 0.175GeV to 0.19 GeV on E^{cms}_γ distribution in the $\Xi^0(\bar{\Xi}^0)$ rest frame are used in the fit, as shown in Fig. 19. The yields of $N^{I,II}_{BKGA}$ and $N^{I,II}_{BKGX}$ in region $E^{cms}_\gamma \sim$ (0.175 GeV to 0.19 GeV) are shown in Table 12.

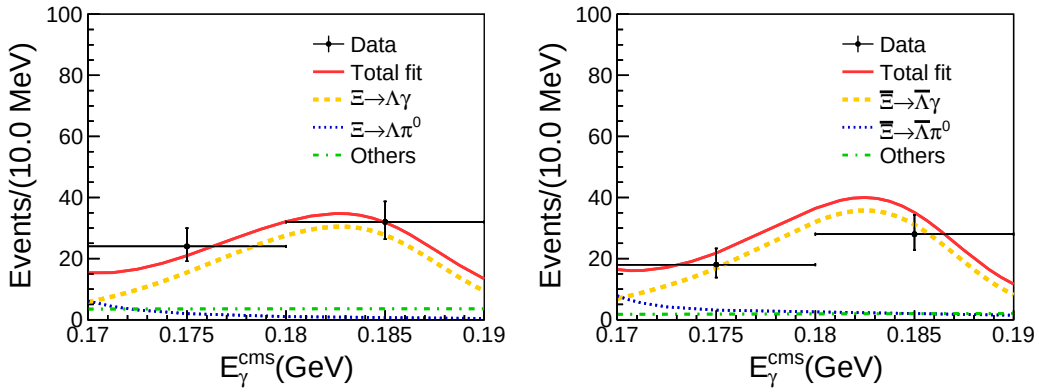

Figure 19: Distribution of E^{cms}_γ in the $\Xi^0(\bar{\Xi}^0)$ rest frame in the region from 0.175 GeV to 0.19 GeV. The accepted events in this region are used in the fit.

In the fit, the α_γ and the phase ϕ_γ are the only two floating parameters, other 7 decay parameters $(\alpha_{J/\psi}, \Delta\Phi, \alpha_{\bar{\Xi}^0}, \phi_{\bar{\Xi}^0}, \alpha_\Lambda, \alpha_{\bar{\Lambda}})$ are fixed to values of in the analysis[*shenhongfei*]. With package MINUIT from the CERN library, all possible α_γ and ϕ_γ values are scaned and the optimized α_γ and ϕ_γ

are determined with a minimized objective function. Individual fit is firstly performed using $\Xi^0 \to \gamma\Lambda$(or $\bar{\Xi}^0 \to \gamma\bar{\Lambda}$) process data, and the results are shown in Table 13. A simultaneous fit using two charge conjugated processes data are implemented, and the decay asymmerty α_γ and $\bar{\alpha}_\gamma$ share the same value with opposite signs. The likelihood functions of the charge conjugate processes are added together, $-\ln\mathcal{L}^I_{SIG} - \ln\mathcal{L}^{II}_{SIG}$, as the object function(O_{fit}). The measured decay asymmetry parameter of $\Xi^0 \to \gamma\Lambda$ is shown in Table 13.

$$O_{fit} = -\ln\mathcal{L}^I_{SIG} - \ln\mathcal{L}^{II}_{SIG} \tag{15}$$

Table 12: Yields of backgroud in the region $E^{cms}_\gamma \sim$ (0.175 GeV to 0.19 GeV).

Process	Yield($\Xi^0 \to \gamma\Lambda$)	Yield($\bar{\Xi}^0 \to \gamma\bar{\Lambda}$)
Signal	35	39
BKG A	1	3
BKG X	7	2

Table 13: Results of the α_γ using individual fit and simultaneous fit.

Modes	α_γ	ϕ_γ
$\Xi^0 \to \gamma\Lambda$	$-0.186 \pm 0.3_{stat.}$	$-0.77 \pm 0.54_{stat.}$
$\bar{\Xi}^0 \to \gamma\bar{\Lambda}$	$0.08 \pm 0.3_{stat.}$	$0.15 \pm 0.70_{stat.}$
Simultaneous fit	$0.03 \pm 0.2stat.$	$-0.1 \pm 0.56_{stat.}$

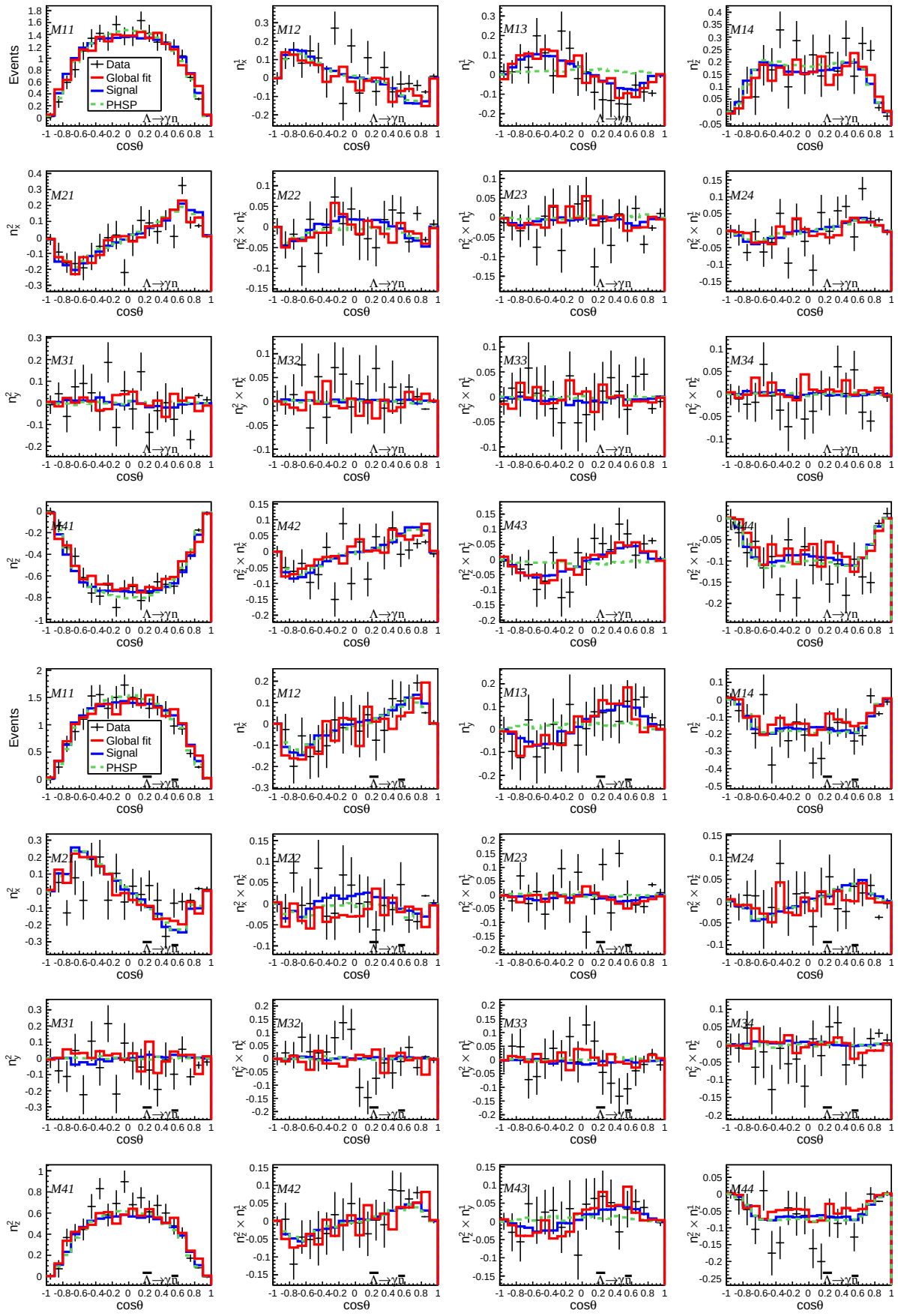

Figure 20: Moments for accepted data as a function of cosθ for the (16 plots on the top) $\bar{p}\pi^{+}n\gamma$ and (16 plots on the bottom)$p\pi^{-}\bar{n}\gamma$. The points with error bars are the data, and the red solid-line is the global fit. The blue solid-line shows the signal and the green dashed-line shows the no polarization scenario $\omega(\xi, \alpha_{J/\psi}, \Delta\Phi, \alpha_{-}, \alpha_{\gamma}) = 1$.

6 Systematic Uncertainty

Basically the systematic uncertainties in this analysis involve two parts: (1) Systematic uncertainty of branching ratio measurement. (2) Systematic uncertainty of the decay parameter measurement.

The sources of the uncertainties are mainly from the MC efficiency, the fit method, backgrounds estimation and the decay parameter of $\Lambda \to n\gamma$ when generating signal MC, etc. All the systematic uncertainties are summarized in Table 14. The detail of each systematic uncertainty is described following the table.

Table 14: Summary of the systematic uncertainties from different sources . The branching fraction uncertainties are showed as the percentage while the decay parameter uncertainties are shown as the absolute value.

Types	Sources	BRs. uncertainty	α_γ uncertainty
Common	Photon detection efficiency	1.0%	-
	$E_\gamma > 0.15$ GeV	-	-
Event selection ($\Lambda \to n\gamma$)	$\chi^2_{1C} < 10$	2.0%	0.024
	$\lvert M(\gamma\gamma) - M_{\pi^0}\rvert > 20$ MeV/c^2	1.6%	0.070
	$\theta(\gamma, n) > 20°$	0.5%	0.025
	BDT>0.3	0.15%	0.060
Event selection ($\bar{\Lambda} \to \bar{n}\gamma$)	$\chi^2_{3C} > 15$	1.5%	0.022
	$\lvert M(\gamma\gamma) - M_{\pi^0}\rvert > 20$ MeV/c^2	1.4%	0.040
	$\theta(\gamma, \bar{n}) > 20°$	1.9%	0.012
	BDT>0.3	0.2%	0.013
	$\bar{n}$ correction	0.5%	-
Fit	Signal shape	0.4%	0.001
	BKG A shape	1.0%	0.002
	BKG B shape	4.8%	0.078
	Fit range	0.3%	0.001
Signal MC efficiency	α_γ measurement	0.6%	0.000
Total		6.4%	0.110

- **Photon detection efficiency**

  At BESIII the photon detection efficiency is estimated to be 1.0% per photon[27] , and there is at least one photon in the signal process ($\Lambda \to \gamma n$), so the systematic uncertainty associated with photon detection is 1.0% .

- **Anti-neutron detection efficiency**

  The anti-neutron detection efficiency is corrected by the package based on a data-driven algorithm[24]. The uncertainty caused by the package can be obtained through the input-output check in Appendix I, the efficiency difference of the IO check is 0.5%, so we take it as the systematic uncertainty.

- **χ^2 of kinematic fit**

  For kinematic fit, by changing the cut value of $\chi^2_{1C}(\chi^2_{3C})$, the maximum variation of the BF and α_γ is taken as the systematic uncertainty. There is no obvious tendency of BF and α_γ, as shown in Fig. 21.

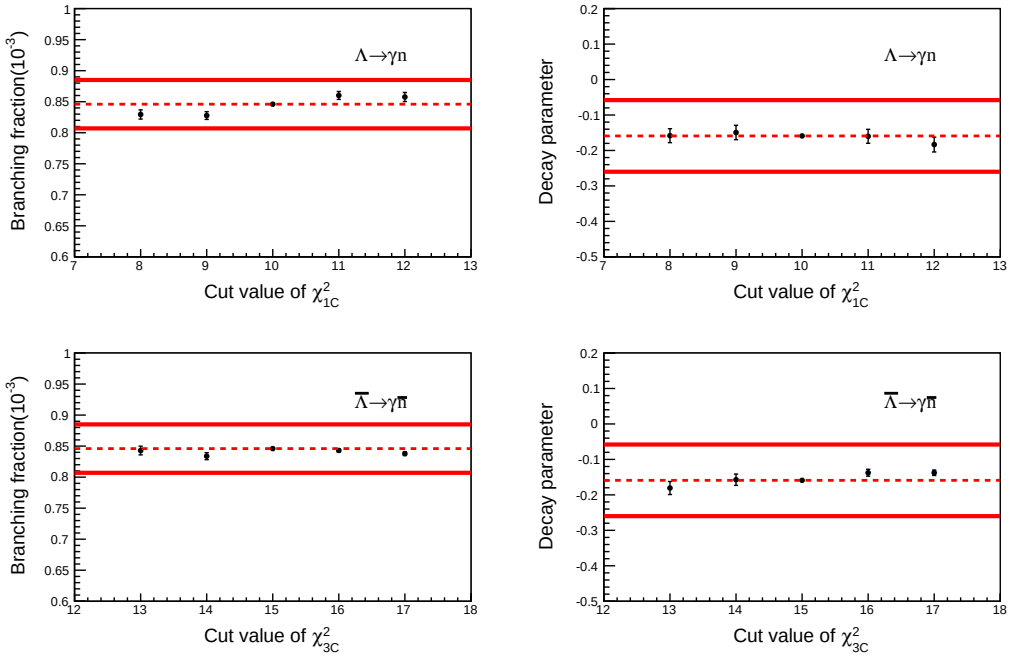

Figure 21: The BF. and α_γ variation tendency for different χ^2_{3C} cut values.

- $\theta(\gamma, n(\bar{n}))$

  For opening angle between γ and $n(\bar{n})$, by changing the cut value of the $\theta(\gamma, n(\bar{n}))$, the maximum variation of the BF. and α_γ is taken as the systematic uncertainty. The variation tendency of BF and α_γ is shown in Fig. 22.

- **BDT**

  The efficiency of BDT is corrected according to chapter **??**, the systematic uncertainty is the statistical error of the correction coefficient, since the amount of the control sample $J/\psi \to \rho\pi$ is huge, the statistical errors are 0.15% and 0.2% for the charge conjugate process, respectively.

- E_γ

  The energy of photon candidate in the laboratory frame, the E_γ, is required as $E_\gamma > 0.15$ GeV. While after BDT, the energy of majority of the photon candidates is larger than 0.2 GeV, so the systematic uncertainty is omitted.

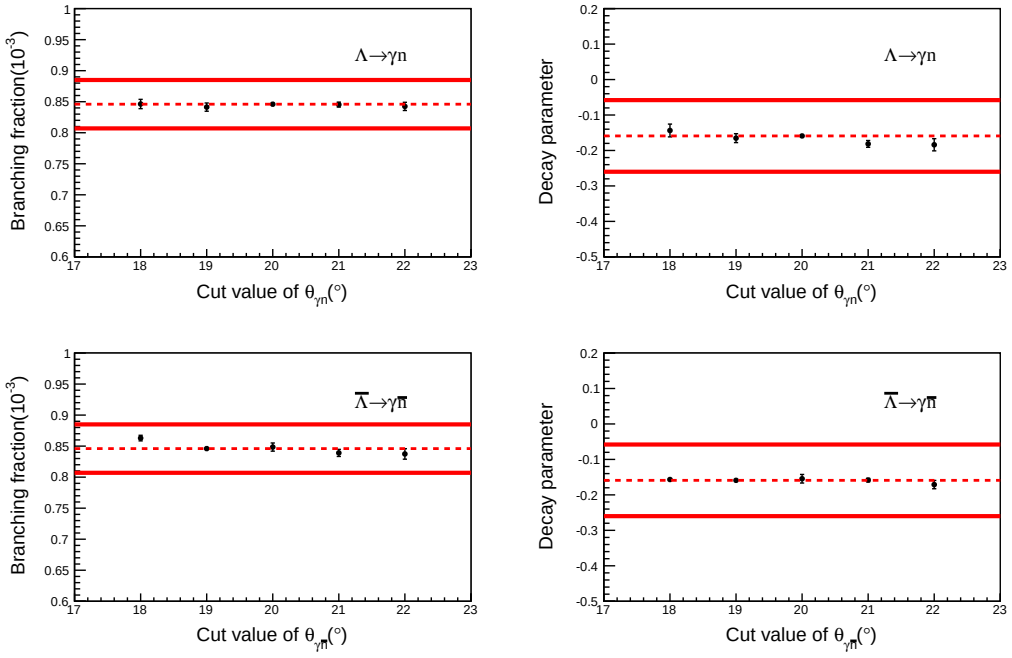

Figure 22: The BF and α_γ variation tendency for different $\theta_{\gamma,n(\bar{n})}$ cut values.

- $|M(\gamma\gamma) - M_{\pi^0}| > \mathbf{20\ MeV}/c^2$

  Two different method are tried to study the systematic uncertainty caused by this cut. The first way, by changing width of the mass window by 1 resolution (σ) of π^0 mass, as $|M(\gamma\gamma) - M_{\pi^0}| > 27$ MeV/c^2 the variation of the BF. and α_γ is taken as the systematic uncertainty, as shown in table 15. However, this method is quite rough and determined the uncertainty might include the statistical fluctuation and influence of the fit. The second way, we try to select a control sample to study the efficiency difference of data and mc. The event selection is as follow: first, selecting the sample of $\Lambda \to \pi^0 n$ ($\bar{\Lambda} \to \pi^0 \bar{n}$) process (same way as in Appendix B); second, applying the default event selection of signal process, performing kinematic fit for hypothesis $J/\psi \to \bar{\Lambda}\gamma n$ and $J/\psi \to \bar{\Lambda}\gamma\gamma n$. It needs to be emphasized that we don't use the softer photon from π^0 decay when looping all photons. Thus, we can get distribution of invariant mass of two γs ($M(\gamma\gamma)$) from control sample, as shown in Fig. 23. The difference of efficiencies between data and mc in control sample is obtained to be 1.6% and 1.4% for $\Lambda \to \gamma n(\bar{\Lambda} \to \gamma\bar{n})$, respectively, what are taken as the systematic uncertainties.

- **Fit range**

  The systematic uncertainty related to fit range is estimated by varying the range from [0.08GeV, 0.24 GeV] to [0.09 GeV, 0.23GeV] or [0.07 GeV, 0.25GeV], the variation of the BF and α_γ is taken as

Table 15: Systematic uncertainties of the π^0 mass window obtained by variation 1 resolution (σ) of the π^0 mass.

Modes	BRs. uncertainty	α_γ uncertainty
$\Lambda \to \gamma n$	1.5%	0.07
$\bar{\Lambda} \to \gamma \bar{n}$	0.9%	0.04

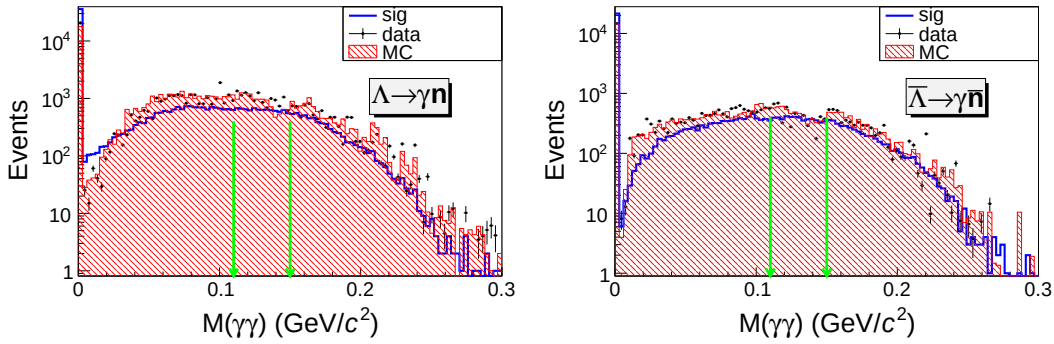

Figure 23: Distributions of invariant mass of two γs. The dots with error bars and red color filled histogrms are control samples of data and mc, respectively. The blue lines are from signal mc.

the systematic uncertainty.

- **Signal / BKG A shape**

  The PDFs of signal or BKG A are extracted from MC samples, the convoluted Gaussian function of signal / BKG A shape represents resolution difference between data and MC simulation. By variating ± 1 resolution (σ) and repeating the fit, the max difference of the results is taken as the systematic uncertainty.

- **BKG B shape**

  The PDFs of signal or BKG A are extracted from data samples, which is a Gaussian function. To study the systematic uncertainty, firstly generating 300 groups of BKG B shape whose Gaussian parameters(mean and resolution) are correlative based on the nominal results in Table 32, the distributions of mean and resolution are shown in Fig. 24; secondly repeating the simultaneous fit with the generated 300 groups of BKG B shapes, the distribution of the results of branching fraction and decay parameter is shown in Fig. 25. whose resolution is taken as the systematic uncertainty.

- **Signal MC α_γ**

  The measurement of α_γ has an uncertainty. By changing the α_γ value $\pm 1\sigma$ and generate new DIY MC to estimate the efficiency, the variation of the fit result is taken as a systematic uncertainty.

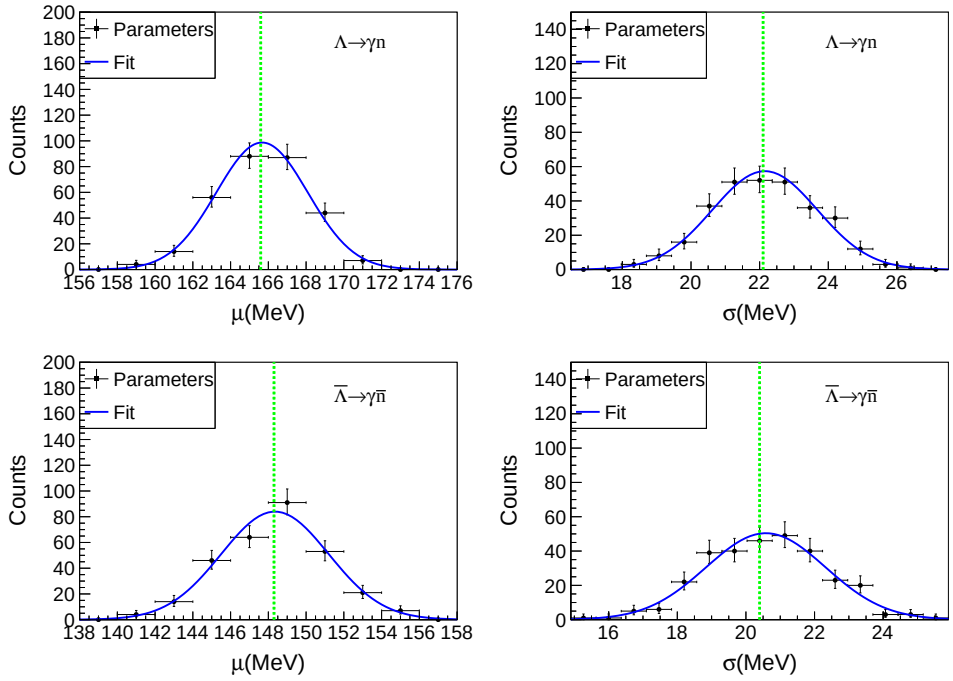

Figure 24: The parameters of the generated 300 groups of Gaussian functions of BKG B shape, μ denotes the mean value and σ denotes the resolution of the Gaussian functions. Dashed blue lines indicate the nominal value in Table 16.

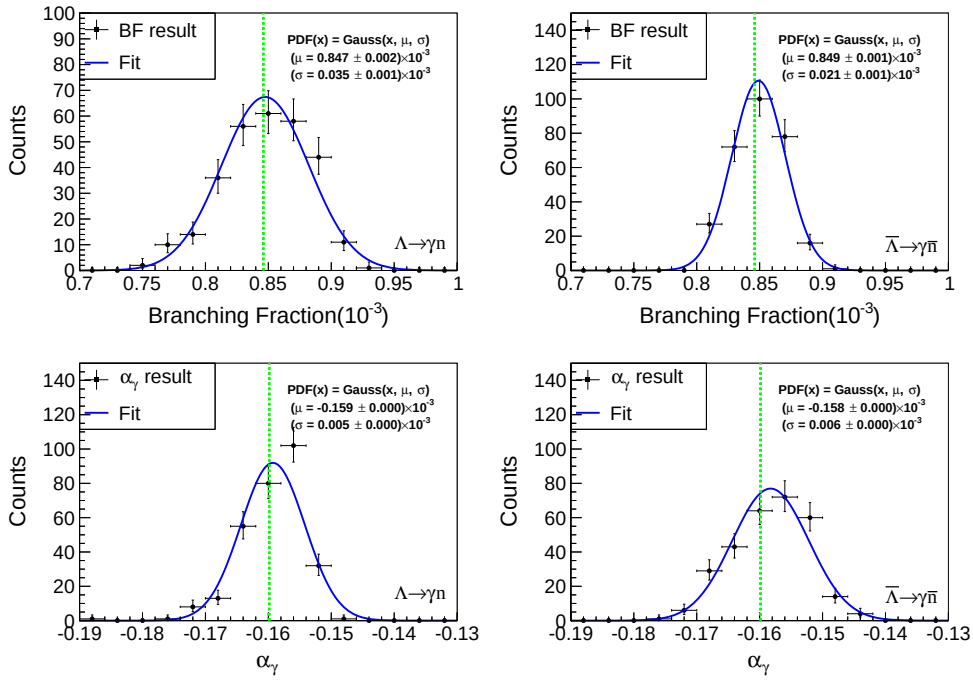

Figure 25: The results of branching fraction and decay parameters from 300 times fit by using the generated 300 groups of BKG B parameters.

7 Summary

In summary, by analyzing the accumulated 10 billion J/ψ data collected with the BESIII spectrometer in 2009, 2012, 2018 and 2019, the weak radiative decay $\Lambda \to \gamma n$ is studied through the $J/\psi \to \Lambda\bar{\Lambda}$,$\Lambda \to p\pi^-$,$\bar{\Lambda} \to \gamma\bar{n}$ process. After background subtraction, 1215±40 events are observed from the charge conjugate processes. The absolute branching fraction (BF) is determined to be $\mathscr{B}(\Lambda \to \gamma n) = (0.846 \pm 0.039_{stat.} \pm 0.054_{syst.}) \times 10^{-3}$, the decay parameter is determined to be $\alpha(\Lambda \to \gamma n) = (-0.160 \pm 0.101_{stat.} \pm 0.110_{syst.})$.

Appendices

A Expression of the joint angular distribution

The expression of the joint angular distribution of $e^+e^- \to J/\psi \to \Xi^0\bar{\Xi}^0$ is shown:

$$
\begin{aligned}
&1 + \bar{\alpha}_\Lambda \bar{\alpha}_\Xi \cos\left[\theta_{\bar{p}}\right] + \alpha_\Lambda \alpha_\Xi \cos\left[\theta_p\right] + \bar{\alpha}_\Lambda \bar{\alpha}_\Xi \alpha_\Lambda \alpha_\Xi \cos\left[\theta_{\bar{p}}\right] \cos\left[\theta_p\right] - \bar{\alpha}_\Xi \alpha_\Xi \alpha\psi \cos\left[\theta_{\bar{\Lambda}}\right] \cos[\theta_\Lambda] - \\
&\bar{\alpha}_\Lambda \alpha_\Xi \alpha\psi \cos\left[\theta_{\bar{p}}\right] \cos\left[\theta_{\bar{\Lambda}}\right] \cos[\theta_\Lambda] - \bar{\alpha}_\Xi \alpha_\Lambda \alpha\psi \cos\left[\theta_{\bar{\Lambda}}\right] \cos\left[\theta_p\right] \cos[\theta_\Lambda] - \\
&\bar{\alpha}_\Lambda \alpha_\Lambda \alpha\psi \cos\left[\theta_{\bar{p}}\right] \cos\left[\theta_{\bar{\Lambda}}\right] \cos\left[\theta_p\right] \cos[\theta_\Lambda] + \alpha\psi \cos[\theta]^2 + \bar{\alpha}_\Lambda \bar{\alpha}_\Xi \alpha\psi \cos\left[\theta_{\bar{p}}\right] \cos[\theta]^2 + \\
&\alpha_\Lambda \alpha_\Xi \alpha\psi \cos\left[\theta_p\right] \cos[\theta]^2 + \bar{\alpha}_\Lambda \bar{\alpha}_\Xi \alpha_\Lambda \alpha_\Xi \alpha\psi \cos\left[\theta_{\bar{p}}\right] \cos\left[\theta_p\right] \cos[\theta]^2 - \\
&\bar{\alpha}_\Xi \alpha_\Xi \cos\left[\theta_{\bar{\Lambda}}\right] \cos[\theta_\Lambda] \cos[\theta]^2 - \bar{\alpha}_\Lambda \alpha_\Xi \cos\left[\theta_{\bar{p}}\right] \cos\left[\theta_{\bar{\Lambda}}\right] \cos[\theta_\Lambda] \cos[\theta]^2 - \\
&\bar{\alpha}_\Xi \alpha_\Lambda \cos\left[\theta_{\bar{\Lambda}}\right] \cos\left[\theta_p\right] \cos[\theta_\Lambda] \cos[\theta]^2 - \bar{\alpha}_\Lambda \alpha_\Lambda \cos\left[\theta_{\bar{p}}\right] \cos\left[\theta_{\bar{\Lambda}}\right] \cos\left[\theta_p\right] \cos[\theta_\Lambda] \cos[\theta]^2 + \\
&\bar{\alpha}_\Lambda \bar{\gamma}_\Xi \alpha_\Xi \alpha\psi \cos[\theta_\Lambda] \cos\left[\phi_{\bar{p}}\right] \sin\left[\theta_{\bar{p}}\right] \sin\left[\theta_{\bar{\Lambda}}\right] + \\
&\bar{\alpha}_\Lambda \bar{\gamma}_\Xi \alpha_\Lambda \alpha\psi \cos\left[\theta_p\right] \cos[\theta_\Lambda] \cos\left[\phi_{\bar{p}}\right] \sin\left[\theta_{\bar{p}}\right] \sin\left[\theta_{\bar{\Lambda}}\right] + \\
&\bar{\alpha}_\Lambda \bar{\gamma}_\Xi \alpha_\Xi \cos[\theta_\Lambda] \cos\left[\phi_{\bar{p}}\right] \cos[\theta]^2 \sin\left[\theta_{\bar{p}}\right] \sin\left[\theta_{\bar{\Lambda}}\right] + \\
&\bar{\alpha}_\Lambda \bar{\gamma}_\Xi \alpha_\Lambda \cos\left[\theta_p\right] \cos[\theta_\Lambda] \cos\left[\phi_{\bar{p}}\right] \cos[\theta]^2 \sin\left[\theta_{\bar{p}}\right] \sin\left[\theta_{\bar{\Lambda}}\right] + \\
&\bar{\alpha}_\Xi \alpha_\Lambda \gamma_\Xi \alpha\psi \cos\left[\theta_{\bar{\Lambda}}\right] \cos\left[\phi_p\right] \sin\left[\theta_p\right] \sin[\theta_\Lambda] + \\
&\bar{\alpha}_\Lambda \alpha_\Lambda \gamma_\Xi \alpha\psi \cos\left[\theta_{\bar{p}}\right] \cos\left[\theta_{\bar{\Lambda}}\right] \cos\left[\phi_p\right] \sin\left[\theta_p\right] \sin[\theta_\Lambda] + \\
&\bar{\alpha}_\Xi \alpha_\Lambda \gamma_\Xi \cos\left[\theta_{\bar{\Lambda}}\right] \cos\left[\phi_p\right] \cos[\theta]^2 \sin\left[\theta_p\right] \sin[\theta_\Lambda] + \\
&\bar{\alpha}_\Lambda \alpha_\Lambda \gamma_\Xi \cos\left[\theta_{\bar{p}}\right] \cos\left[\theta_{\bar{\Lambda}}\right] \cos\left[\phi_p\right] \cos[\theta]^2 \sin\left[\theta_p\right] \sin[\theta_\Lambda] - \\
&\bar{\alpha}_\Lambda \bar{\gamma}_\Xi \alpha_\Lambda \gamma_\Xi \alpha\psi \cos\left[\phi_{\bar{p}}\right] \cos\left[\phi_p\right] \sin\left[\theta_{\bar{p}}\right] \sin\left[\theta_{\bar{\Lambda}}\right] \sin\left[\theta_p\right] \sin[\theta_\Lambda] - \\
&\bar{\alpha}_\Lambda \bar{\gamma}_\Xi \alpha_\Lambda \gamma_\Xi \cos\left[\phi_{\bar{p}}\right] \cos\left[\phi_p\right] \cos[\theta]^2 \sin\left[\theta_{\bar{p}}\right] \sin\left[\theta_{\bar{\Lambda}}\right] \sin\left[\theta_p\right] \sin[\theta_\Lambda] - \\
&\bar{\alpha}_\Lambda \bar{\beta}_\Xi \alpha_\Lambda \alpha\psi \cos\left[\theta_p\right] \cos[\theta_\Lambda] \sin\left[\theta_{\bar{p}}\right] \sin\left[\theta_{\bar{\Lambda}}\right] \sin\left[\phi_{\bar{p}}\right] - \\
&\bar{\alpha}_\Lambda \bar{\beta}_\Xi \alpha_\Xi \alpha\psi \cos[\theta_\Lambda] \cos\left[\phi_{\bar{\Lambda}}\right]^2 \sin\left[\theta_{\bar{p}}\right] \sin\left[\theta_{\bar{\Lambda}}\right] \sin\left[\phi_{\bar{p}}\right] - \\
&\bar{\alpha}_\Lambda \bar{\beta}_\Xi \alpha_\Xi \cos[\theta_\Lambda] \cos[\theta]^2 \sin\left[\theta_{\bar{p}}\right] \sin\left[\theta_{\bar{\Lambda}}\right] \sin\left[\phi_{\bar{p}}\right] -
\end{aligned}
$$

Figure 26: joint angular distribution of $e^+e^- \to J/\psi \to \Xi^0\bar{\Xi}^0$(a)

$$
\begin{aligned}
&\bar{\alpha}_\Lambda \bar{\beta}_\Xi \alpha_\Lambda \cos\left[\theta_p\right] \cos\left[\theta_\Lambda\right] \cos\left[\theta\right]^2 \sin\left[\theta_{\bar{p}}\right] \sin\left[\theta_{\bar{\Lambda}}\right] \sin\left[\phi_{\bar{p}}\right] + \\
&\bar{\alpha}_\Lambda \bar{\beta}_\Xi \alpha_\Lambda \gamma_\Xi \alpha\psi \cos\left[\phi_p\right] \sin\left[\theta_{\bar{p}}\right] \sin\left[\theta_{\bar{\Lambda}}\right] \sin\left[\theta_p\right] \sin\left[\theta_\Lambda\right] \sin\left[\phi_{\bar{p}}\right] + \\
&\bar{\alpha}_\Lambda \bar{\beta}_\Xi \alpha_\Lambda \gamma_\Xi \cos\left[\phi_p\right] \cos\left[\theta\right]^2 \sin\left[\theta_{\bar{p}}\right] \sin\left[\theta_{\bar{\Lambda}}\right] \sin\left[\theta_p\right] \sin\left[\theta_\Lambda\right] \sin\left[\phi_{\bar{p}}\right] - \\
&\bar{\alpha}_\Lambda \bar{\beta}_\Xi \alpha_\Xi \alpha\psi \cos\left[\theta_\Lambda\right] \sin\left[\theta_{\bar{p}}\right] \sin\left[\theta_{\bar{\Lambda}}\right] \sin\left[\phi_{\bar{p}}\right] \sin\left[\phi_{\bar{\Lambda}}\right]^2 - \\
&\bar{\alpha}_\Lambda \alpha_\Lambda \beta_\Xi \alpha\psi \cos\left[\theta_p\right] \cos\left[\theta_{\bar{\Lambda}}\right] \sin\left[\theta_p\right] \sin\left[\theta_\Lambda\right] \sin\left[\phi_p\right] - \\
&\bar{\alpha}_\Xi \alpha_\Lambda \beta_\Xi \alpha\psi \cos\left[\theta_{\bar{\Lambda}}\right] \cos\left[\phi_\Lambda\right]^2 \sin\left[\theta_p\right] \sin\left[\theta_\Lambda\right] \sin\left[\phi_p\right] - \\
&\bar{\alpha}_\Xi \alpha_\Lambda \beta_\Xi \cos\left[\theta_{\bar{\Lambda}}\right] \cos\left[\theta\right]^2 \sin\left[\theta_p\right] \sin\left[\theta_\Lambda\right] \sin\left[\phi_p\right] - \\
&\bar{\alpha}_\Lambda \alpha_\Lambda \beta_\Xi \cos\left[\theta_p\right] \cos\left[\theta_{\bar{\Lambda}}\right] \cos\left[\theta\right]^2 \sin\left[\theta_p\right] \sin\left[\theta_\Lambda\right] \sin\left[\phi_p\right] + \\
&\bar{\alpha}_\Lambda \bar{\gamma}_\Xi \alpha_\Lambda \beta_\Xi \alpha\psi \cos\left[\phi_{\bar{p}}\right] \sin\left[\theta_{\bar{p}}\right] \sin\left[\theta_{\bar{\Lambda}}\right] \sin\left[\theta_p\right] \sin\left[\theta_\Lambda\right] \sin\left[\phi_p\right] + \\
&\bar{\alpha}_\Lambda \bar{\gamma}_\Xi \alpha_\Lambda \beta_\Xi \cos\left[\phi_{\bar{p}}\right] \cos\left[\theta\right]^2 \sin\left[\theta_{\bar{p}}\right] \sin\left[\theta_{\bar{\Lambda}}\right] \sin\left[\theta_p\right] \sin\left[\theta_\Lambda\right] \sin\left[\phi_p\right] - \\
&\bar{\alpha}_\Lambda \bar{\beta}_\Xi \alpha_\Lambda \beta_\Xi \alpha\psi \sin\left[\theta_{\bar{p}}\right] \sin\left[\theta_{\bar{\Lambda}}\right] \sin\left[\theta_p\right] \sin\left[\theta_\Lambda\right] \sin\left[\phi_{\bar{p}}\right] \sin\left[\phi_p\right] - \\
&\bar{\alpha}_\Lambda \bar{\beta}_\Xi \alpha_\Lambda \beta_\Xi \cos\left[\theta\right]^2 \sin\left[\theta_{\bar{p}}\right] \sin\left[\theta_{\bar{\Lambda}}\right] \sin\left[\theta_p\right] \sin\left[\theta_\Lambda\right] \sin\left[\phi_{\bar{p}}\right] \sin\left[\phi_p\right] - \\
&\bar{\alpha}_\Xi \alpha_\Lambda \beta_\Xi \alpha\psi \cos\left[\theta_{\bar{\Lambda}}\right] \sin\left[\theta_p\right] \sin\left[\theta_\Lambda\right] \sin\left[\phi_p\right] \sin\left[\phi_\Lambda\right]^2 - \\
&\bar{\alpha}_\Lambda \bar{\gamma}_\Xi \alpha_\Xi \sqrt{1-\alpha\psi^2} \cos\left[\theta_{\bar{\Lambda}}\right] \cos\left[\theta_\Lambda\right] \cos\left[\phi_{\bar{p}}\right] \cos\left[\phi_{\bar{\Lambda}}\right] \cos\left[\theta\right] \cos\left[\Phi\right] \sin\left[\theta_{\bar{p}}\right] \sin\left[\theta\right] - \\
&\bar{\alpha}_\Lambda \bar{\gamma}_\Xi \alpha_\Lambda \sqrt{1-\alpha\psi^2} \cos\left[\theta_{\bar{\Lambda}}\right] \cos\left[\theta_p\right] \cos\left[\theta_\Lambda\right] \cos\left[\phi_{\bar{p}}\right] \cos\left[\phi_{\bar{\Lambda}}\right] \cos\left[\theta\right] \cos\left[\Phi\right] \sin\left[\theta_{\bar{p}}\right] \sin\left[\theta\right] - \\
&\bar{\alpha}_\Xi \alpha_\Xi \sqrt{1-\alpha\psi^2} \cos\left[\theta_\Lambda\right] \cos\left[\phi_{\bar{\Lambda}}\right] \cos\left[\theta\right] \cos\left[\Phi\right] \sin\left[\theta_{\bar{\Lambda}}\right] \sin\left[\theta\right] - \\
&\bar{\alpha}_\Lambda \alpha_\Xi \sqrt{1-\alpha\psi^2} \cos\left[\theta_{\bar{p}}\right] \cos\left[\theta_\Lambda\right] \cos\left[\phi_{\bar{\Lambda}}\right] \cos\left[\theta\right] \cos\left[\Phi\right] \sin\left[\theta_{\bar{\Lambda}}\right] \sin\left[\theta\right] - \\
&\bar{\alpha}_\Xi \alpha_\Lambda \sqrt{1-\alpha\psi^2} \cos\left[\theta_p\right] \cos\left[\theta_\Lambda\right] \cos\left[\phi_{\bar{\Lambda}}\right] \cos\left[\theta\right] \cos\left[\Phi\right] \sin\left[\theta_{\bar{\Lambda}}\right] \sin\left[\theta\right] - \\
&\bar{\alpha}_\Lambda \alpha_\Lambda \sqrt{1-\alpha\psi^2} \cos\left[\theta_{\bar{p}}\right] \cos\left[\theta_p\right] \cos\left[\theta_\Lambda\right] \cos\left[\phi_{\bar{\Lambda}}\right] \cos\left[\theta\right] \cos\left[\Phi\right] \sin\left[\theta_{\bar{\Lambda}}\right] \sin\left[\theta\right] + \\
&\bar{\alpha}_\Xi \alpha_\Lambda \gamma_\Xi \sqrt{1-\alpha\psi^2} \cos\left[\theta_{\bar{\Lambda}}\right] \cos\left[\theta_\Lambda\right] \cos\left[\phi_p\right] \cos\left[\phi_\Lambda\right] \cos\left[\theta\right] \cos\left[\Phi\right] \sin\left[\theta_p\right] \sin\left[\theta\right] + \\
&\bar{\alpha}_\Lambda \alpha_\Lambda \gamma_\Xi \sqrt{1-\alpha\psi^2} \cos\left[\theta_{\bar{p}}\right] \cos\left[\theta_{\bar{\Lambda}}\right] \cos\left[\theta_\Lambda\right] \cos\left[\phi_p\right] \cos\left[\phi_\Lambda\right] \cos\left[\theta\right] \cos\left[\Phi\right] \sin\left[\theta_p\right] \sin\left[\theta\right] - \\
&\bar{\alpha}_\Lambda \bar{\gamma}_\Xi \alpha_\Lambda \gamma_\Xi \sqrt{1-\alpha\psi^2} \cos\left[\theta_\Lambda\right] \cos\left[\phi_{\bar{p}}\right] \cos\left[\phi_p\right] \cos\left[\phi_\Lambda\right] \cos\left[\theta\right] \cos\left[\Phi\right] \sin\left[\theta_{\bar{p}}\right] \sin\left[\theta_{\bar{\Lambda}}\right] \\
&\quad \sin\left[\theta_p\right] \sin\left[\theta\right] + \bar{\alpha}_\Xi \alpha_\Xi \sqrt{1-\alpha\psi^2} \cos\left[\theta_{\bar{\Lambda}}\right] \cos\left[\phi_\Lambda\right] \cos\left[\theta\right] \cos\left[\Phi\right] \sin\left[\theta_\Lambda\right] \sin\left[\theta\right] + \\
&\bar{\alpha}_\Lambda \alpha_\Xi \sqrt{1-\alpha\psi^2} \cos\left[\theta_{\bar{p}}\right] \cos\left[\theta_{\bar{\Lambda}}\right] \cos\left[\phi_\Lambda\right] \cos\left[\theta\right] \cos\left[\Phi\right] \sin\left[\theta_\Lambda\right] \sin\left[\theta\right] + \\
&\bar{\alpha}_\Xi \alpha_\Lambda \sqrt{1-\alpha\psi^2} \cos\left[\theta_{\bar{\Lambda}}\right] \cos\left[\theta_p\right] \cos\left[\phi_\Lambda\right] \cos\left[\theta\right] \cos\left[\Phi\right] \sin\left[\theta_\Lambda\right] \sin\left[\theta\right] + \\
&\bar{\alpha}_\Lambda \alpha_\Lambda \sqrt{1-\alpha\psi^2} \cos\left[\theta_{\bar{p}}\right] \cos\left[\theta_{\bar{\Lambda}}\right] \cos\left[\theta_p\right] \cos\left[\phi_\Lambda\right] \cos\left[\theta\right] \cos\left[\Phi\right] \sin\left[\theta_\Lambda\right] \sin\left[\theta\right] - \\
&\bar{\alpha}_\Lambda \bar{\gamma}_\Xi \alpha_\Lambda \gamma_\Xi \sqrt{1-\alpha\psi^2} \cos\left[\phi_{\bar{p}}\right] \cos\left[\phi_\Lambda\right] \cos\left[\theta\right] \cos\left[\Phi\right] \sin\left[\theta_{\bar{p}}\right] \sin\left[\theta_{\bar{\Lambda}}\right] \sin\left[\theta_\Lambda\right] \sin\left[\theta\right] - \\
&\bar{\alpha}_\Lambda \bar{\gamma}_\Xi \alpha_\Lambda \sqrt{1-\alpha\psi^2} \cos\left[\theta_p\right] \cos\left[\phi_{\bar{p}}\right] \cos\left[\phi_\Lambda\right] \cos\left[\theta\right] \cos\left[\Phi\right] \sin\left[\theta_{\bar{p}}\right] \sin\left[\theta_{\bar{\Lambda}}\right] \sin\left[\theta_\Lambda\right] \sin\left[\theta\right] + \\
&\bar{\alpha}_\Lambda \bar{\gamma}_\Xi \alpha_\Lambda \gamma_\Xi \sqrt{1-\alpha\psi^2} \cos\left[\theta_{\bar{\Lambda}}\right] \cos\left[\phi_{\bar{p}}\right] \cos\left[\phi_p\right] \cos\left[\phi_{\bar{\Lambda}}\right] \\
&\quad \cos\left[\phi_p\right] \cos\left[\theta\right] \cos\left[\Phi\right] \sin\left[\theta_{\bar{p}}\right] \sin\left[\theta_p\right] \sin\left[\theta_\Lambda\right] \sin\left[\theta\right] + \\
&\bar{\alpha}_\Xi \alpha_\Lambda \gamma_\Xi \sqrt{1-\alpha\psi^2} \cos\left[\phi_{\bar{\Lambda}}\right] \cos\left[\phi_p\right] \cos\left[\theta\right] \cos\left[\Phi\right] \sin\left[\theta_{\bar{\Lambda}}\right] \sin\left[\theta_p\right] \sin\left[\theta_\Lambda\right] \sin\left[\theta\right] + \\
&\bar{\alpha}_\Lambda \alpha_\Lambda \gamma_\Xi \sqrt{1-\alpha\psi^2} \cos\left[\theta_{\bar{p}}\right] \cos\left[\phi_{\bar{\Lambda}}\right] \cos\left[\phi_p\right] \cos\left[\theta\right] \cos\left[\Phi\right] \sin\left[\theta_{\bar{\Lambda}}\right] \sin\left[\theta_p\right] \sin\left[\theta_\Lambda\right] \sin\left[\theta\right] + \\
&\bar{\alpha}_\Lambda \bar{\beta}_\Xi \alpha_\Xi \sqrt{1-\alpha\psi^2} \cos\left[\theta_{\bar{\Lambda}}\right] \cos\left[\theta_\Lambda\right] \cos\left[\phi_{\bar{\Lambda}}\right] \cos\left[\theta\right] \cos\left[\Phi\right] \sin\left[\theta_{\bar{p}}\right] \sin\left[\phi_{\bar{p}}\right] \sin\left[\theta\right] + \\
&\bar{\alpha}_\Lambda \bar{\beta}_\Xi \alpha_\Lambda \sqrt{1-\alpha\psi^2} \cos\left[\theta_{\bar{\Lambda}}\right] \cos\left[\theta_p\right] \cos\left[\theta_\Lambda\right] \cos\left[\phi_{\bar{\Lambda}}\right] \cos\left[\theta\right] \cos\left[\Phi\right] \sin\left[\theta_{\bar{p}}\right] \sin\left[\phi_{\bar{p}}\right] \sin\left[\theta\right] + \\
&\bar{\alpha}_\Lambda \bar{\beta}_\Xi \alpha_\Lambda \gamma_\Xi \sqrt{1-\alpha\psi^2} \cos\left[\theta_\Lambda\right] \cos\left[\phi_p\right] \cos\left[\phi_\Lambda\right]
\end{aligned}
$$

Figure 27: joint angular distribution of $e^+e^- \to J/\psi \to \Xi^0\bar{\Xi}^0$(b)

$$
\begin{aligned}
&\mathrm{Cos}[\theta]\,\mathrm{Cos}[\Phi]\,\mathrm{Sin}\left[\theta_{\mathrm{p}}^{-}\right]\,\mathrm{Sin}\left[\theta_{\bar{\Lambda}}^{-}\right]\,\mathrm{Sin}\left[\theta_{\mathrm{p}}\right]\,\mathrm{Sin}\left[\phi_{\mathrm{p}}^{-}\right]\,\mathrm{Sin}[\theta]\,+\\
&\bar{\alpha}_{\Lambda}\,\bar{\beta}_{\Xi}\,\alpha_{\Xi}\,\sqrt{1-\alpha\psi^{2}}\,\mathrm{Cos}[\phi_{\Lambda}]\,\mathrm{Cos}[\theta]\,\mathrm{Cos}[\Phi]\,\mathrm{Sin}\left[\theta_{\mathrm{p}}^{-}\right]\,\mathrm{Sin}\left[\theta_{\bar{\Lambda}}^{-}\right]\,\mathrm{Sin}[\theta_{\Lambda}]\,\mathrm{Sin}\left[\phi_{\mathrm{p}}^{-}\right]\,\mathrm{Sin}[\theta]\,+\\
&\bar{\alpha}_{\Lambda}\,\bar{\beta}_{\Xi}\,\alpha_{\Lambda}\,\sqrt{1-\alpha\psi^{2}}\,\mathrm{Cos}\left[\theta_{\mathrm{p}}\right]\,\mathrm{Cos}[\phi_{\Lambda}]\,\mathrm{Cos}[\theta]\,\mathrm{Cos}[\Phi]\,\mathrm{Sin}\left[\theta_{\mathrm{p}}^{-}\right]\,\mathrm{Sin}\left[\theta_{\bar{\Lambda}}^{-}\right]\,\mathrm{Sin}[\theta_{\Lambda}]\,\mathrm{Sin}\left[\phi_{\mathrm{p}}^{-}\right]\,\mathrm{Sin}[\theta]\,-\\
&\bar{\alpha}_{\Lambda}\,\bar{\beta}_{\Xi}\,\alpha_{\Lambda}\,\gamma_{\Xi}\,\sqrt{1-\alpha\psi^{2}}\,\mathrm{Cos}\left[\theta_{\bar{\Lambda}}^{-}\right]\,\mathrm{Cos}\left[\phi_{\bar{\Lambda}}^{-}\right]\,\mathrm{Cos}\left[\phi_{\mathrm{p}}\right]\\
&\mathrm{Cos}[\theta]\,\mathrm{Cos}[\Phi]\,\mathrm{Sin}\left[\theta_{\mathrm{p}}^{-}\right]\,\mathrm{Sin}\left[\theta_{\mathrm{p}}\right]\,\mathrm{Sin}[\theta_{\Lambda}]\,\mathrm{Sin}\left[\phi_{\mathrm{p}}^{-}\right]\,\mathrm{Sin}[\theta]\,+\\
&\bar{\alpha}_{\Lambda}\,\bar{\beta}_{\Xi}\,\alpha_{\Xi}\,\sqrt{1-\alpha\psi^{2}}\,\mathrm{Cos}[\theta_{\Lambda}]\,\mathrm{Cos}\left[\phi_{\mathrm{p}}^{-}\right]\,\mathrm{Cos}[\theta]\,\mathrm{Cos}[\Phi]\,\mathrm{Sin}\left[\theta_{\mathrm{p}}^{-}\right]\,\mathrm{Sin}\left[\phi_{\bar{\Lambda}}^{-}\right]\,\mathrm{Sin}[\theta]\,+\\
&\bar{\alpha}_{\Lambda}\,\bar{\beta}_{\Xi}\,\alpha_{\Lambda}\,\sqrt{1-\alpha\psi^{2}}\,\mathrm{Cos}\left[\theta_{\mathrm{p}}\right]\,\mathrm{Cos}[\theta_{\Lambda}]\,\mathrm{Cos}\left[\phi_{\mathrm{p}}^{-}\right]\,\mathrm{Cos}[\theta]\,\mathrm{Cos}[\Phi]\,\mathrm{Sin}\left[\theta_{\mathrm{p}}^{-}\right]\,\mathrm{Sin}\left[\phi_{\bar{\Lambda}}^{-}\right]\,\mathrm{Sin}[\theta]\,-\\
&\bar{\alpha}_{\Lambda}\,\bar{\beta}_{\Xi}\,\alpha_{\Lambda}\,\gamma_{\Xi}\,\sqrt{1-\alpha\psi^{2}}\,\mathrm{Cos}\left[\phi_{\mathrm{p}}^{-}\right]\,\mathrm{Cos}\left[\phi_{\mathrm{p}}\right]\,\mathrm{Cos}[\theta]\,\mathrm{Cos}[\Phi]\,\mathrm{Sin}\left[\theta_{\mathrm{p}}^{-}\right]\,\mathrm{Sin}\left[\theta_{\mathrm{p}}\right]\,\mathrm{Sin}[\theta_{\Lambda}]\,\mathrm{Sin}\left[\phi_{\bar{\Lambda}}^{-}\right]\\
&\mathrm{Sin}[\theta]\,+\,\bar{\alpha}_{\Lambda}\,\bar{\gamma}_{\Xi}\,\alpha_{\Xi}\,\sqrt{1-\alpha\psi^{2}}\,\mathrm{Cos}[\theta_{\Lambda}]\,\mathrm{Cos}[\theta]\,\mathrm{Cos}[\Phi]\,\mathrm{Sin}\left[\theta_{\mathrm{p}}^{-}\right]\,\mathrm{Sin}\left[\phi_{\mathrm{p}}^{-}\right]\,\mathrm{Sin}\left[\phi_{\bar{\Lambda}}^{-}\right]\,\mathrm{Sin}[\theta]\,+\\
&\bar{\alpha}_{\Lambda}\,\bar{\gamma}_{\Xi}\,\alpha_{\Lambda}\,\sqrt{1-\alpha\psi^{2}}\,\mathrm{Cos}\left[\theta_{\mathrm{p}}\right]\,\mathrm{Cos}[\theta_{\Lambda}]\,\mathrm{Cos}[\theta]\,\mathrm{Cos}[\Phi]\,\mathrm{Sin}\left[\theta_{\mathrm{p}}^{-}\right]\,\mathrm{Sin}\left[\phi_{\mathrm{p}}^{-}\right]\,\mathrm{Sin}\left[\phi_{\bar{\Lambda}}^{-}\right]\,\mathrm{Sin}[\theta]\,-\,\bar{\alpha}_{\Lambda}\,\bar{\gamma}_{\Xi}\\
&\alpha_{\Lambda}\,\gamma_{\Xi}\,\sqrt{1-\alpha\psi^{2}}\,\mathrm{Cos}\left[\phi_{\mathrm{p}}\right]\,\mathrm{Cos}[\theta]\,\mathrm{Cos}[\Phi]\,\mathrm{Sin}\left[\theta_{\mathrm{p}}^{-}\right]\,\mathrm{Sin}\left[\theta_{\mathrm{p}}\right]\,\mathrm{Sin}[\theta_{\Lambda}]\,\mathrm{Sin}\left[\phi_{\mathrm{p}}^{-}\right]\,\mathrm{Sin}\left[\phi_{\bar{\Lambda}}^{-}\right]\,\mathrm{Sin}[\theta]\,-\\
&\bar{\alpha}_{\Xi}\,\alpha_{\Lambda}\,\beta_{\Xi}\,\sqrt{1-\alpha\psi^{2}}\,\mathrm{Cos}\left[\theta_{\bar{\Lambda}}^{-}\right]\,\mathrm{Cos}[\theta_{\Lambda}]\,\mathrm{Cos}[\phi_{\Lambda}]\,\mathrm{Cos}[\theta]\,\mathrm{Cos}[\Phi]\,\mathrm{Sin}\left[\theta_{\mathrm{p}}\right]\,\mathrm{Sin}\left[\phi_{\mathrm{p}}\right]\,\mathrm{Sin}[\theta]\,-\\
&\bar{\alpha}_{\Lambda}\,\alpha_{\Lambda}\,\beta_{\Xi}\,\sqrt{1-\alpha\psi^{2}}\,\mathrm{Cos}\left[\theta_{\mathrm{p}}\right]\,\mathrm{Cos}\left[\theta_{\bar{\Lambda}}^{-}\right]\,\mathrm{Cos}[\theta_{\Lambda}]\,\mathrm{Cos}[\phi_{\Lambda}]\,\mathrm{Cos}[\theta]\,\mathrm{Cos}[\Phi]\,\mathrm{Sin}\left[\theta_{\mathrm{p}}\right]\,\mathrm{Sin}\left[\phi_{\mathrm{p}}\right]\,\mathrm{Sin}[\theta]\,+\\
&\bar{\alpha}_{\Lambda}\,\bar{\gamma}_{\Xi}\,\alpha_{\Lambda}\,\beta_{\Xi}\,\sqrt{1-\alpha\psi^{2}}\,\mathrm{Cos}[\theta_{\Lambda}]\,\mathrm{Cos}\left[\phi_{\mathrm{p}}^{-}\right]\,\mathrm{Cos}[\phi_{\Lambda}]\,\mathrm{Cos}[\theta]\,\mathrm{Cos}[\Phi]\,\mathrm{Sin}\left[\theta_{\mathrm{p}}^{-}\right]\\
&\mathrm{Sin}\left[\theta_{\bar{\Lambda}}^{-}\right]\,\mathrm{Sin}\left[\theta_{\mathrm{p}}\right]\,\mathrm{Sin}\left[\phi_{\mathrm{p}}\right]\,\mathrm{Sin}[\theta]\,-\,\bar{\alpha}_{\Lambda}\,\bar{\gamma}_{\Xi}\,\alpha_{\Lambda}\,\beta_{\Xi}\,\sqrt{1-\alpha\psi^{2}}\,\mathrm{Cos}\left[\theta_{\bar{\Lambda}}^{-}\right]\,\mathrm{Cos}\left[\phi_{\mathrm{p}}^{-}\right]\\
&\mathrm{Cos}\left[\phi_{\bar{\Lambda}}^{-}\right]\,\mathrm{Cos}[\theta]\,\mathrm{Cos}[\Phi]\,\mathrm{Sin}\left[\theta_{\mathrm{p}}^{-}\right]\,\mathrm{Sin}\left[\theta_{\mathrm{p}}\right]\,\mathrm{Sin}[\theta_{\Lambda}]\,\mathrm{Sin}\left[\phi_{\mathrm{p}}\right]\,\mathrm{Sin}[\theta]\,-\\
&\bar{\alpha}_{\Xi}\,\alpha_{\Lambda}\,\beta_{\Xi}\,\sqrt{1-\alpha\psi^{2}}\,\mathrm{Cos}\left[\phi_{\bar{\Lambda}}^{-}\right]\,\mathrm{Cos}[\theta]\,\mathrm{Cos}[\Phi]\,\mathrm{Sin}\left[\theta_{\bar{\Lambda}}^{-}\right]\,\mathrm{Sin}\left[\theta_{\mathrm{p}}\right]\,\mathrm{Sin}[\theta_{\Lambda}]\,\mathrm{Sin}\left[\phi_{\mathrm{p}}\right]\,\mathrm{Sin}[\theta]\,-\\
&\bar{\alpha}_{\Lambda}\,\alpha_{\Lambda}\,\beta_{\Xi}\,\sqrt{1-\alpha\psi^{2}}\,\mathrm{Cos}\left[\theta_{\mathrm{p}}^{-}\right]\,\mathrm{Cos}\left[\phi_{\bar{\Lambda}}^{-}\right]\,\mathrm{Cos}[\theta]\,\mathrm{Cos}[\Phi]\,\mathrm{Sin}\left[\theta_{\bar{\Lambda}}^{-}\right]\,\mathrm{Sin}\left[\theta_{\mathrm{p}}\right]\,\mathrm{Sin}[\theta_{\Lambda}]\,\mathrm{Sin}\left[\phi_{\mathrm{p}}\right]\,\mathrm{Sin}[\theta]\,-\\
&\bar{\alpha}_{\Lambda}\,\bar{\beta}_{\Xi}\,\alpha_{\Lambda}\,\beta_{\Xi}\,\sqrt{1-\alpha\psi^{2}}\,\mathrm{Cos}[\theta_{\Lambda}]\,\mathrm{Cos}[\phi_{\Lambda}]\,\mathrm{Cos}[\theta]\,\mathrm{Cos}[\Phi]\,\mathrm{Sin}\left[\theta_{\mathrm{p}}^{-}\right]\,\mathrm{Sin}\left[\theta_{\bar{\Lambda}}^{-}\right]\,\mathrm{Sin}\left[\theta_{\mathrm{p}}\right]\,\mathrm{Sin}\left[\phi_{\mathrm{p}}^{-}\right]\\
&\mathrm{Sin}\left[\phi_{\mathrm{p}}\right]\,\mathrm{Sin}[\theta]\,+\,\bar{\alpha}_{\Lambda}\,\bar{\beta}_{\Xi}\,\alpha_{\Lambda}\,\beta_{\Xi}\,\sqrt{1-\alpha\psi^{2}}\,\mathrm{Cos}\left[\theta_{\bar{\Lambda}}^{-}\right]\,\mathrm{Cos}\left[\phi_{\bar{\Lambda}}^{-}\right]\,\mathrm{Cos}[\theta]\,\mathrm{Cos}[\Phi]\,\mathrm{Sin}\left[\theta_{\mathrm{p}}^{-}\right]\\
&\mathrm{Sin}\left[\theta_{\mathrm{p}}\right]\,\mathrm{Sin}[\theta_{\Lambda}]\,\mathrm{Sin}\left[\phi_{\mathrm{p}}^{-}\right]\,\mathrm{Sin}\left[\phi_{\mathrm{p}}\right]\,\mathrm{Sin}[\theta]\,+\,\bar{\alpha}_{\Lambda}\,\bar{\beta}_{\Xi}\,\alpha_{\Lambda}\,\beta_{\Xi}\,\sqrt{1-\alpha\psi^{2}}\,\mathrm{Cos}\left[\phi_{\mathrm{p}}^{-}\right]\,\mathrm{Cos}[\theta]\\
&\mathrm{Cos}[\Phi]\,\mathrm{Sin}\left[\theta_{\mathrm{p}}^{-}\right]\,\mathrm{Sin}\left[\theta_{\mathrm{p}}\right]\,\mathrm{Sin}[\theta_{\Lambda}]\,\mathrm{Sin}\left[\phi_{\bar{\Lambda}}^{-}\right]\,\mathrm{Sin}\left[\phi_{\mathrm{p}}\right]\,\mathrm{Sin}[\theta]\,+\,\bar{\alpha}_{\Lambda}\,\bar{\gamma}_{\Xi}\,\alpha_{\Lambda}\,\beta_{\Xi}\,\sqrt{1-\alpha\psi^{2}}\\
&\mathrm{Cos}[\theta]\,\mathrm{Cos}[\Phi]\,\mathrm{Sin}\left[\theta_{\mathrm{p}}^{-}\right]\,\mathrm{Sin}\left[\theta_{\mathrm{p}}\right]\,\mathrm{Sin}[\theta_{\Lambda}]\,\mathrm{Sin}\left[\phi_{\bar{\Lambda}}^{-}\right]\,\mathrm{Sin}\left[\phi_{\mathrm{p}}^{-}\right]\,\mathrm{Sin}\left[\phi_{\mathrm{p}}\right]\,\mathrm{Sin}[\theta]\,-\\
&\bar{\alpha}_{\Xi}\,\alpha_{\Lambda}\,\beta_{\Xi}\,\sqrt{1-\alpha\psi^{2}}\,\mathrm{Cos}\left[\theta_{\bar{\Lambda}}^{-}\right]\,\mathrm{Cos}\left[\phi_{\mathrm{p}}\right]\,\mathrm{Cos}[\theta]\,\mathrm{Cos}[\Phi]\,\mathrm{Sin}\left[\theta_{\mathrm{p}}\right]\,\mathrm{Sin}[\phi_{\Lambda}]\,\mathrm{Sin}[\theta]\,-\\
&\bar{\alpha}_{\Lambda}\,\alpha_{\Lambda}\,\beta_{\Xi}\,\sqrt{1-\alpha\psi^{2}}\,\mathrm{Cos}\left[\theta_{\mathrm{p}}\right]\,\mathrm{Cos}\left[\theta_{\bar{\Lambda}}^{-}\right]\,\mathrm{Cos}\left[\phi_{\mathrm{p}}\right]\,\mathrm{Cos}[\theta]\,\mathrm{Cos}[\Phi]\,\mathrm{Sin}\left[\theta_{\mathrm{p}}\right]\,\mathrm{Sin}[\phi_{\Lambda}]\,\mathrm{Sin}[\theta]\,+\,\bar{\alpha}_{\Lambda}\,\bar{\gamma}_{\Xi}\,\alpha_{\Lambda}\\
&\beta_{\Xi}\,\sqrt{1-\alpha\psi^{2}}\,\mathrm{Cos}\left[\phi_{\mathrm{p}}^{-}\right]\,\mathrm{Cos}\left[\phi_{\mathrm{p}}\right]\,\mathrm{Cos}[\theta]\,\mathrm{Cos}[\Phi]\,\mathrm{Sin}\left[\theta_{\mathrm{p}}^{-}\right]\,\mathrm{Sin}\left[\theta_{\bar{\Lambda}}^{-}\right]\,\mathrm{Sin}\left[\theta_{\mathrm{p}}\right]\,\mathrm{Sin}[\phi_{\Lambda}]\,\mathrm{Sin}[\theta]\,-\\
&\bar{\alpha}_{\Lambda}\,\bar{\beta}_{\Xi}\,\alpha_{\Lambda}\,\beta_{\Xi}\,\sqrt{1-\alpha\psi^{2}}\,\mathrm{Cos}\left[\phi_{\mathrm{p}}\right]\,\mathrm{Cos}[\theta]\,\mathrm{Cos}[\Phi]\,\mathrm{Sin}\left[\theta_{\mathrm{p}}^{-}\right]\,\mathrm{Sin}\left[\theta_{\bar{\Lambda}}^{-}\right]\,\mathrm{Sin}\left[\theta_{\mathrm{p}}\right]\,\mathrm{Sin}\left[\phi_{\mathrm{p}}^{-}\right]\,\mathrm{Sin}[\phi_{\Lambda}]\\
&\mathrm{Sin}[\theta]\,-\,\bar{\alpha}_{\Xi}\,\alpha_{\Lambda}\,\gamma_{\Xi}\,\sqrt{1-\alpha\psi^{2}}\,\mathrm{Cos}\left[\theta_{\bar{\Lambda}}^{-}\right]\,\mathrm{Cos}[\theta]\,\mathrm{Cos}[\Phi]\,\mathrm{Sin}\left[\theta_{\mathrm{p}}\right]\,\mathrm{Sin}\left[\phi_{\mathrm{p}}\right]\,\mathrm{Sin}[\phi_{\Lambda}]\,\mathrm{Sin}[\theta]\,-\\
&\bar{\alpha}_{\Lambda}\,\alpha_{\Lambda}\,\gamma_{\Xi}\,\sqrt{1-\alpha\psi^{2}}\,\mathrm{Cos}\left[\theta_{\mathrm{p}}^{-}\right]\,\mathrm{Cos}\left[\theta_{\bar{\Lambda}}^{-}\right]\,\mathrm{Cos}[\theta]\,\mathrm{Cos}[\Phi]\,\mathrm{Sin}\left[\theta_{\mathrm{p}}\right]\,\mathrm{Sin}\left[\phi_{\mathrm{p}}\right]\,\mathrm{Sin}[\phi_{\Lambda}]\,\mathrm{Sin}[\theta]\,+\,\bar{\alpha}_{\Lambda}\,\bar{\gamma}_{\Xi}\\
&\alpha_{\Lambda}\,\gamma_{\Xi}\,\sqrt{1-\alpha\psi^{2}}\,\mathrm{Cos}\left[\phi_{\mathrm{p}}^{-}\right]\,\mathrm{Cos}[\theta]\,\mathrm{Cos}[\Phi]\,\mathrm{Sin}\left[\theta_{\mathrm{p}}^{-}\right]\,\mathrm{Sin}\left[\theta_{\bar{\Lambda}}^{-}\right]\,\mathrm{Sin}\left[\theta_{\mathrm{p}}\right]\,\mathrm{Sin}\left[\phi_{\mathrm{p}}\right]\,\mathrm{Sin}[\phi_{\Lambda}]\,\mathrm{Sin}[\theta]\,-\\
&\bar{\alpha}_{\Lambda}\,\bar{\beta}_{\Xi}\,\alpha_{\Lambda}\,\gamma_{\Xi}\,\sqrt{1-\alpha\psi^{2}}\,\mathrm{Cos}[\theta]\,\mathrm{Cos}[\Phi]\,\mathrm{Sin}\left[\theta_{\mathrm{p}}^{-}\right]\,\mathrm{Sin}\left[\theta_{\bar{\Lambda}}^{-}\right]\,\mathrm{Sin}\left[\theta_{\mathrm{p}}\right]\,\mathrm{Sin}\left[\phi_{\mathrm{p}}^{-}\right]\,\mathrm{Sin}\left[\phi_{\mathrm{p}}\right]\,\mathrm{Sin}[\phi_{\Lambda}]\\
&\mathrm{Sin}[\theta]\,+\,\bar{\alpha}_{\Lambda}\,\bar{\beta}_{\Xi}\,\alpha_{\Lambda}\,\beta_{\Xi}\,\alpha\psi\,\mathrm{Cos}\left[\phi_{\mathrm{p}}^{-}\right]\,\mathrm{Cos}\left[\phi_{\bar{\Lambda}}^{-}\right]\,\mathrm{Cos}\left[\phi_{\mathrm{p}}\right]\,\mathrm{Cos}[\phi_{\Lambda}]\,\mathrm{Sin}\left[\theta_{\mathrm{p}}^{-}\right]\,\mathrm{Sin}\left[\theta_{\mathrm{p}}\right]\,\mathrm{Sin}[\theta]^{2}\,+\\
&\bar{\alpha}_{\Lambda}\,\bar{\gamma}_{\Xi}\,\alpha_{\Lambda}\,\gamma_{\Xi}\,\mathrm{Cos}\left[\theta_{\bar{\Lambda}}^{-}\right]\,\mathrm{Cos}[\theta_{\Lambda}]\,\mathrm{Cos}\left[\phi_{\mathrm{p}}^{-}\right]\,\mathrm{Cos}\left[\phi_{\bar{\Lambda}}^{-}\right]\,\mathrm{Cos}\left[\phi_{\mathrm{p}}\right]\,\mathrm{Cos}[\phi_{\Lambda}]\,\mathrm{Sin}\left[\theta_{\mathrm{p}}^{-}\right]\,\mathrm{Sin}\left[\theta_{\mathrm{p}}\right]\,\mathrm{Sin}[\theta]^{2}\,+\\
&\bar{\alpha}_{\Xi}\,\alpha_{\Lambda}\,\gamma_{\Xi}\,\mathrm{Cos}[\theta_{\Lambda}]\,\mathrm{Cos}\left[\phi_{\bar{\Lambda}}^{-}\right]\,\mathrm{Cos}\left[\phi_{\mathrm{p}}\right]\,\mathrm{Cos}[\phi_{\Lambda}]\,\mathrm{Sin}\left[\theta_{\bar{\Lambda}}^{-}\right]\,\mathrm{Sin}\left[\theta_{\mathrm{p}}\right]\,\mathrm{Sin}[\theta]^{2}\,+\\
&\bar{\alpha}_{\Lambda}\,\alpha_{\Lambda}\,\gamma_{\Xi}\,\mathrm{Cos}\left[\theta_{\mathrm{p}}^{-}\right]\,\mathrm{Cos}[\theta_{\Lambda}]\,\mathrm{Cos}\left[\phi_{\bar{\Lambda}}^{-}\right]\,\mathrm{Cos}\left[\phi_{\mathrm{p}}\right]\,\mathrm{Cos}[\phi_{\Lambda}]\,\mathrm{Sin}\left[\theta_{\bar{\Lambda}}^{-}\right]\,\mathrm{Sin}\left[\theta_{\mathrm{p}}\right]\,\mathrm{Sin}[\theta]^{2}\,+
\end{aligned}
$$

Figure 28: joint angular distribution of $e^{+}e^{-} \to J/\psi \to \Xi^{0}\bar{\Xi}^{0}$(c)

$$
\begin{aligned}
&\bar{\alpha}_\Lambda \bar{\gamma}_\Xi \alpha_\Xi \cos\left[\theta_{\bar{\Lambda}}\right] \cos\left[\phi_{\bar{p}}\right] \cos\left[\phi_{\bar{\Lambda}}\right] \cos[\phi_\Lambda] \sin\left[\theta_{\bar{p}}\right] \sin[\theta_\Lambda] \sin[\theta]^2 + \\
&\bar{\alpha}_\Lambda \bar{\gamma}_\Xi \alpha_\Lambda \cos\left[\theta_{\bar{\Lambda}}\right] \cos\left[\theta_p\right] \cos\left[\phi_{\bar{p}}\right] \cos\left[\phi_{\bar{\Lambda}}\right] \cos[\phi_\Lambda] \sin\left[\theta_{\bar{p}}\right] \sin[\theta_\Lambda] \sin[\theta]^2 + \\
&\bar{\alpha}_\Xi \alpha_\Xi \cos\left[\phi_{\bar{\Lambda}}\right] \cos[\phi_\Lambda] \sin\left[\theta_{\bar{\Lambda}}\right] \sin[\theta_\Lambda] \sin[\theta]^2 + \\
&\bar{\alpha}_\Lambda \alpha_\Xi \cos\left[\theta_p\right] \cos\left[\phi_{\bar{\Lambda}}\right] \cos[\phi_\Lambda] \sin\left[\theta_{\bar{\Lambda}}\right] \sin[\theta_\Lambda] \sin[\theta]^2 + \\
&\bar{\alpha}_\Xi \alpha_\Lambda \cos\left[\theta_p\right] \cos\left[\phi_{\bar{\Lambda}}\right] \cos[\phi_\Lambda] \sin\left[\theta_{\bar{\Lambda}}\right] \sin[\theta_\Lambda] \sin[\theta]^2 + \\
&\bar{\alpha}_\Lambda \alpha_\Lambda \cos\left[\theta_{\bar{p}}\right] \cos\left[\theta_p\right] \cos\left[\phi_{\bar{\Lambda}}\right] \cos[\phi_\Lambda] \sin\left[\theta_{\bar{\Lambda}}\right] \sin[\theta_\Lambda] \sin[\theta]^2 + \\
&\bar{\alpha}_\Lambda \bar{\gamma}_\Xi \alpha_\Lambda \beta_\Xi \alpha\psi \cos\left[\phi_{\bar{\Lambda}}\right] \cos\left[\phi_p\right] \cos[\phi_\Lambda] \sin\left[\theta_{\bar{p}}\right] \sin\left[\theta_p\right] \sin\left[\phi_{\bar{p}}\right] \sin[\theta]^2 - \\
&\bar{\alpha}_\Lambda \bar{\beta}_\Xi \alpha_\Lambda \gamma_\Xi \cos\left[\theta_{\bar{\Lambda}}\right] \cos[\theta_\Lambda] \cos\left[\phi_{\bar{\Lambda}}\right] \cos\left[\phi_p\right] \cos[\phi_\Lambda] \sin\left[\theta_{\bar{p}}\right] \sin\left[\theta_p\right] \sin\left[\phi_{\bar{p}}\right] \sin[\theta]^2 - \\
&\bar{\alpha}_\Lambda \bar{\beta}_\Xi \alpha_\Xi \cos\left[\theta_{\bar{\Lambda}}\right] \cos\left[\phi_{\bar{\Lambda}}\right] \cos[\phi_\Lambda] \sin\left[\theta_{\bar{p}}\right] \sin[\theta_\Lambda] \sin\left[\phi_{\bar{p}}\right] \sin[\theta]^2 - \\
&\bar{\alpha}_\Lambda \bar{\beta}_\Xi \alpha_\Lambda \cos\left[\theta_{\bar{\Lambda}}\right] \cos\left[\theta_p\right] \cos\left[\phi_{\bar{\Lambda}}\right] \cos[\phi_\Lambda] \sin\left[\theta_{\bar{p}}\right] \sin[\theta_\Lambda] \sin\left[\phi_{\bar{p}}\right] \sin[\theta]^2 + \\
&\bar{\alpha}_\Lambda \bar{\gamma}_\Xi \alpha_\Lambda \beta_\Xi \alpha\psi \cos\left[\theta_{\bar{\Lambda}}\right] \cos\left[\phi_{\bar{p}}\right] \cos\left[\phi_p\right] \cos[\phi_\Lambda] \sin\left[\theta_{\bar{p}}\right] \sin\left[\theta_p\right] \sin\left[\phi_{\bar{\Lambda}}\right] \sin[\theta]^2 - \\
&\bar{\alpha}_\Lambda \bar{\beta}_\Xi \alpha_\Lambda \gamma_\Xi \cos[\theta_\Lambda] \cos\left[\phi_{\bar{p}}\right] \cos\left[\phi_p\right] \cos[\phi_\Lambda] \sin\left[\theta_{\bar{p}}\right] \sin\left[\theta_p\right] \sin\left[\phi_{\bar{\Lambda}}\right] \sin[\theta]^2 + \\
&\bar{\alpha}_\Lambda \alpha_\Lambda \beta_\Xi \alpha\psi \cos\left[\theta_{\bar{p}}\right] \cos\left[\phi_p\right] \cos[\phi_\Lambda] \sin\left[\theta_{\bar{\Lambda}}\right] \sin\left[\theta_p\right] \sin\left[\phi_{\bar{\Lambda}}\right] \sin[\theta]^2 + \\
&\bar{\alpha}_\Xi \alpha_\Lambda \beta_\Xi \alpha\psi \cos[\theta_\Lambda]^2 \cos\left[\phi_p\right] \cos[\phi_\Lambda] \sin\left[\theta_{\bar{\Lambda}}\right] \sin\left[\theta_p\right] \sin\left[\phi_{\bar{\Lambda}}\right] \sin[\theta]^2 - \\
&\bar{\alpha}_\Lambda \bar{\beta}_\Xi \alpha_\Xi \cos\left[\theta_{\bar{\Lambda}}\right]^2 \cos\left[\phi_{\bar{p}}\right] \cos[\phi_\Lambda] \sin\left[\theta_{\bar{p}}\right] \sin[\theta_\Lambda] \sin\left[\phi_{\bar{\Lambda}}\right] \sin[\theta]^2 - \\
&\bar{\alpha}_\Lambda \bar{\beta}_\Xi \alpha_\Lambda \cos\left[\theta_p\right] \cos\left[\phi_{\bar{p}}\right] \cos[\phi_\Lambda] \sin\left[\theta_p\right] \sin[\theta_\Lambda] \sin\left[\phi_{\bar{\Lambda}}\right] \sin[\theta]^2 - \\
&\bar{\alpha}_\Lambda \bar{\beta}_\Xi \alpha_\Xi \cos\left[\phi_{\bar{p}}\right] \cos[\phi_\Lambda] \sin\left[\theta_p\right] \sin\left[\theta_{\bar{\Lambda}}\right]^2 \sin[\theta_\Lambda] \sin\left[\phi_{\bar{\Lambda}}\right] \sin[\theta]^2 + \\
&\bar{\alpha}_\Xi \alpha_\Lambda \beta_\Xi \alpha\psi \cos\left[\phi_p\right] \cos[\phi_\Lambda] \sin\left[\theta_{\bar{\Lambda}}\right] \sin\left[\theta_p\right] \sin[\theta_\Lambda]^2 \sin\left[\phi_{\bar{\Lambda}}\right] \sin[\theta]^2 - \\
&\bar{\alpha}_\Lambda \bar{\beta}_\Xi \alpha_\Lambda \beta_\Xi \alpha\psi \cos\left[\theta_{\bar{\Lambda}}\right] \cos\left[\phi_p\right] \cos[\phi_\Lambda] \sin\left[\theta_{\bar{p}}\right] \sin\left[\theta_p\right] \sin\left[\phi_{\bar{p}}\right] \sin\left[\phi_{\bar{\Lambda}}\right] \sin[\theta]^2 - \\
&\bar{\alpha}_\Lambda \bar{\gamma}_\Xi \alpha_\Lambda \gamma_\Xi \cos[\theta_\Lambda] \cos\left[\phi_p\right] \cos[\phi_\Lambda] \sin\left[\theta_{\bar{p}}\right] \sin\left[\theta_p\right] \sin\left[\phi_{\bar{p}}\right] \sin\left[\phi_{\bar{\Lambda}}\right] \sin[\theta]^2 - \\
&\bar{\alpha}_\Lambda \bar{\gamma}_\Xi \alpha_\Xi \cos[\phi_\Lambda] \sin\left[\theta_{\bar{p}}\right] \sin[\theta_\Lambda] \sin\left[\phi_{\bar{p}}\right] \sin\left[\phi_{\bar{\Lambda}}\right] \sin[\theta]^2 - \\
&\bar{\alpha}_\Lambda \bar{\gamma}_\Xi \alpha_\Lambda \cos\left[\theta_p\right] \cos[\phi_\Lambda] \sin\left[\theta_{\bar{p}}\right] \sin[\theta_\Lambda] \sin\left[\phi_{\bar{p}}\right] \sin\left[\phi_{\bar{\Lambda}}\right] \sin[\theta]^2 + \\
&\bar{\alpha}_\Lambda \bar{\beta}_\Xi \alpha_\Lambda \gamma_\Xi \alpha\psi \cos\left[\phi_{\bar{p}}\right] \cos\left[\phi_{\bar{\Lambda}}\right] \cos[\phi_\Lambda] \sin\left[\theta_{\bar{p}}\right] \sin\left[\theta_p\right] \sin\left[\phi_p\right] \sin[\theta]^2 - \\
&\bar{\alpha}_\Lambda \bar{\gamma}_\Xi \alpha_\Lambda \beta_\Xi \cos\left[\theta_{\bar{\Lambda}}\right] \cos[\theta_\Lambda] \cos\left[\phi_{\bar{p}}\right] \cos\left[\phi_{\bar{\Lambda}}\right] \cos[\phi_\Lambda] \sin\left[\theta_{\bar{p}}\right] \sin\left[\theta_p\right] \sin\left[\phi_p\right] \sin[\theta]^2 - \\
&\bar{\alpha}_\Xi \alpha_\Lambda \beta_\Xi \cos[\theta_\Lambda] \cos\left[\phi_{\bar{\Lambda}}\right] \cos[\phi_\Lambda] \sin\left[\theta_{\bar{\Lambda}}\right] \sin\left[\theta_p\right] \sin\left[\phi_p\right] \sin[\theta]^2 - \\
&\bar{\alpha}_\Lambda \alpha_\Lambda \beta_\Xi \cos\left[\theta_{\bar{p}}\right] \cos[\theta_\Lambda] \cos\left[\phi_{\bar{\Lambda}}\right] \cos[\phi_\Lambda] \sin\left[\theta_{\bar{\Lambda}}\right] \sin\left[\theta_p\right] \sin\left[\phi_p\right] \sin[\theta]^2 + \\
&\bar{\alpha}_\Lambda \bar{\gamma}_\Xi \alpha_\Lambda \gamma_\Xi \alpha\psi \cos\left[\phi_{\bar{\Lambda}}\right] \cos[\phi_\Lambda] \sin\left[\theta_{\bar{p}}\right] \sin\left[\theta_p\right] \sin\left[\phi_{\bar{p}}\right] \sin\left[\phi_p\right] \sin[\theta]^2 + \\
&\bar{\alpha}_\Lambda \bar{\beta}_\Xi \alpha_\Lambda \beta_\Xi \cos\left[\theta_{\bar{\Lambda}}\right] \cos[\theta_\Lambda] \cos\left[\phi_{\bar{\Lambda}}\right] \cos[\phi_\Lambda] \sin\left[\theta_{\bar{p}}\right] \sin\left[\theta_p\right] \sin\left[\phi_{\bar{p}}\right] \sin\left[\phi_p\right] \sin[\theta]^2 + \\
&\bar{\alpha}_\Lambda \bar{\gamma}_\Xi \alpha_\Lambda \gamma_\Xi \alpha\psi \cos\left[\theta_{\bar{\Lambda}}\right] \cos\left[\phi_{\bar{p}}\right] \cos[\phi_\Lambda] \sin\left[\theta_{\bar{p}}\right] \sin\left[\theta_p\right] \sin\left[\phi_{\bar{\Lambda}}\right] \sin\left[\phi_p\right] \sin[\theta]^2 + \\
&\bar{\alpha}_\Lambda \bar{\beta}_\Xi \alpha_\Lambda \beta_\Xi \cos[\theta_\Lambda] \cos\left[\phi_{\bar{p}}\right] \cos[\phi_\Lambda] \sin\left[\theta_{\bar{p}}\right] \sin\left[\theta_p\right] \sin\left[\phi_{\bar{\Lambda}}\right] \sin\left[\phi_p\right] \sin[\theta]^2 + \\
&\bar{\alpha}_\Xi \alpha_\Lambda \gamma_\Xi \alpha\psi \cos[\phi_\Lambda] \sin\left[\theta_{\bar{\Lambda}}\right] \sin\left[\theta_p\right] \sin\left[\phi_{\bar{\Lambda}}\right] \sin\left[\phi_p\right] \sin[\theta]^2 + \\
&\bar{\alpha}_\Lambda \alpha_\Lambda \gamma_\Xi \alpha\psi \cos\left[\theta_p\right] \cos[\phi_\Lambda] \sin\left[\theta_{\bar{\Lambda}}\right] \sin\left[\theta_p\right] \sin\left[\phi_{\bar{\Lambda}}\right] \sin\left[\phi_p\right] \sin[\theta]^2 - \\
&\bar{\alpha}_\Lambda \bar{\beta}_\Xi \alpha_\Lambda \gamma_\Xi \alpha\psi \cos\left[\theta_{\bar{\Lambda}}\right] \cos[\phi_\Lambda] \sin\left[\theta_p\right] \sin\left[\theta_p\right] \sin\left[\phi_{\bar{p}}\right] \sin\left[\phi_{\bar{\Lambda}}\right] \sin\left[\phi_p\right] \sin[\theta]^2 + \\
&\bar{\alpha}_\Lambda \bar{\gamma}_\Xi \alpha_\Lambda \beta_\Xi \cos[\theta_\Lambda] \cos[\phi_\Lambda] \sin\left[\theta_p\right] \sin\left[\theta_p\right] \sin\left[\phi_{\bar{p}}\right] \sin\left[\phi_{\bar{\Lambda}}\right] \sin[\theta]^2 - \\
&\bar{\alpha}_\Lambda \bar{\gamma}_\Xi \alpha_\Lambda \beta_\Xi \cos\left[\theta_{\bar{\Lambda}}\right] \cos\left[\phi_{\bar{p}}\right] \cos\left[\phi_{\bar{\Lambda}}\right] \cos\left[\phi_p\right] \sin\left[\theta_{\bar{p}}\right] \sin\left[\theta_p\right] \sin[\phi_\Lambda] \sin[\theta]^2 + \\
&\bar{\alpha}_\Lambda \bar{\beta}_\Xi \alpha_\Lambda \gamma_\Xi \alpha\psi \cos[\theta_\Lambda] \cos\left[\phi_{\bar{p}}\right] \cos\left[\phi_{\bar{\Lambda}}\right] \cos\left[\phi_p\right] \sin\left[\theta_{\bar{p}}\right] \sin\left[\theta_p\right] \sin[\phi_\Lambda] \sin[\theta]^2 -
\end{aligned}
$$

Figure 29: joint angular distribution of $e^+e^- \to J/\psi \to \Xi^0\bar{\Xi}^0$(d)

$$
\begin{aligned}
&\bar{\alpha}_\Lambda \bar{\gamma}_\Xi \alpha_\Xi \cos\left[\theta_{\bar{\Lambda}}\right] \cos\left[\phi_{\bar{p}}\right] \cos\left[\phi_{\bar{\Lambda}}\right] \cos[\phi_\Lambda] \sin\left[\theta_{\bar{p}}\right] \sin[\theta_\Lambda] \sin[\theta]^2 + \\
&\bar{\alpha}_\Lambda \bar{\gamma}_\Xi \alpha_\Lambda \cos\left[\theta_{\bar{\Lambda}}\right] \cos\left[\theta_p\right] \cos\left[\phi_{\bar{p}}\right] \cos\left[\phi_{\bar{\Lambda}}\right] \cos[\phi_\Lambda] \sin\left[\theta_{\bar{p}}\right] \sin[\theta_\Lambda] \sin[\theta]^2 + \\
&\bar{\alpha}_\Xi \alpha_\Xi \cos\left[\phi_{\bar{\Lambda}}\right] \cos[\phi_\Lambda] \sin\left[\theta_{\bar{\Lambda}}\right] \sin[\theta_\Lambda] \sin[\theta]^2 + \\
&\bar{\alpha}_\Lambda \alpha_\Xi \cos\left[\theta_p\right] \cos\left[\phi_{\bar{\Lambda}}\right] \cos[\phi_\Lambda] \sin\left[\theta_{\bar{\Lambda}}\right] \sin[\theta_\Lambda] \sin[\theta]^2 + \\
&\bar{\alpha}_\Xi \alpha_\Lambda \cos\left[\theta_p\right] \cos\left[\phi_{\bar{\Lambda}}\right] \cos[\phi_\Lambda] \sin\left[\theta_{\bar{\Lambda}}\right] \sin[\theta_\Lambda] \sin[\theta]^2 + \\
&\bar{\alpha}_\Lambda \alpha_\Lambda \cos\left[\theta_{\bar{p}}\right] \cos\left[\theta_p\right] \cos\left[\phi_{\bar{\Lambda}}\right] \cos[\phi_\Lambda] \sin\left[\theta_{\bar{\Lambda}}\right] \sin[\theta_\Lambda] \sin[\theta]^2 + \\
&\bar{\alpha}_\Lambda \bar{\gamma}_\Xi \alpha_\Lambda \beta_\Xi \alpha\psi \cos\left[\phi_{\bar{\Lambda}}\right] \cos\left[\phi_p\right] \cos[\phi_\Lambda] \sin\left[\theta_{\bar{p}}\right] \sin\left[\theta_p\right] \sin\left[\phi_{\bar{p}}\right] \sin[\theta]^2 - \\
&\bar{\alpha}_\Lambda \bar{\beta}_\Xi \alpha_\Lambda \gamma_\Xi \cos\left[\theta_{\bar{\Lambda}}\right] \cos[\theta_\Lambda] \cos\left[\phi_{\bar{\Lambda}}\right] \cos\left[\phi_p\right] \cos[\phi_\Lambda] \sin\left[\theta_{\bar{p}}\right] \sin\left[\theta_p\right] \sin\left[\phi_{\bar{p}}\right] \sin[\theta]^2 - \\
&\bar{\alpha}_\Lambda \bar{\beta}_\Xi \alpha_\Xi \cos\left[\theta_{\bar{\Lambda}}\right] \cos\left[\phi_{\bar{\Lambda}}\right] \cos[\phi_\Lambda] \sin\left[\theta_{\bar{p}}\right] \sin[\theta_\Lambda] \sin\left[\phi_{\bar{p}}\right] \sin[\theta]^2 - \\
&\bar{\alpha}_\Lambda \bar{\beta}_\Xi \alpha_\Lambda \cos\left[\theta_{\bar{\Lambda}}\right] \cos\left[\theta_p\right] \cos\left[\phi_{\bar{\Lambda}}\right] \cos[\phi_\Lambda] \sin\left[\theta_{\bar{p}}\right] \sin[\theta_\Lambda] \sin\left[\phi_{\bar{p}}\right] \sin[\theta]^2 + \\
&\bar{\alpha}_\Lambda \bar{\gamma}_\Xi \alpha_\Lambda \beta_\Xi \alpha\psi \cos\left[\theta_{\bar{\Lambda}}\right] \cos\left[\phi_{\bar{p}}\right] \cos\left[\phi_p\right] \cos[\phi_\Lambda] \sin\left[\theta_{\bar{p}}\right] \sin\left[\theta_p\right] \sin\left[\phi_{\bar{\Lambda}}\right] \sin[\theta]^2 - \\
&\bar{\alpha}_\Lambda \bar{\beta}_\Xi \alpha_\Lambda \gamma_\Xi \cos[\theta_\Lambda] \cos\left[\phi_{\bar{p}}\right] \cos\left[\phi_p\right] \cos[\phi_\Lambda] \sin\left[\theta_{\bar{p}}\right] \sin\left[\theta_p\right] \sin\left[\phi_{\bar{\Lambda}}\right] \sin[\theta]^2 + \\
&\bar{\alpha}_\Lambda \alpha_\Lambda \beta_\Xi \alpha\psi \cos\left[\theta_{\bar{p}}\right] \cos\left[\phi_p\right] \cos[\phi_\Lambda] \sin\left[\theta_{\bar{\Lambda}}\right] \sin\left[\theta_p\right] \sin\left[\phi_{\bar{\Lambda}}\right] \sin[\theta]^2 + \\
&\bar{\alpha}_\Xi \alpha_\Lambda \beta_\Xi \alpha\psi \cos[\theta_\Lambda]^2 \cos\left[\phi_p\right] \cos[\phi_\Lambda] \sin\left[\theta_{\bar{\Lambda}}\right] \sin\left[\theta_p\right] \sin\left[\phi_{\bar{\Lambda}}\right] \sin[\theta]^2 - \\
&\bar{\alpha}_\Lambda \bar{\beta}_\Xi \alpha_\Xi \cos\left[\theta_{\bar{\Lambda}}\right]^2 \cos\left[\phi_p\right] \cos[\phi_\Lambda] \sin\left[\theta_{\bar{p}}\right] \sin[\theta_\Lambda] \sin\left[\phi_{\bar{\Lambda}}\right] \sin[\theta]^2 - \\
&\bar{\alpha}_\Lambda \bar{\beta}_\Xi \alpha_\Lambda \cos\left[\theta_p\right] \cos\left[\phi_{\bar{p}}\right] \cos[\phi_\Lambda] \sin\left[\theta_{\bar{p}}\right] \sin[\theta_\Lambda] \sin\left[\phi_{\bar{\Lambda}}\right] \sin[\theta]^2 - \\
&\bar{\alpha}_\Lambda \bar{\beta}_\Xi \alpha_\Xi \cos\left[\phi_{\bar{p}}\right] \cos[\phi_\Lambda] \sin\left[\theta_{\bar{p}}\right] \sin\left[\theta_{\bar{\Lambda}}\right]^2 \sin[\theta_\Lambda] \sin\left[\phi_{\bar{\Lambda}}\right] \sin[\theta]^2 + \\
&\bar{\alpha}_\Xi \alpha_\Lambda \beta_\Xi \alpha\psi \cos\left[\phi_p\right] \cos[\phi_\Lambda] \sin\left[\theta_{\bar{\Lambda}}\right] \sin\left[\theta_p\right] \sin[\theta_\Lambda]^2 \sin\left[\phi_{\bar{\Lambda}}\right] \sin[\theta]^2 - \\
&\bar{\alpha}_\Lambda \bar{\beta}_\Xi \alpha_\Lambda \beta_\Xi \alpha\psi \cos\left[\theta_{\bar{\Lambda}}\right] \cos\left[\phi_p\right] \cos[\phi_\Lambda] \sin\left[\theta_{\bar{p}}\right] \sin\left[\theta_p\right] \sin\left[\phi_{\bar{p}}\right] \sin\left[\phi_{\bar{\Lambda}}\right] \sin[\theta]^2 - \\
&\bar{\alpha}_\Lambda \bar{\gamma}_\Xi \alpha_\Lambda \gamma_\Xi \cos[\theta_\Lambda] \cos\left[\phi_p\right] \cos[\phi_\Lambda] \sin\left[\theta_{\bar{p}}\right] \sin\left[\theta_p\right] \sin\left[\phi_{\bar{p}}\right] \sin\left[\phi_{\bar{\Lambda}}\right] \sin[\theta]^2 - \\
&\bar{\alpha}_\Lambda \bar{\gamma}_\Xi \alpha_\Xi \cos[\phi_\Lambda] \sin\left[\theta_{\bar{p}}\right] \sin[\theta_\Lambda] \sin\left[\phi_{\bar{p}}\right] \sin\left[\phi_{\bar{\Lambda}}\right] \sin[\theta]^2 - \\
&\bar{\alpha}_\Lambda \bar{\gamma}_\Xi \alpha_\Lambda \cos\left[\theta_p\right] \cos[\phi_\Lambda] \sin\left[\theta_{\bar{p}}\right] \sin[\theta_\Lambda] \sin\left[\phi_{\bar{p}}\right] \sin\left[\phi_{\bar{\Lambda}}\right] \sin[\theta]^2 + \\
&\bar{\alpha}_\Lambda \bar{\beta}_\Xi \alpha_\Lambda \gamma_\Xi \alpha\psi \cos\left[\phi_{\bar{p}}\right] \cos\left[\phi_{\bar{\Lambda}}\right] \cos[\phi_\Lambda] \sin\left[\theta_{\bar{p}}\right] \sin\left[\theta_p\right] \sin\left[\phi_p\right] \sin[\theta]^2 - \\
&\bar{\alpha}_\Lambda \bar{\gamma}_\Xi \alpha_\Lambda \beta_\Xi \cos\left[\theta_{\bar{\Lambda}}\right] \cos[\theta_\Lambda] \cos\left[\phi_{\bar{p}}\right] \cos\left[\phi_{\bar{\Lambda}}\right] \cos[\phi_\Lambda] \sin\left[\theta_{\bar{p}}\right] \sin\left[\theta_p\right] \sin\left[\phi_p\right] \sin[\theta]^2 - \\
&\bar{\alpha}_\Xi \alpha_\Lambda \beta_\Xi \cos[\theta_\Lambda] \cos\left[\phi_{\bar{\Lambda}}\right] \cos[\phi_\Lambda] \sin\left[\theta_{\bar{\Lambda}}\right] \sin\left[\theta_p\right] \sin\left[\phi_p\right] \sin[\theta]^2 - \\
&\bar{\alpha}_\Lambda \alpha_\Lambda \beta_\Xi \cos\left[\theta_p\right] \cos[\theta_\Lambda] \cos\left[\phi_{\bar{\Lambda}}\right] \cos[\phi_\Lambda] \sin\left[\theta_{\bar{\Lambda}}\right] \sin\left[\theta_p\right] \sin\left[\phi_p\right] \sin[\theta]^2 + \\
&\bar{\alpha}_\Lambda \bar{\gamma}_\Xi \alpha_\Lambda \gamma_\Xi \alpha\psi \cos\left[\phi_{\bar{\Lambda}}\right] \cos[\phi_\Lambda] \sin\left[\theta_{\bar{p}}\right] \sin\left[\theta_p\right] \sin\left[\phi_{\bar{p}}\right] \sin\left[\phi_p\right] \sin[\theta]^2 + \\
&\bar{\alpha}_\Lambda \bar{\beta}_\Xi \alpha_\Lambda \beta_\Xi \cos\left[\theta_{\bar{\Lambda}}\right] \cos[\theta_\Lambda] \cos\left[\phi_{\bar{\Lambda}}\right] \cos[\phi_\Lambda] \sin\left[\theta_{\bar{p}}\right] \sin\left[\theta_p\right] \sin\left[\phi_{\bar{p}}\right] \sin\left[\phi_p\right] \sin[\theta]^2 + \\
&\bar{\alpha}_\Lambda \bar{\gamma}_\Xi \alpha_\Lambda \gamma_\Xi \alpha\psi \cos\left[\theta_{\bar{\Lambda}}\right] \cos\left[\phi_{\bar{p}}\right] \cos[\phi_\Lambda] \sin\left[\theta_{\bar{p}}\right] \sin\left[\theta_p\right] \sin\left[\phi_{\bar{\Lambda}}\right] \sin\left[\phi_p\right] \sin[\theta]^2 + \\
&\bar{\alpha}_\Lambda \bar{\beta}_\Xi \alpha_\Lambda \beta_\Xi \cos[\theta_\Lambda] \cos\left[\phi_{\bar{p}}\right] \cos[\phi_\Lambda] \sin\left[\theta_{\bar{p}}\right] \sin\left[\theta_p\right] \sin\left[\phi_{\bar{\Lambda}}\right] \sin\left[\phi_p\right] \sin[\theta]^2 + \\
&\bar{\alpha}_\Xi \alpha_\Lambda \gamma_\Xi \alpha\psi \cos[\phi_\Lambda] \sin\left[\theta_{\bar{\Lambda}}\right] \sin\left[\theta_p\right] \sin\left[\phi_{\bar{\Lambda}}\right] \sin\left[\phi_p\right] \sin[\theta]^2 + \\
&\bar{\alpha}_\Lambda \alpha_\Lambda \gamma_\Xi \alpha\psi \cos\left[\theta_{\bar{p}}\right] \cos[\phi_\Lambda] \sin\left[\theta_{\bar{\Lambda}}\right] \sin\left[\theta_p\right] \sin\left[\phi_{\bar{\Lambda}}\right] \sin\left[\phi_p\right] \sin[\theta]^2 - \\
&\bar{\alpha}_\Lambda \bar{\beta}_\Xi \alpha_\Lambda \gamma_\Xi \alpha\psi \cos\left[\theta_{\bar{\Lambda}}\right] \cos[\phi_\Lambda] \sin\left[\theta_{\bar{p}}\right] \sin\left[\theta_p\right] \sin\left[\phi_{\bar{p}}\right] \sin\left[\phi_{\bar{\Lambda}}\right] \sin\left[\phi_p\right] \sin[\theta]^2 + \\
&\bar{\alpha}_\Lambda \bar{\gamma}_\Xi \alpha_\Lambda \beta_\Xi \cos[\theta_\Lambda] \cos[\phi_\Lambda] \sin\left[\theta_{\bar{p}}\right] \sin\left[\theta_p\right] \sin\left[\phi_{\bar{p}}\right] \sin\left[\phi_{\bar{\Lambda}}\right] \sin\left[\phi_p\right] \sin[\theta]^2 - \\
&\bar{\alpha}_\Lambda \bar{\gamma}_\Xi \alpha_\Lambda \beta_\Xi \cos\left[\theta_{\bar{\Lambda}}\right] \cos\left[\phi_p\right] \cos\left[\phi_{\bar{\Lambda}}\right] \cos\left[\phi_p\right] \sin\left[\theta_{\bar{p}}\right] \sin\left[\theta_p\right] \sin[\phi_\Lambda] \sin[\theta]^2 + \\
&\bar{\alpha}_\Lambda \bar{\beta}_\Xi \alpha_\Lambda \gamma_\Xi \alpha\psi \cos[\theta_\Lambda] \cos\left[\phi_{\bar{p}}\right] \cos\left[\phi_{\bar{\Lambda}}\right] \cos\left[\phi_p\right] \sin\left[\theta_{\bar{p}}\right] \sin\left[\theta_p\right] \sin[\phi_\Lambda] \sin[\theta]^2 -
\end{aligned}
$$

Figure 30: joint angular distribution of $e^+e^- \to J/\psi \to \Xi^0\bar{\Xi}^0$(e)

$$
\begin{aligned}
&\bar{\alpha}_\Lambda \bar{\beta}_\Xi \sqrt{1-\alpha\psi^2}\, \mathrm{Cos}\left[\bar{\phi}_p\right] \mathrm{Cos}\left[\bar{\phi}_\Lambda\right] \mathrm{Cos}[\theta]\, \mathrm{Sin}\left[\bar{\theta}_p\right] \mathrm{Sin}[\theta]\, \mathrm{Sin}[\Phi] + \\
&\bar{\alpha}_\Lambda \bar{\beta}_\Xi \alpha_\Lambda \alpha_\Xi \sqrt{1-\alpha\psi^2}\, \mathrm{Cos}\left[\theta_p\right] \mathrm{Cos}\left[\phi_p\right] \mathrm{Cos}\left[\phi_{\bar{\Lambda}}\right] \mathrm{Cos}[\theta]\, \mathrm{Sin}\left[\theta_p\right] \mathrm{Sin}[\theta]\, \mathrm{Sin}[\Phi] - \\
&\alpha_\Lambda \beta_\Xi \sqrt{1-\alpha\psi^2}\, \mathrm{Cos}\left[\phi_p\right] \mathrm{Cos}[\phi_\Lambda] \mathrm{Cos}[\theta]\, \mathrm{Sin}\left[\theta_p\right] \mathrm{Sin}[\theta]\, \mathrm{Sin}[\Phi] - \\
&\bar{\alpha}_\Lambda \bar{\alpha}_\Xi \alpha_\Lambda \beta_\Xi \sqrt{1-\alpha\psi^2}\, \mathrm{Cos}\left[\theta_p\right] \mathrm{Cos}\left[\phi_p\right] \mathrm{Cos}[\phi_\Lambda] \mathrm{Cos}[\theta]\, \mathrm{Sin}\left[\theta_p\right] \mathrm{Sin}[\theta]\, \mathrm{Sin}[\Phi] + \\
&\bar{\alpha}_\Lambda \bar{\gamma}_\Xi \sqrt{1-\alpha\psi^2}\, \mathrm{Cos}\left[\bar{\phi}_\Lambda\right] \mathrm{Cos}[\theta]\, \mathrm{Sin}\left[\theta_p\right] \mathrm{Sin}\left[\phi_p\right] \mathrm{Sin}[\theta]\, \mathrm{Sin}[\Phi] + \\
&\bar{\alpha}_\Lambda \bar{\gamma}_\Xi \alpha_\Lambda \alpha_\Xi \sqrt{1-\alpha\psi^2}\, \mathrm{Cos}\left[\theta_p\right] \mathrm{Cos}\left[\bar{\phi}_\Lambda\right] \mathrm{Cos}[\theta]\, \mathrm{Sin}\left[\theta_p\right] \mathrm{Sin}\left[\phi_p\right] \mathrm{Sin}[\theta]\, \mathrm{Sin}[\Phi] + \\
&\bar{\alpha}_\Lambda \bar{\gamma}_\Xi \sqrt{1-\alpha\psi^2}\, \mathrm{Cos}\left[\bar{\theta}_\Lambda\right] \mathrm{Cos}\left[\bar{\phi}_p\right] \mathrm{Cos}[\theta]\, \mathrm{Sin}\left[\bar{\theta}_p\right] \mathrm{Sin}\left[\bar{\phi}_\Lambda\right] \mathrm{Sin}[\theta]\, \mathrm{Sin}[\Phi] + \\
&\bar{\alpha}_\Lambda \bar{\gamma}_\Xi \alpha_\Lambda \alpha_\Xi \sqrt{1-\alpha\psi^2}\, \mathrm{Cos}\left[\bar{\theta}_\Lambda\right] \mathrm{Cos}\left[\theta_p\right] \mathrm{Cos}\left[\bar{\phi}_p\right] \mathrm{Cos}[\theta]\, \mathrm{Sin}\left[\bar{\theta}_p\right] \mathrm{Sin}\left[\bar{\phi}_\Lambda\right] \mathrm{Sin}[\theta]\, \mathrm{Sin}[\Phi] + \\
&\bar{\alpha}_\Xi \sqrt{1-\alpha\psi^2}\, \mathrm{Cos}[\theta]\, \mathrm{Sin}\left[\theta_{\bar{\Lambda}}\right] \mathrm{Sin}\left[\phi_{\bar{\Lambda}}\right] \mathrm{Sin}[\theta]\, \mathrm{Sin}[\Phi] + \\
&\bar{\alpha}_\Lambda \sqrt{1-\alpha\psi^2}\, \mathrm{Cos}\left[\bar{\theta}_p\right] \mathrm{Cos}[\theta]\, \mathrm{Sin}\left[\bar{\theta}_\Lambda\right] \mathrm{Sin}\left[\bar{\phi}_\Lambda\right] \mathrm{Sin}[\theta]\, \mathrm{Sin}[\Phi] + \\
&\bar{\alpha}_\Xi \alpha_\Lambda \alpha_\Xi \sqrt{1-\alpha\psi^2}\, \mathrm{Cos}\left[\theta_p\right] \mathrm{Cos}[\theta]\, \mathrm{Sin}\left[\bar{\theta}_\Lambda\right] \mathrm{Sin}\left[\bar{\phi}_\Lambda\right] \mathrm{Sin}[\theta]\, \mathrm{Sin}[\Phi] + \\
&\bar{\alpha}_\Lambda \alpha_\Lambda \alpha_\Xi \sqrt{1-\alpha\psi^2}\, \mathrm{Cos}\left[\theta_p\right] \mathrm{Cos}\left[\theta_p\right] \mathrm{Cos}[\theta]\, \mathrm{Sin}\left[\bar{\theta}_\Lambda\right] \mathrm{Sin}\left[\bar{\phi}_\Lambda\right] \mathrm{Sin}[\theta]\, \mathrm{Sin}[\Phi] - \\
&\bar{\alpha}_\Lambda \bar{\beta}_\Xi \sqrt{1-\alpha\psi^2}\, \mathrm{Cos}\left[\bar{\theta}_\Lambda\right] \mathrm{Cos}[\theta]\, \mathrm{Sin}\left[\bar{\theta}_p\right] \mathrm{Sin}\left[\bar{\phi}_p\right] \mathrm{Sin}\left[\bar{\phi}_\Lambda\right] \mathrm{Sin}[\theta]\, \mathrm{Sin}[\Phi] - \\
&\bar{\alpha}_\Lambda \bar{\beta}_\Xi \alpha_\Lambda \alpha_\Xi \sqrt{1-\alpha\psi^2}\, \mathrm{Cos}\left[\bar{\theta}_\Lambda\right] \mathrm{Cos}\left[\theta_p\right] \mathrm{Cos}[\theta]\, \mathrm{Sin}\left[\bar{\theta}_p\right] \mathrm{Sin}\left[\bar{\phi}_p\right] \mathrm{Sin}\left[\bar{\phi}_\Lambda\right] \mathrm{Sin}[\theta]\, \mathrm{Sin}[\Phi] - \\
&\alpha_\Lambda \gamma_\Xi \sqrt{1-\alpha\psi^2}\, \mathrm{Cos}[\phi_\Lambda] \mathrm{Cos}[\theta]\, \mathrm{Sin}\left[\theta_p\right] \mathrm{Sin}\left[\phi_p\right] \mathrm{Sin}[\theta]\, \mathrm{Sin}[\Phi] - \\
&\bar{\alpha}_\Lambda \bar{\alpha}_\Xi \alpha_\Lambda \gamma_\Xi \sqrt{1-\alpha\psi^2}\, \mathrm{Cos}\left[\bar{\theta}_p\right] \mathrm{Cos}[\phi_\Lambda] \mathrm{Cos}[\theta]\, \mathrm{Sin}\left[\theta_p\right] \mathrm{Sin}\left[\phi_p\right] \mathrm{Sin}[\theta]\, \mathrm{Sin}[\Phi] - \\
&\alpha_\Lambda \gamma_\Xi \sqrt{1-\alpha\psi^2}\, \mathrm{Cos}[\theta_\Lambda] \mathrm{Cos}\left[\phi_p\right] \mathrm{Cos}[\theta]\, \mathrm{Sin}\left[\theta_p\right] \mathrm{Sin}[\phi_\Lambda] \mathrm{Sin}[\theta]\, \mathrm{Sin}[\Phi] - \\
&\bar{\alpha}_\Lambda \bar{\alpha}_\Xi \alpha_\Lambda \gamma_\Xi \sqrt{1-\alpha\psi^2}\, \mathrm{Cos}\left[\bar{\theta}_p\right] \mathrm{Cos}[\theta_\Lambda] \mathrm{Cos}\left[\phi_p\right] \mathrm{Cos}[\theta]\, \mathrm{Sin}\left[\theta_p\right] \mathrm{Sin}[\phi_\Lambda] \mathrm{Sin}[\theta]\, \mathrm{Sin}[\Phi] - \\
&\alpha_\Xi \sqrt{1-\alpha\psi^2}\, \mathrm{Cos}[\theta]\, \mathrm{Sin}[\theta_\Lambda] \mathrm{Sin}[\phi_\Lambda] \mathrm{Sin}[\theta]\, \mathrm{Sin}[\Phi] - \\
&\bar{\alpha}_\Lambda \bar{\alpha}_\Xi \alpha_\Xi \sqrt{1-\alpha\psi^2}\, \mathrm{Cos}\left[\bar{\theta}_p\right] \mathrm{Cos}[\theta]\, \mathrm{Sin}[\theta_\Lambda] \mathrm{Sin}[\phi_\Lambda] \mathrm{Sin}[\theta]\, \mathrm{Sin}[\Phi] - \\
&\alpha_\Lambda \sqrt{1-\alpha\psi^2}\, \mathrm{Cos}\left[\theta_p\right] \mathrm{Cos}[\theta]\, \mathrm{Sin}[\theta_\Lambda] \mathrm{Sin}[\phi_\Lambda] \mathrm{Sin}[\theta]\, \mathrm{Sin}[\Phi] - \\
&\bar{\alpha}_\Lambda \bar{\alpha}_\Xi \alpha_\Lambda \sqrt{1-\alpha\psi^2}\, \mathrm{Cos}\left[\bar{\theta}_p\right] \mathrm{Cos}\left[\theta_p\right] \mathrm{Cos}[\theta]\, \mathrm{Sin}[\theta_\Lambda] \mathrm{Sin}[\phi_\Lambda] \mathrm{Sin}[\theta]\, \mathrm{Sin}[\Phi] + \\
&\alpha_\Lambda \beta_\Xi \sqrt{1-\alpha\psi^2}\, \mathrm{Cos}[\theta_\Lambda] \mathrm{Cos}[\theta]\, \mathrm{Sin}\left[\theta_p\right] \mathrm{Sin}\left[\phi_p\right] \mathrm{Sin}[\phi_\Lambda] \mathrm{Sin}[\theta]\, \mathrm{Sin}[\Phi] + \\
&\bar{\alpha}_\Lambda \bar{\alpha}_\Xi \alpha_\Lambda \beta_\Xi \sqrt{1-\alpha\psi^2}\, \mathrm{Cos}\left[\bar{\theta}_p\right] \mathrm{Cos}[\theta_\Lambda] \mathrm{Cos}[\theta]\, \mathrm{Sin}\left[\theta_p\right] \mathrm{Sin}\left[\phi_p\right] \mathrm{Sin}[\phi_\Lambda] \mathrm{Sin}[\theta]\, \mathrm{Sin}[\Phi]
\end{aligned}
$$

Figure 31: joint angular distribution of $e^+e^- \to J/\psi \to \Xi^0\bar{\Xi}^0$(f)

B Control sample of BKG B

For $\Lambda \to \gamma n$ ($\bar{\Lambda} \to \gamma \bar{n}$) process, the BKG Bs are events of $\Lambda \to \pi^0 n$ ($\bar{\Lambda} \to \pi^0 \bar{n}$) process, whose photon candidate determined by the kinematic fit for $\bar{\Lambda}\Lambda\bar{n}\gamma$ hypothesis is none of the π^0 decay photons, but other noise showers(possibly secondary showers of the n($\bar{n}$) reaction with matters in the EMC). At this point Geant4(MC) can not simulate the noise showers accurately so we try to obtain the shape of BKG B through a data control sample.

The control sample is obtained from $J/\psi \to \Lambda\bar{\Lambda}$, $\Lambda \to p\pi^-$, $\bar{\Lambda} \to \pi^0\bar{n}$ ($J/\psi \to \Lambda\bar{\Lambda}$, $\bar{\Lambda} \to \bar{p}\pi^+$, $\Lambda \to \pi^0 n$) process, respectively. The general steps of event selection is: first, reconstruct the $\Lambda \to p\pi^-$ with a proton, a π^-; second, reconstruct $\bar{\Lambda} \to \pi^0\bar{n}$ with two photons(π^0) and a anti-neutron; third, applying kinematic fit of signal final state hypothesis of $\Lambda\gamma\bar{n}$; finally, require the photon candidate of $\bar{\Lambda} \to \gamma\bar{n}$ is not the two photons of reconstructed π^0 in second step. The detail selection creteria are introduced at the end of this chapter.

The shape extraction of BKG B from control sample is shown in Fig. 32. There are three components to describe the distribution of data sample. The green line is the shape of BKG B, which is modeled by a gaussian function whose parameters are floated and determined by the fit, as shown in Table 16. The blue line is the shape of process of $\Lambda \to \gamma n$, which is modeled by the MC shape extracted from exclusive MC of $\Lambda \to \gamma n$. The red line corresponds to the special cases that the photon candidate is the signal γ from π^0, these events refers to the two γs of π^0 are not signal photons during the reconstrction of π^0.

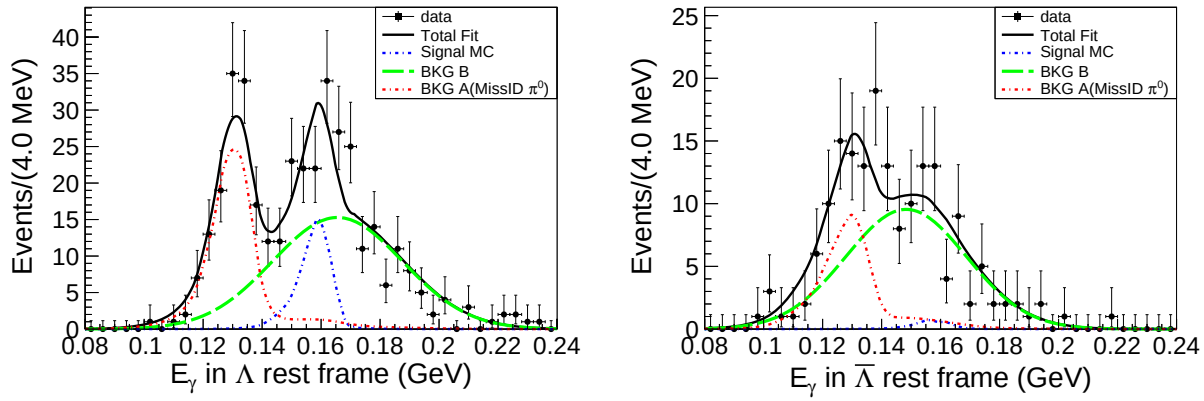

(a) (b)

Figure 32: Distribution of the E_γ in $\Lambda(\bar{\Lambda})$ rest frame of the control sample. The left (right) plot is for $\Lambda \to \gamma n$ ($\bar{\Lambda} \to \gamma\bar{n}$), respectively. To extract the BKG B shape, a gaussian function with floated parameters is used to model the shape, which is in dashed green line. The other two constituents are modeled with shapes obtained from exclusive MC, as mentioned in previous content.

Actually the control sample of BKG B is obtained from $J/\psi \to \Lambda\bar{\Lambda}$, $\Lambda \to p\pi^-$, $\bar{\Lambda} \to \pi^0\bar{n}$ process,

Table 16: Parameters of the BKG B shape described by Gaussian function

Fit Parameters	mean (MeV)	sigma (MeV)
$\Lambda \to \gamma n$	165.6±2.6	22.1±1.5
$\bar{\Lambda} \to \gamma \bar{n}$	148.3±2.9	20.4±1.7

however, sometimes the π^0 can not be reconstructed when the signal photons are not detected by the EMC. So we use MC to validate that the shape of BKG B in control sample can represent the shape of all the BKG B events, as shown in Fig. 33, the shapes of BKG B whether the π^0 is reconstructed are basically consistent.

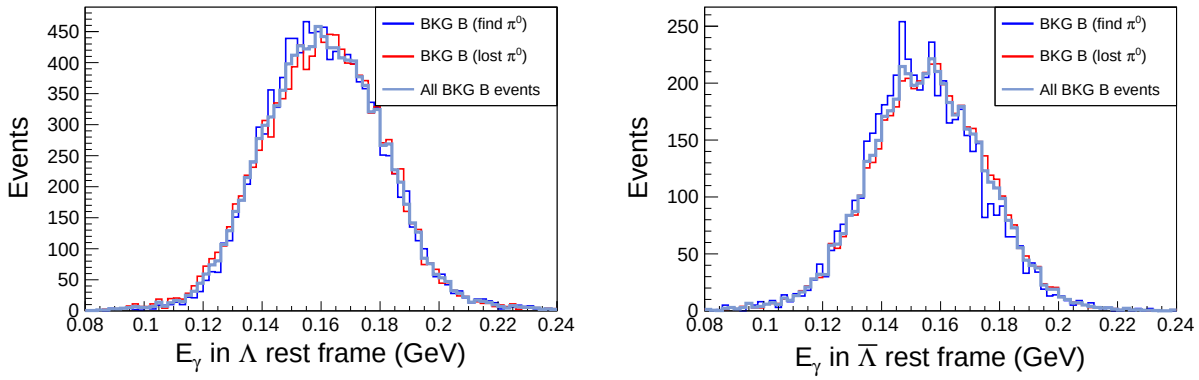

(a) (b)

Figure 33: Comparison of distribution of the E_γ in $\Lambda(\bar{\Lambda})$ rest frame of BKG B for $\Lambda \to \gamma n$ (left) and $\bar{\Lambda} \to \gamma \bar{n}$ (right). The blue line indicates the case that π^0 is reconstructed and the red line indicates the case the π^0s is not successfully reconstructed. The stone blue indicates all BKG B events.

The detail selection criteria of BKG B control sample from $J/\psi \to \Lambda\bar{\Lambda}, \Lambda \to p\pi^-, \bar{\Lambda} \to \bar{n}\pi^0$ process, the detail creteria are listed as :

- **Good charged tracks**

  $\to V_{xy}$ <10 cm, $|V_z|$ <30 cm, $|cos\theta| < 0.93$

  $\to N_p \geq 1$, $N_{\pi^-} \geq 1$,

- $p^\pm, \pi^\pm$ **identification**

  $\to p^\pm : p > 0.5$ GeV/c and $prob(p) > prob(\pi)\&\&prob(p) > prob(K)$

  $\to \pi^\pm : p < 0.5$ GeV/c

- **Vertex fit**

  $\to \chi^2_{\text{sec}} < 20, L/\sigma_L > 2.0$

→ $|M(p\pi^-) - 1115.7| < 8$ MeV/c^2,

- **Good EMC showers**

  → $E > 25$ MeV (barrel:$|cos\theta| < 0.8$), $E > 50$ MeV (endcap:$0.86 < |cos\theta| < 0.92$)

  → $N_{shower} \geq 2$ for $\Lambda \to n\pi^0$, while 3 for $\bar{\Lambda} \to \bar{n}\pi^0$.

  → $0 \leq t_{TDC} \leq 700$ ns.

  → $\theta(\gamma, \text{track}) > 20°$ for anti-proton, while $\theta(\gamma, \text{track}) > 10°$ for other tracks, where $\theta(\gamma, \text{track})$ is the open angle between the charged tracks and the showers in EMC.

- $\bar{n}$ **selection**

  → The most energetic shower in the EMC,

  → $E_{\bar{n}} > 400$ MeV.

- π^0 **selection**

  → 1C kinematic fit for all possible combinations of photons .

  → $\chi^2_{\pi^0} < 25$.

  → $N_{\pi^0} > 0$.

- **Kinematic fit**

  → $\chi^2_{1C}(\Lambda \to n\pi^0) < 100$ (optimized according to Figure 34(a b).)

  → $\chi^2_{3C}(\bar{\Lambda} \to \bar{n}\pi^0) < 200$ (optimized according to Figure 34(c d).)

- **Selection criteria for** $\Lambda \to \gamma n$ ($\bar{\Lambda} \to \gamma\bar{n}$)

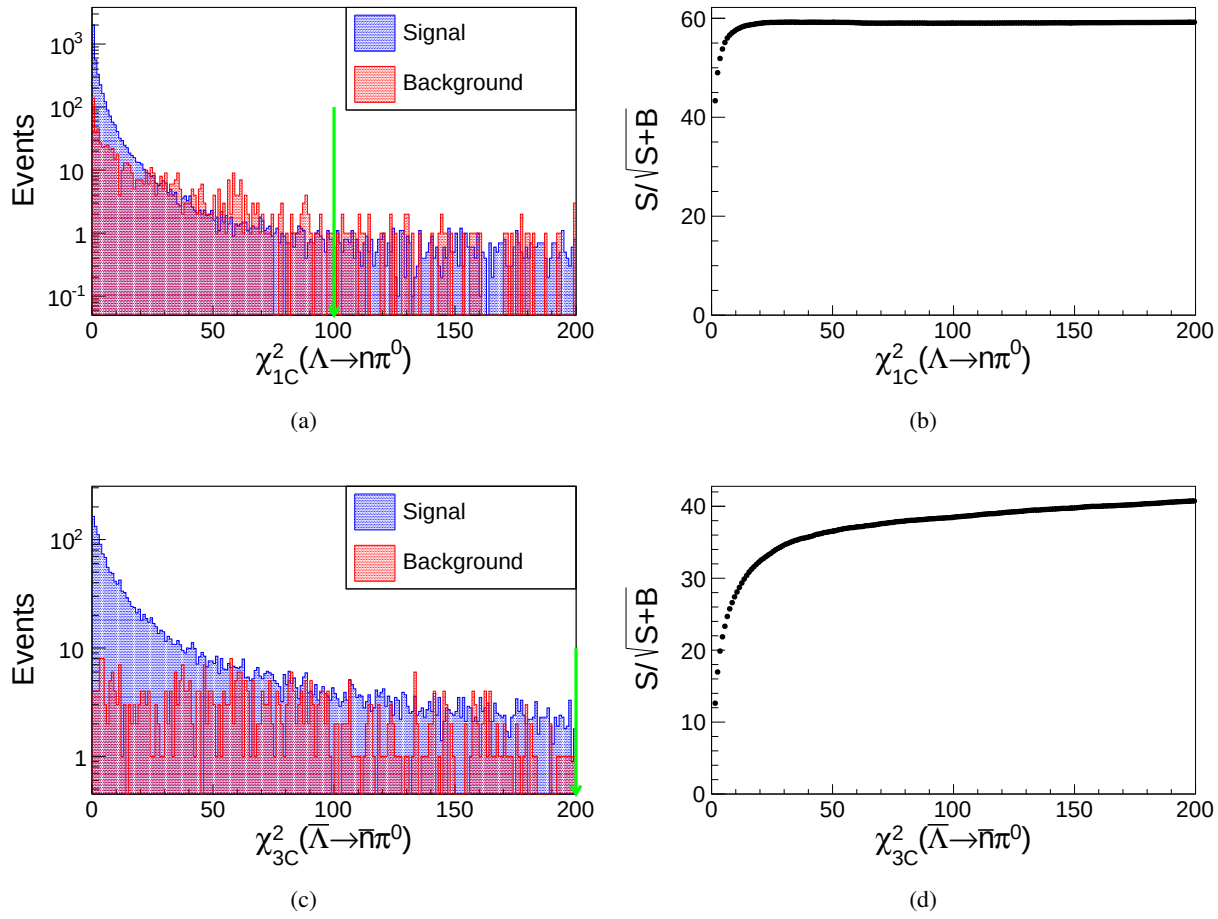

Figure 34: (a b) The distribution of $\chi^2_{1C}(\Lambda \to n\pi^0)$ and $\chi^2_{3C}(\bar{\Lambda} \to \bar{n}\pi^0)$ (c d) the optimization curve, where S and B stands for Signal and background yields, respectively.

C Performance comparison of MVA models

To further reject the BKG B, BDT(G) model has been adopted. In fact, the several Multivariate Data Analysis(MVA) models are compared. As mentioned in the previous content, the input vaiables of MVA models are emc shower information, as shown in Table 17. Trainning and testinf samples of MVA models of photon candidates are obtained from signal MC and BKG B MC. The correlation matrix of the input variables are shown in Fig. 35, which indicate the relational degree between two shower variables. The performace of MVA models is evaluated by the signal efficiency vs background rejection rate curve, which is shown in Fig. 36, obviously the BDT(G) has the best performace.

The energy of photon candidate is also used in BDT because the performace will be better when using the energy as one of the iuput variables of BDT, according to Fig. 37.

Table 17: MVA input variables of EMC shower information of photon candidates.

Photon Shower Information	Description
E_γ	Energy
N_{hit}	Hit number
$\sum_{i=1}^{i=N} E_i r_i^2 / \sum_{i=1}^{i=N} E_i$	Second moment
M_{42}	$A42$ moment
$(e5x5 - e3x3)/e5x5$	Shower shape

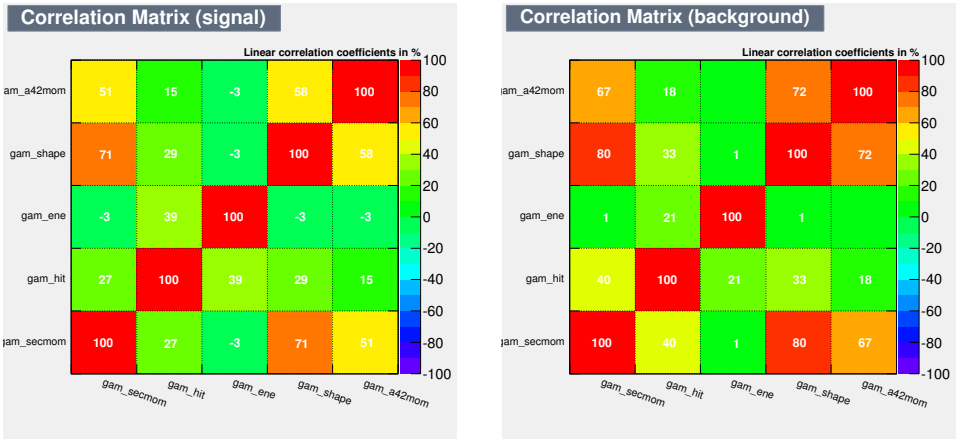

(a) $\Lambda \to \gamma n$ (b) $\Lambda \to \gamma n$

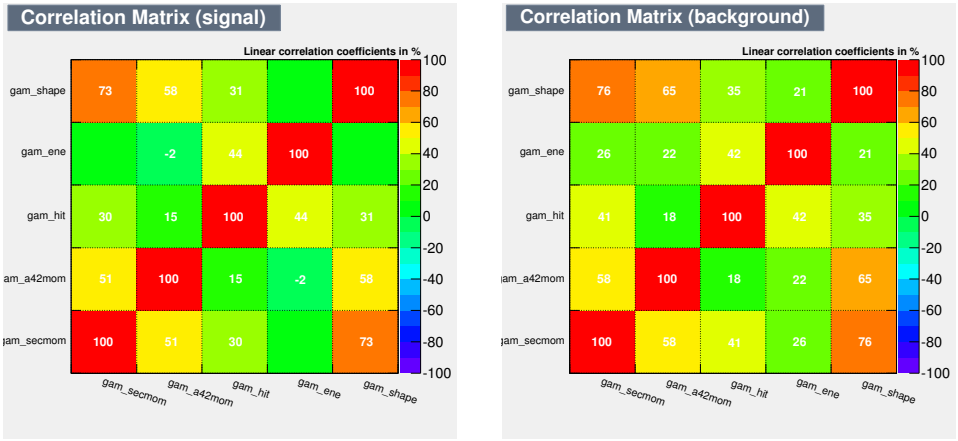

(c) $\bar{\Lambda} \to \gamma \bar{n}$ (d) $\bar{\Lambda} \to \gamma \bar{n}$

Figure 35: The correlation matrix of the input variables of signal and BKG B.

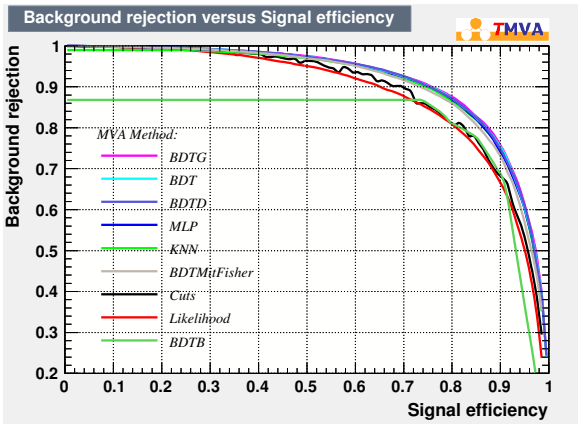

Figure 36: Performance comparison of different MVA classifier models. The BDT(G) has the best perfirmace.

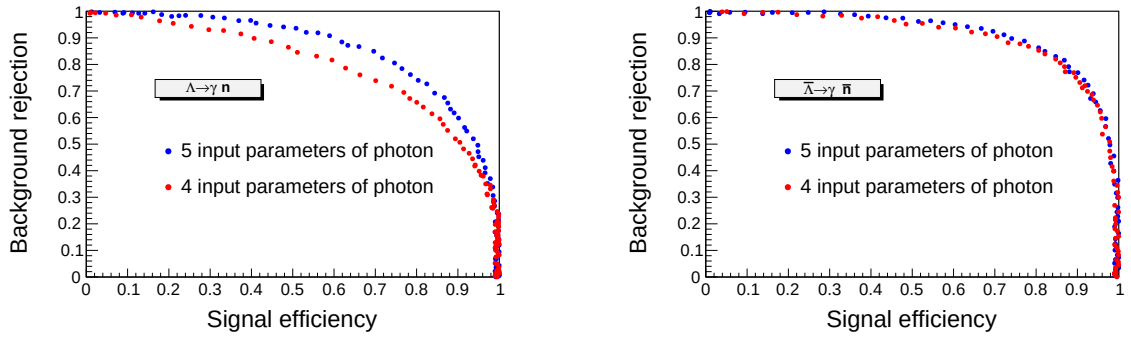

(a) $\Lambda \to \gamma n$ (b) $\Lambda \to \gamma n$

Figure 37: Performace comparison of BDT(G). When using the E_γ as input variables(5 input parameters of photon candidate) , the performace is much better than that not using the E_γ as input variables(4 input parameters of photon candidate).

D Correction of ST efficiency

To reconstruct the Λ signal with its decay mode $\Lambda \to \pi^- p$. Candidate events are required to have at least one proton and one π^-, vertex fit and secondary vertex fit for $\Lambda \to \pi^- p$ decay are used to reconstruct Λ . Since the signal yields of single tag exist 3.5% difference between two charge conjugated modes after the efficiency correction. Detail studies indicate that this difference is due to the MC efficiency of single tag. Detail check for the single tag efficiency of (anti-)proton selection, π^+ (π^-) selection and vertex fit and secondary vertex fit will be introduced in this chapter.

The efficiency of single tag includes three parts: tracking, PID, and (second)vertex fit. The process of $J/\psi \to \Lambda\bar{\Lambda}, \Lambda \to \pi^- p, \bar{\Lambda} \to \pi^+ \bar{p}$ is used to study the efficiency. All the J/ψ data and equal luminosity of generated exclusive MC are used.

- **Tracking efficiency**

  The tracking effiency is defined by the formula:

$$\varepsilon_{trk} = \frac{N}{N+n}, \tag{16}$$

  where **N** is the number of events in which the missing particle is found and **n** is the number of events in which the missing particle is not found. Taking proton for example, to get the tracking efficiency, the recoil mass of proton is obtained by using other particles of the final state: first use signal tag (ST) to reconstruct a $\bar{\Lambda}$ with its charged decay mode $\bar{\Lambda} \to \pi^+ \bar{p}$, same as the event selection in chapter 3; second recoil the proton with the tag $\bar{\Lambda}$ and one π^- to get the recoil mass distribution of proton, which is shown in Fig. 38. The N is the yield of recoil mass distribution

of proton with no requirement for the number of the track. The n is the yield of recoil mass distribution of proton with requirement of track number of proton: $N^{trk}_{proton} > 0$. Note that for N^{trk}_{proton} the protons are identified by the momentum, as the the charged track pion and proton are well seperated in kinematic and (anti-)proton inherits most of the energy of (anti-)Λ, thus, a charged track with momentum larger than 0.5 GeV/c is assigned to be (anti-)proton, otherwise pion.

The efficiency vs $cos\theta$ and transverse momentum of (anti-)proton is shown in Fig. 39. Combining all the phase space, the tracking efficiency of the (anti-)proton and π^+/π^- is sumarized in table 18.

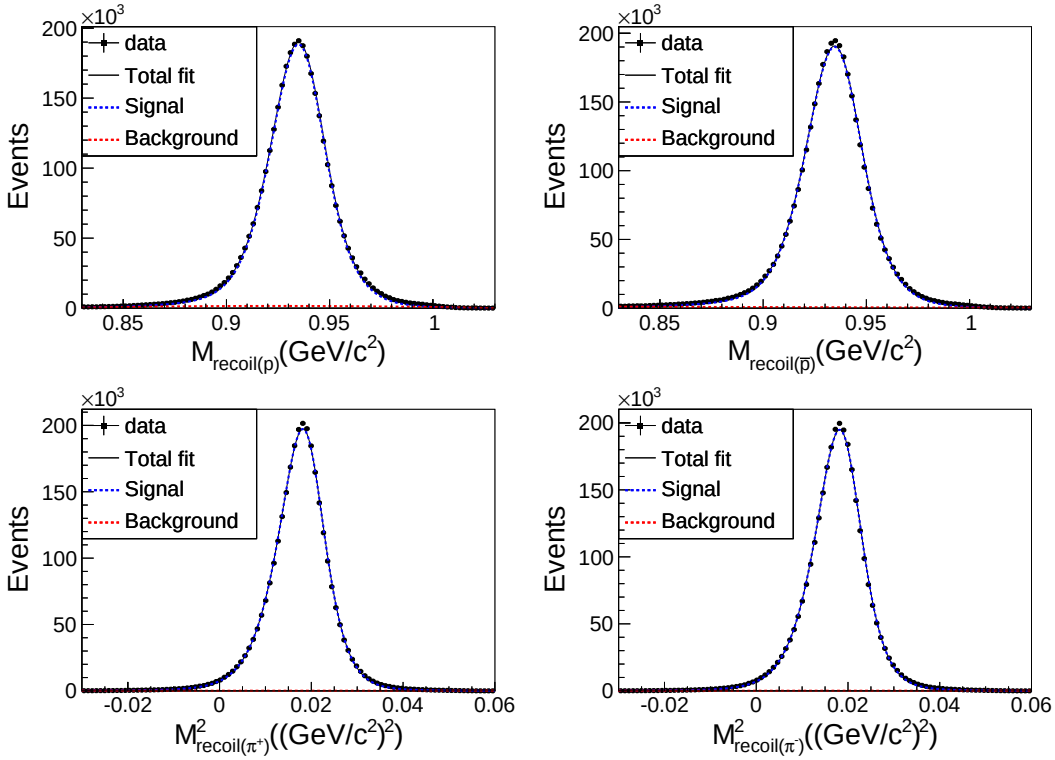

Figure 38: Distribution of the recoil mass distribution of proton(topleft), anti-proton(topright), distribution of the square of the recoil mass of π^+(bottomleft) and π^-(bottomright).

Table 18: Tracking efficiency of the (anti-)proton and π^+/π^-.

Efficiency	Data	MC
proton	98.5%	98.7%
anti-proton	97.7%	98.1%
π^+	72.8%	71.8%
π^-	72.9%	70.9%

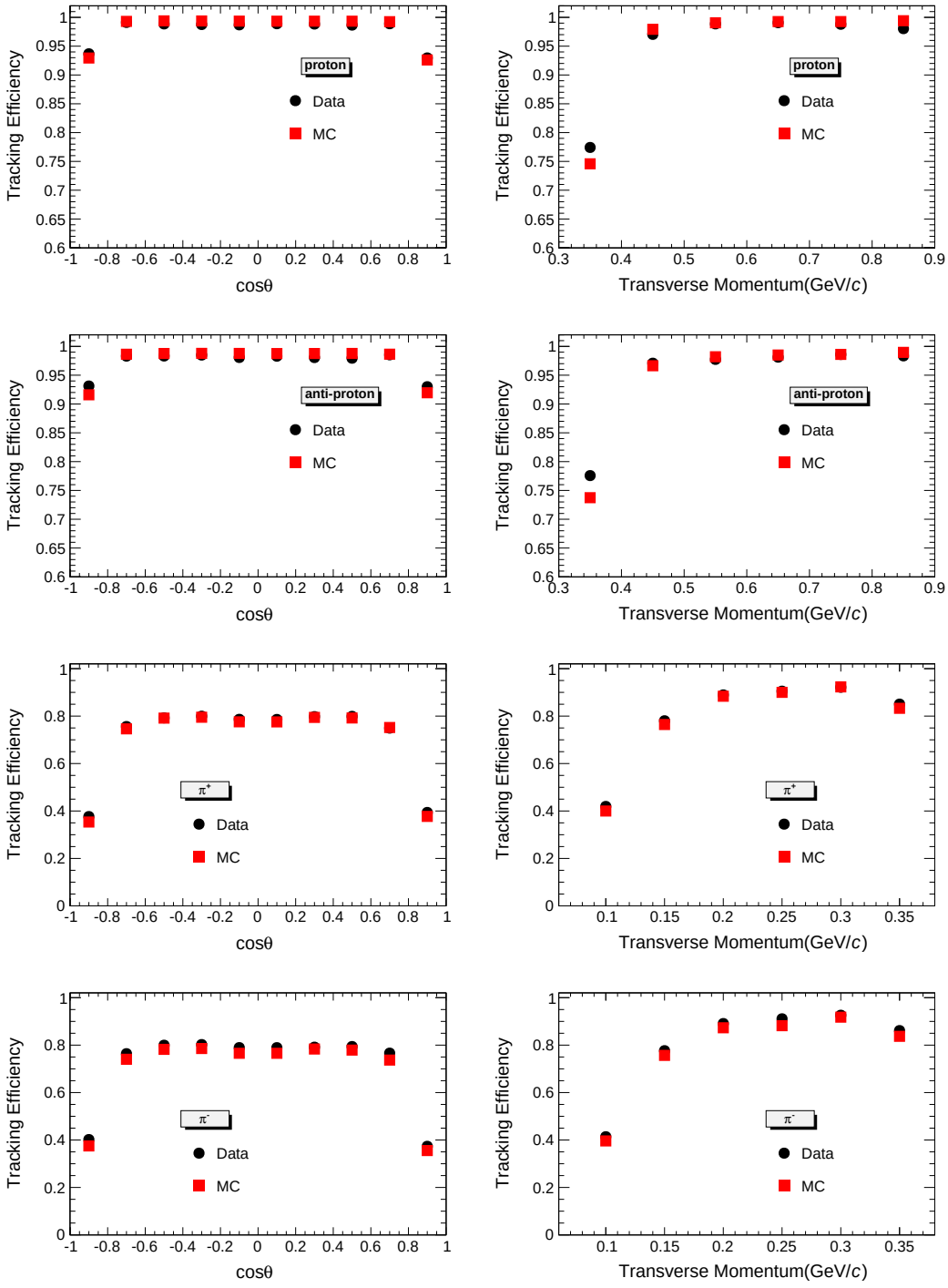

Figure 39: Tracking efficiency vs the cosθ and transverse momentum of charged particles. From the top down, the plots are for proton, anti-proton and π^+ and π^-, respectively.

- **PID efficiency**

The Pid effiency is defined by the formula:

$$\varepsilon_{PID} = \frac{n}{N}, \tag{17}$$

where **N** is the number of signal events without PID requirement for the given particle and **n** is the number of events with PID for the given particle. We use the same sample of checking tracking efficiency. The PID efficiency vs $cos\theta$ and transverse momentum of (anti-)proton is shown in Fig. 40. Combining all the phase space, the PID efficiency of the (anti-)proton is sumarized in table 19.

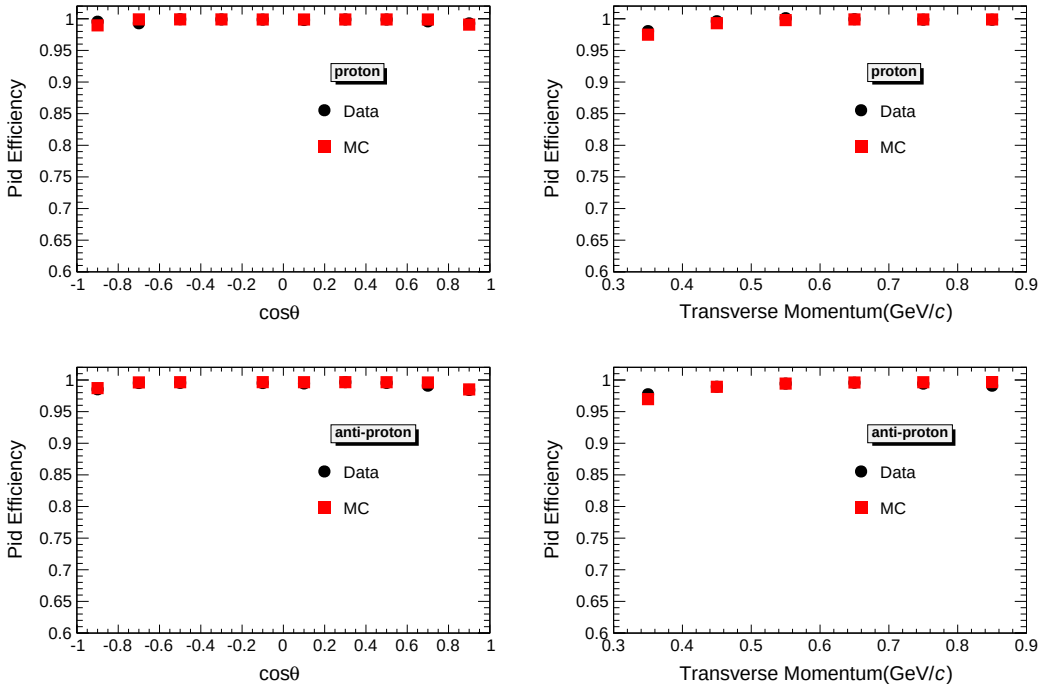

Figure 40: PID efficiency vs the cosθ and transverse momentum of charged particles. From the top down, the plots are for proton, anti-proton, respectively.

Table 19: PID efficiency of the (anti-)proton.

Efficiency	Data	MC
proton	99.7%	99.8%
anti-proton	99.5%	99.6%

- **Vertex fit efficiency**

To reconstruct a Λ signal with its decay mode $\Lambda \to \pi^- p$, the efficiency of vertex fit and secondary vertex fit is defined by the formula:

$$\varepsilon_{vtxfit} = \frac{n}{N}, \tag{18}$$

where **N** is the number of signal events before vertex fit and secondary vertex fit and **n** is the number of events after vertex fit and secondary vertex fit.

To obtain the efficiency of vertex fit and secondary vertex fit for $\bar{\Lambda} \to \pi^+ \bar{p}$, first, we need to select the $J/\psi \to \Lambda\bar{\Lambda}, \Lambda \to \pi^- p, \bar{\Lambda} \to$ *anything* by using the ST method in chapter 3.1. then, require at least one anti-proton and one π^+ and obtain the **N**; finally, perform vertex fit and secondary vertex fit for $\bar{\Lambda}$ with the anti-proton and π^+ and obtain the **n**. The efficiency of vertex fit and secondary vertex fit of the $\Lambda(\bar{\Lambda})$ is sumarized in table 20.

Table 20: Vertex fit and second vertex fit efficiency of the Λ ($\bar{\Lambda}$)

Efficiency	Data	MC
Tag Λ	79.1%	79.1%
Tag $\bar{\Lambda}$	77.9%	78.7%

Accordingly, the efficiency of the data and mc exist differences, therefore the signal MC efficiency of tracking, PID and (second)vertex fit is corrected to eliminate the bias, after which we got the consistant yields of the two charge conjugate modes. The result is shown in table 21.

Table 21: The ST yields of charged conjugated modes with efficiency.

Modes	$J/\psi \to \Lambda\bar{\Lambda}$,$\Lambda \to p\pi^-$,$\bar{\Lambda} \to$ *anything*	$J/\psi \to \Lambda\bar{\Lambda}$,$\bar{\Lambda} \to \bar{p}\pi^+$,$\Lambda \to$ *anything*
Yield	6922930 ± 2788	6736380 ± 2750
Efficiency(default)	51.2%	51.2%
Efficiency (corrected)	52.5%	51.1%

E Check the resolution of M_{Λ}^{DT} after fix the M_{Λ}^{ST} to PDG

Since kinematic fit is used to reconstruct the DT Λ, to further improve the resolution of M_{Λ}^{DT}, a test is tried after fixing the the single tag Λ mass (M_{Λ}^{ST}) to PDG or use the vertex fit result, the resolution of M_{Λ}^{DT} (E_{γ}) are very close, according to Fig. 41. Note the efficiency of signal will decrease about 15%, this is because when we fix the M_{Λ}^{ST} to PDG, we need to create resonance by $p\pi^{-}$, but the $p\pi^{-}$ don't from initial point but from the Λ decay, so the χ^2 of kinematic fit will much larger, as shown in Fig. 42

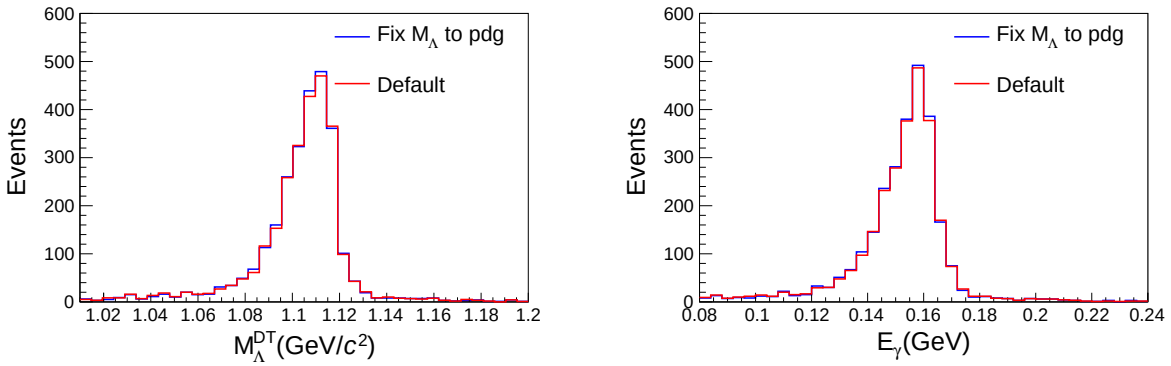

(a) invariant mass of DT (anti-)Λ (b) photon energy in rest frame of DT (anti-)Λ

Figure 41: Comparison of the resolution of invariant mass of DT (anti-)Λ or photon energy in rest frame of DT (anti-)Λ.

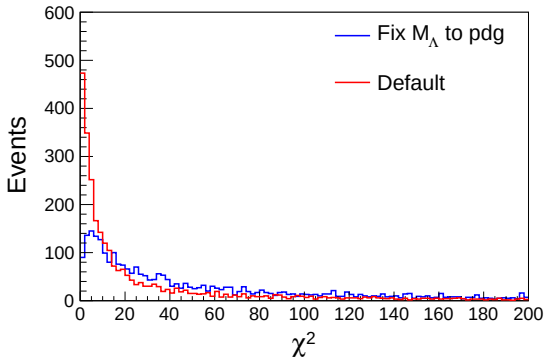

(a)

Figure 42: χ^2 distribution of kinematic fit after fixing the the single tag Λ mass (M_{Λ}^{ST}) to PDG.

F Comparison of observables of E_γ and $M_{\gamma n}$

The E_γ in the Λ rest frame and invariant mass of γ and (anti-)neutron ($M_{\gamma n(\bar{n})}$) are the potential variables to extract the yields of signal, as shown in Fig. 43. Actually the two variables are completely correlated, according to the 2D distribution of E_γ and $M_{\gamma n}$, as shown in Fig. 44

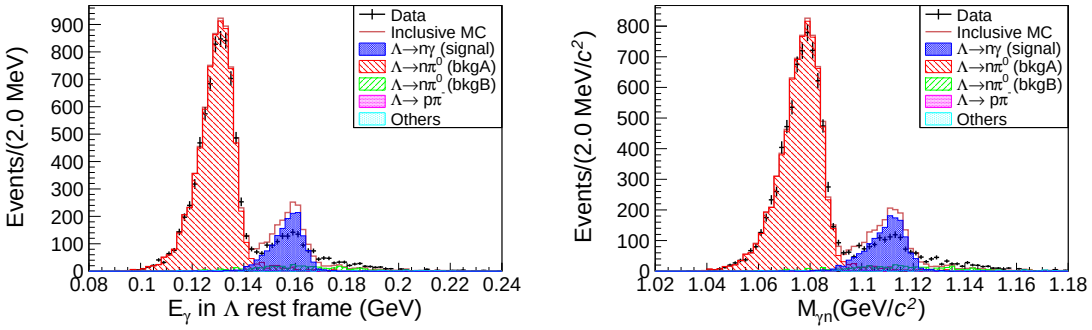

Figure 43: The distributions of gamma energy in the $\Lambda(\bar{\Lambda})$ rest frame (E_γ) (left) and the invariant mass of γ and (anti-)neutron ($M_{\gamma n/\bar{n}}$) (right) after applying all the above selection criteria.

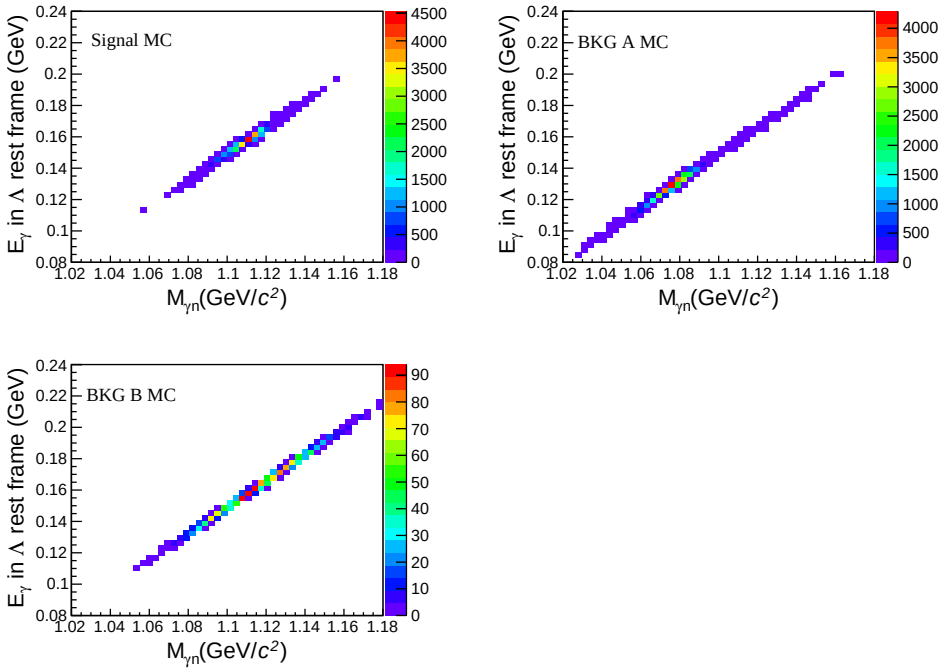

Figure 44: The 2D distributions of gamma energy in the Λ rest frame (E_γ) (left) and the invariant mass of γ and neutron

G Input and output check of the fit for decay parametor

To check the reliability of the fit method, an input/output check is implemented by using 40 sets of MC samples mixed with sianal, BKG A and BKG B with the same number as yields of data, as shown in Table 12. The distribution of the output value of α_γ is shown in Fig.45, with fit result shown in Table 22.

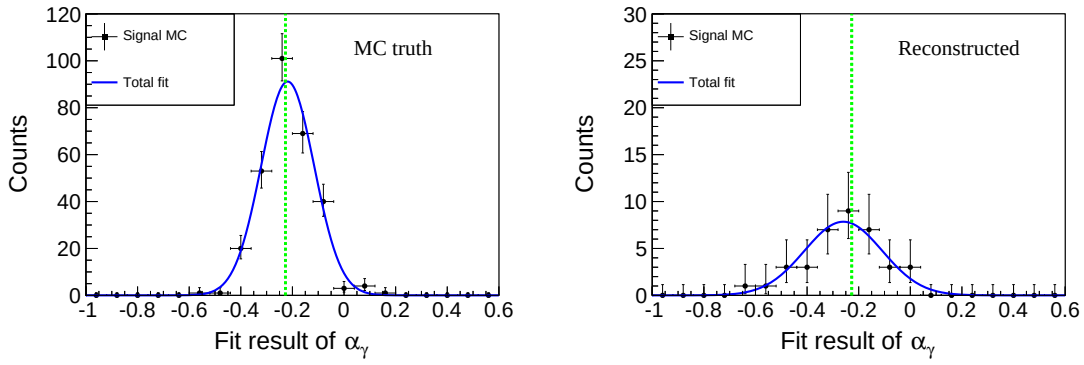

Figure 45: Distribution of output value of α_γ by using 200 sets of signal MC truth (left) and 40 sets of MC samples mixed with signal and BKG A B with same number of the yield (right). The distribution is fitted with a gaussian function, The dashed green line in the plot indicates the input value of α_γ.

Table 22: Input/Output check result.

Parameters	Input value	Output value
$\alpha_{J/\psi}$	0.461	0.461 (Fixed)
$\Delta\Phi$	0.74	0.74 (Fixed)
α_-	0.75	0.75 (Fixed)
α_+	−0.758	−0.758 (Fixed)
α_γ	−0.227	-0.259 ± 0.025

H Input and output check of the fit for the DT yield extraction

As mentioned in Sec.4.4, the double tag yield $N_{double-tag}$ is extracted by fitting the distribution of γ energy in the $\Lambda(\bar{\Lambda})$ rest frame. A 1-D unbinned extended maximum likelihood fit is performed on the distribution of the accepted events. As shown in Fig 46, we have generated 100 groups of Toy MC accordig to the E_γ distribution of signal and BKG A B with yields same as that in data, after which we fit the samples with the same stategy (BKG B is described with a Gaussian function whose parameters are extracted from data sample) as that for data and record the fitting results in Fig. 47. If we try to describe the BKG B with a Gaussian function which parameters are floated, the errors of the yield caused by fitting will be larger, as shown in Fig. 48. If we try to describe the BKG B with a Gaussian function which sigma are 5% larger than that extracted from data sample, the errors of the yield caused by fitting will also be larger, as shown in Fig. 49

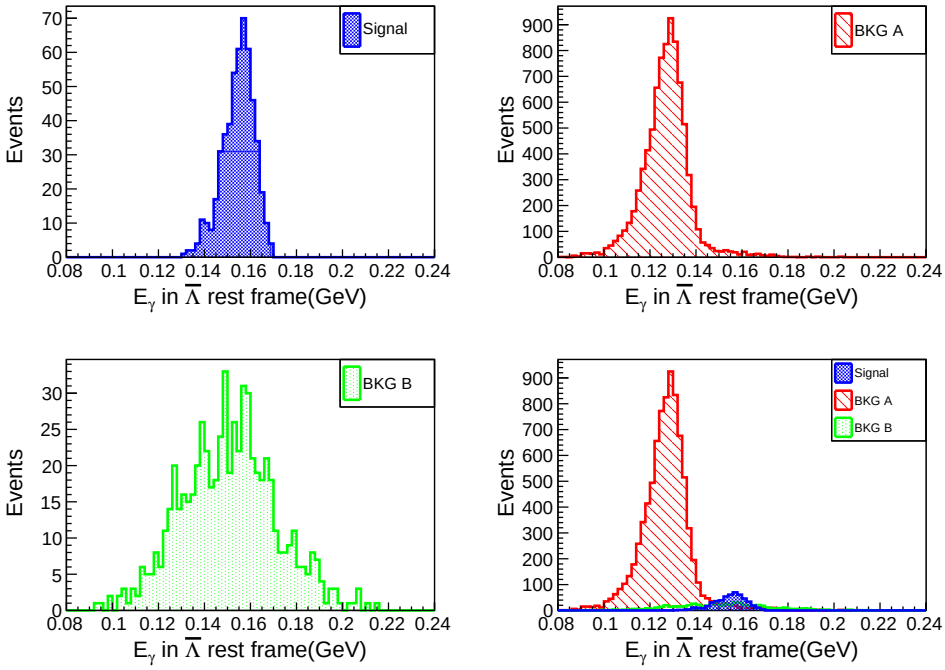

Figure 46: The gamma energy in the Λ rest frame (E_γ) distribution of signal, BKG A and BKG B of the generated toy MC

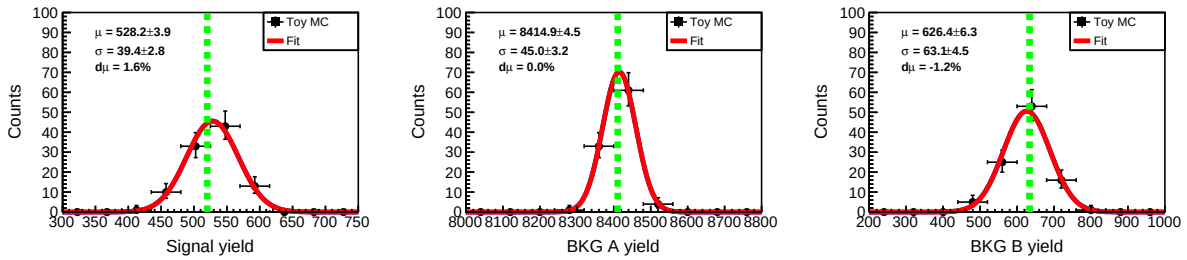

Figure 47: The yield of signal, BKG A and BKG B of the toy MC for 100 times, the green dashed line indicates the inout value of the signal/BKG A/B. BKG B is described with a Gaussian function whose parameters are extracted from data sample.

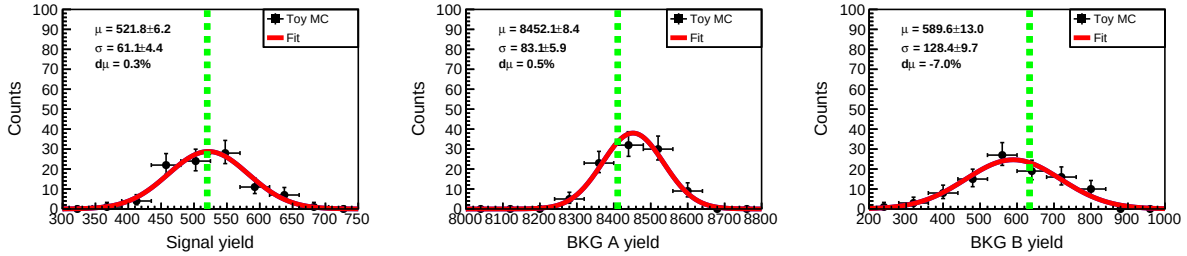

Figure 48: The yield of signal, BKG A and BKG B of the toy MC for 100 times, the green dashed line indicates the inout value of the signal/BKG A/B. BKG B is described with a Gaussian function whose parameters are floated.

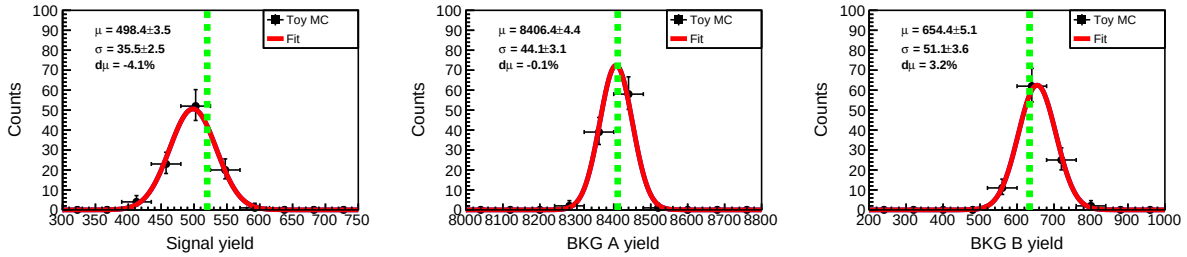

Figure 49: The yield of signal, BKG A and BKG B of the toy MC for 100 times, the green dashed line indicates the inout value of the signal/BKG A/B. BKG B is described with a Gaussian function whose parameters are floated.

I Input and output check of the the anti-neutron efficiency correction

The strong interaction of anti-neutrons can not be described accurately by the MC, especially the shower information and efficiency. But in 3C kinematic fit, the $\bar{n}$ exact shower properties are required, including the spatial position θ , ϕ and the spatial position error $d\theta$, $d\phi$. To guarantee the consistency of data and MC simulations for the anti-neutron, including the efficiency and kinematic properties, a data-driven algorithm has been adopted to correct the $\bar{n}$ selection efficiency and shower parameters.

Input-output check is done to check reliability of the package by using signal MC. We have compared the efficiencies of the same MC with/without applying the package to correct the efficiency. The default MC don't apply the package while the corrected MC apply the package which anti-neutron efficiency is obtained from the MC control sample ($J/\psi \to p\pi^-\bar{n}$). The cosθ and moment distribution of the anti-neutrons are shown in Fig. 50. The efficiencies of each selection creteria are shown in table 23, indicating that the systematic uncertainty of the correction is negligible.

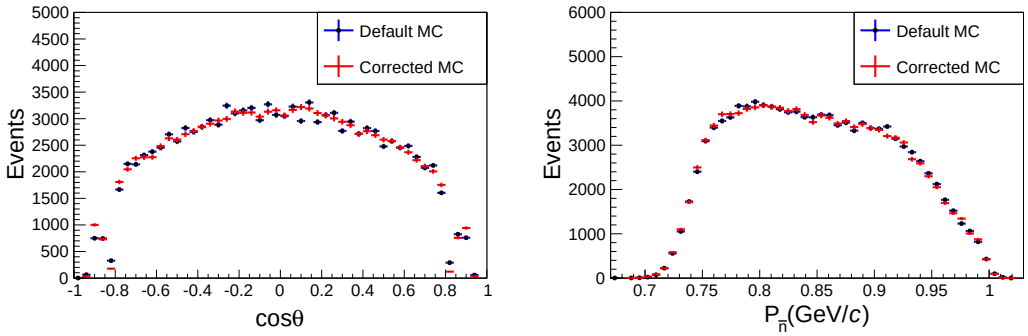

Figure 50: The cosθ and moment distribution of anti-neutrons. The blue dots are based on the default mc sample and the red dots are based on the mc sample whose anti-neutron efficiency is corrected by the package.

Table 23: The input-output check result of anti-neutron correction. The efficiencies of each selection creteria of default mc and corrected mc are compared.

Selection criteria	Defalut MC efficiency	Corrected MC efficiency
Truth	100.00%	100.00%
Good charged track	70.96%	70.96%
Pid	66.63%	66.63%
Single Tag	51.09%	51.09%
3C kinematic fit	25.30%	25.44%
$\chi^2_{3C}(\bar{\Lambda} \to \gamma\bar{n}) < 15$	9.09%	9.18%
$\lvert M(\gamma\gamma) - M_{\pi^0}\rvert > 20$ MeV/c^2	8.17%	8.18%
$E_\gamma > 0.15$ GeV	6.15%	6.16%
$\theta(\gamma, \bar{n}) > 20^\circ$	5.45%	5.47%
BDT>0.3	2.80%	2.81%

References

[1] B.Bassalleck. Hyperon Weak Radiative Decays. *Nuclear Physics*, A585:255c-266c, 1995.

[2] Hai-Bo Li. Prospects for rare and forbidden hyperon decays at BESIII. *Front. Phys.*, 121301:12(5), 2017.

[3] I. I. Balitsky, V. M. Braun, and A. V. Kolesnichenko. Radiative decay $\Sigma^+ \to p\gamma$ in quantum chromodynamics. *Nucl. Phys.*, B 312(3), 509 (1989)

[4] M. K. Gaillard, X. Li, and S. Rudaz. Constituent gluons and a new mechanism for radiative weak decays of hyperons. *Phys. Lett. B.*, B 158(2), 158 (1985)

[5] P. Zenczykowski. Joint description of weak radiative and nonleptonic hyperon decays in broken SU(3). Phys. Rev. D , D 73(7), 076005 (2006)

[6] B. Borasoy and B. R. Holstein. Resonances in radiative hyperon decays. Phys. Rev. D , D 59(5), 054019 (1999)

[7] Y. Hara. Nonleptonic Decays of Baryons and the Eightfold Way. Phys. Rev. Lett., 12, 378 (1964).

[8] G. Feldman, P. T. Matthews and A. Salam. Nonleptonic decay modes of the hyperons. Phys. Rev., 121, 302-303 (1961).

[9] A.Lai, et al., Phys. Lett. B, 584 251 (20064).

[10] V.Fanti, et al., EPJC, 12, 69–76 (2000)

[11] C. James, et al., Phys.Rev.Lett., 64 843-846 (1990)

[12] J.R.Batley, et al., Phys. Lett. B ,693 241 (2010)

[13] P. Y. Niu, J. M. Richard, Q. Wang and Q. Zhao, Chin. Phys. C **45**, no.1, 013101 (2021)

[14] P. Zenczykowski. Joint description of weak radiative and nonleptonic hyperon decays in broken SU(3). Phys. Rev. D.,73, 076005 (2006)

[15] B. Borasoy and B. R. Holstein. Resonances in radiative hyperon decays. Phys. Rev. D.,59, 054019 (1999)

[16] G. Nardulli, A Pole Model Calculation of Weak Radiative Hyperon Decays. Phys. Lett. B.,190, 187 (1987).

[17] M. B. Gavela,etc al. Parity Violating Radiative Weak Decays and the Quark Model. Phys. Lett. B.,417 (1981).

[18] The BESIII Collaboration. MEMO-537,https://hnbes3.ihep.ac.cn/HyperNews/get/paper537.html

[19] S. Agostinelli et al. GEANT4: A Simulation toolkit.. Nucl. Instrum. Meth., A506:250-303, 2003.

[20] John Allison et al. Geant4 developments and applications.. IEEE Trans. Nucl. Sci., 53:270, 2006

[21] S. Jadach, B. F. L. Ward, and Z. Was. Coherent exclusive exponentiation for precision Monte Carlo calculations.. Phys. Rev., D63:113009, 2001.

[22] Rong-Gang Ping. Event generators at BESIII.. Chin. Phys., C32:599, 2008.

[23] D. J. Lange. The EvtGen particle decay simulation package.. Nucl. Instrum. Meth., A462:152-155, 2001.

[24] Liang Liu. Development of a Data-Driven Algorithm to Simulate Anti-neutron with Bootstrapping at BESIII .BESIII DocDB-doc-908-v10.

[25] T. D. Lee and C.-N. Yang, General Partial Wave Analysis of the Decay of a Hyperon of Spin 1/2,. Phys. Rev., 108 (1957) 1645–1647.

[26] G. Faldt and A. Kupsc, Hadronic structure functions in the $e + e- \to \Lambda\bar{\Lambda}$ reaction,. Phys. Lett., B772 (2017) 16–20.

[27] M. Ablikim et al. [BESIII Collaboration]. *Phys. Rev. D*, 052005:81, 2010.